

# Multicritical behavior in the fully frustrated XY model and related systems

Martin Hasenbusch,<sup>1</sup> Andrea Pelissetto,<sup>2</sup> and Ettore Vicari<sup>1</sup>

<sup>1</sup> Dip. Fisica dell'Università di Pisa and INFN, Largo Pontecorvo 2, I-56127 Pisa, Italy

<sup>2</sup> Dip. Fisica dell'Università di Roma "La Sapienza" and INFN, P.le Moro 2, I-00185 Roma, Italy

E-mail: [Martin.Hasenbusch@df.unipi.it](mailto:Martin.Hasenbusch@df.unipi.it),  
[Andrea.Pelissetto@roma1.infn.it](mailto:Andrea.Pelissetto@roma1.infn.it), [Ettore.Vicari@df.unipi.it](mailto:Ettore.Vicari@df.unipi.it)

**Abstract.** We study the phase diagram and critical behavior of the two-dimensional square-lattice fully frustrated XY model (FFXY) and of two related models, a lattice discretization of the Landau-Ginzburg-Wilson Hamiltonian for the critical modes of the FFXY model, and a coupled Ising-XY model. We present a finite-size-scaling analysis of the results of high-precision Monte Carlo simulations on square lattices  $L \times L$ , up to  $L = O(10^3)$ .

In the FFXY model and in the other models, when the transitions are continuous, there are two very close but separate transitions. There is an Ising chiral transition characterized by the onset of chiral long-range order while spins remain paramagnetic. Then, as temperature decreases, the systems undergo a Kosterlitz-Thouless spin transition to a phase with quasi-long-range order.

The FFXY model and the other models in a rather large parameter region show a crossover behavior at the chiral and spin transitions that is universal to some extent. We conjecture that this universal behavior is due to a multicritical point. The numerical data suggest that the relevant multicritical point is a zero-temperature transition. A possible candidate is the  $O(4)$  point that controls the low-temperature behavior of the 4-vector model.

## 1. Introduction

In the last few decades there has been considerable interest in the nature of the phase diagram of the two-dimensional ( $2-d$ ) fully frustrated XY (FFXY) model, whose Hamiltonian is [1]

$$\mathcal{H}_{\text{FFXY}} = -J \sum_{\langle xy \rangle} \cos(\theta_x - \theta_y + A_{xy}). \quad (1)$$

Here  $J > 0$ , the angle variables  $\theta_x$  are defined on the sites of a regular  $2-d$  lattice, the summation is over nearest-neighbor pairs, and the quantities  $A_{xy}$  are fixed and satisfy the constraint  $\sum A_{xy} = \pi$  around each plaquette. The FFX model is experimentally relevant for Josephson-junction arrays in a magnetic field. It should describe the superconducting-to-normal transition at half a flux quantum per plaquette, see, e.g., Refs. [2, 3, 4] and references therein.

As a consequence of frustration, the ground state of the FFX model presents an  $O(2) \otimes \mathbb{Z}_2$  degeneracy [1]. While the  $O(2)$  degeneracy is the usual one and is related to the  $O(2)$  global invariance of the Hamiltonian that is broken in the low-temperature (LT) phase, the additional  $\mathbb{Z}_2$  degeneracy [1, 5]. A variable that distinguishes the different ground states is the chirality [1], which is defined by

$$\chi_n = \text{sign} \left[ \sum_{\langle xy \rangle \in \Pi_n} \sin(\theta_x - \theta_y + A_{xy}) \right], \quad (2)$$

where  $\Pi_n$  is a lattice plaquette and  $n$  is the dual-lattice site at its center. At zero temperature there are two degenerate ground states related by a global flip of the chiral variables  $\chi_n$ . Therefore, the staggered chirality magnetization defines an order parameter related to the chiral  $\mathbb{Z}_2$  symmetry, which competes with the spin magnetization in determining the phase diagram and critical behavior of the FFX model. Much work has been dedicated to the study of the phase diagram of the FFX model and related models that have the same ground-state degeneracy [5, 6, 7, 8, 9, 10, 11, 12, 13, 14, 15, 16, 17, 18, 19, 20, 21, 22, 23, 24, 25, 26, 27, 28, 29, 30, 31, 32, 33, 34, 35, 36, 37, 38, 39, 40, 41, 42, 43, 44, 45, 46, 47, 48, 49, 50, 51, 52, 53, 54, 55, 56, 57, 58, 59, 60, 61, 62, 63, 64, 65, 66, 67, 68, 69, 70, 71, 72, 73, 74, 75]. In spite of that, there is not yet a general consensus on the critical behavior of these systems. In this paper, we address again this issue and, by performing simulations on very large lattices and by means of a careful finite-size scaling (FSS) analysis of the results, we provide what we believe is the definite answer on this problem.

Two scenarios have been put forward for the critical behavior of the FFX and related  $2-d$  models. In one of them the system undergoes two transitions as temperature decreases. First, chiral modes undergo an Ising-type transition at  $T_{\text{ch}}$ , characterized by the onset of chiral long-range order while spins remain paramagnetic. Then, at a lower temperature  $T_{\text{sp}}$ , spin modes exhibit a transition to a phase with quasi-long-range order, which coexists with the long-range order of the chiral modes. This second transition is expected to belong to the same universality class as the Kosterlitz-Thouless (KT)

transition in the standard 2- $d$  XY model [76, 77]. In this scenario spin and chiral modes decouple and order at different temperatures. This scenario is supported by arguments based on a kink-antikink unbinding picture [68, 74]. A second possibility is that spin and chirality order at the same temperature,  $T_c$ , where both chiral long-range order and spin quasi-long-range order set in simultaneously. In this case spin and chiral modes may be coupled at the transition and may give rise to a qualitatively new critical behavior. Therefore, one may observe values of the chiral critical exponents that differ from the Ising ones,  $\nu = 1$  and  $\eta = 1/4$ . Field-theoretical calculations within the corresponding Landau-Ginzburg-Wilson (LGW) theory [65, 70] support the existence of such a new universality class.

Previous results are presented in Table 1. We report results for the fully frustrated XY model on the square lattice (FFXY<sub>sq</sub>) and on the triangular lattice (FFXY<sub>tr</sub>), and also for some generalizations: a model with next-to-nearest-neighbor interactions (FFXY<sub>nn+nnn</sub>), a nearest-neighbor model with Villain Hamiltonian, and XY models in which frustration is induced by the competition of nearest-neighbor and next-to-nearest-neighbor interactions (FXY<sub>J<sub>1</sub>,J<sub>2</sub></sub>) or by a zig-zag pattern of ferromagnetic and antiferromagnetic couplings (FXY<sub>zz</sub>). We also include results for some related models that have the same ground-state degeneracy: the fractional-charge Coulomb-gas (CG) model that is obtained from the FFXXY model by the usual duality mapping, a model with two coupled XY fields (2cXY) or with an Ising and XY field (IsXY), the antiferromagnetic XXZ model with easy-plane exchange anisotropy on the triangular lattice (FFXXZ<sub>tr</sub>), the frustrated antiferromagnetic six-state clock model on a triangular lattice (FA6SC), the 19-vertex model, the quantum ladder of Josephson junctions (QLJJ), the solid-on-solid model coupled to the Ising model (SOS-Is), and the corresponding LGW  $\phi^4$  theory. In Table 1 we report the method that has been employed to investigate the phase diagram, the number of transitions that are observed (whenever there are two transitions, we also give the difference of the critical temperatures) and the estimates of the critical exponents at the chiral transition. Most of the results have been obtained by Monte Carlo (MC) simulations. But we should also mention transfer-matrix (TM) and real-space renormalization-group (RG) calculations, as well as perturbative field-theoretical (FT) analyses. Note that most MC studies focussed on the finite-size behavior at criticality; only in a few cases [30, 33, 43, 47] was the temperature dependence investigated in the large-volume limit. In some cases the critical behavior was investigated by studying the nonequilibrium relaxation (NER) at criticality.

The results summarized in Table 1 are rather contradictory. The most recent MC simulations favor the existence of two transitions. If this is correct, the results of the MC simulations observing only one transition may be reasonably explained by noting that the two transitions are very close and that high accuracy is required to disentangle them. If there are two transitions, chiral and spin modes decouple and thus one expects Ising behavior at the chiral transition. But this is not supported by numerical simulations that have found  $\nu \approx 0.8$  in most cases. To explain this result, one may conclude that there is a single transition that belongs to a new universality class. In this case, the

observation of two very close transitions might be explained by uncontrolled systematic errors in the analysis of the MC data. Of course, it is also possible, as discussed in Refs. [40, 47, 67], that the departure of the chiral exponents from the Ising values is due to a slow crossover towards the Ising asymptotic behavior, somehow caused by the interaction with the spin modes, which will eventually give rise to a KT transition. However, this argument does not explain why the same estimate  $\nu \approx 0.8$  is obtained in several different models. Finally, there is a third, less conventional possibility: There are two transitions, but the chiral transition does not belong to the Ising universality class for some unknown reasons.

In this paper we study the phase diagram of the 2- $d$  square-lattice FFXY and of two related models, a coupled Ising-XY (IsXY) model and a  $\phi^4$  model obtained from a straightforward lattice discretization of the LGW Hamiltonian for the critical modes of the FFXY model, see, e.g., Refs. [29, 5]. We present MC simulations on square lattices  $L \times L$ , up to  $L = O(10^3)$ . The phase diagrams and critical behaviors are obtained by means of a FSS analysis of the MC results. Short reports already appeared in Ref. [78]. In the LT phase the  $\mathbb{Z}_2$  chiral symmetry is broken and the spin degrees of freedom show the same quasi-long-range order as in the 2- $d$  XY model. We conclusively show that the square-lattice FFXY model undergoes two very close but separate transitions: a KT and then, as temperature increases, an Ising transition with  $\delta \equiv (T_{\text{ch}} - T_{\text{sp}})/T_{\text{ch}} = 0.0159(2)$ . The same transition pattern is observed in the  $\phi^4$  and IsXY models when the transitions are continuous.

Beside confirming the two-transition scenario, we have also observed an unexpected crossover behavior that is universal to some extent. In the FFXY model and in the  $\phi^4$  and IsXY models in a large parameter region, the finite-size behavior at the chiral and spin transitions is model independent, apart from a length rescaling. In particular, the universal approach to the Ising regime at the chiral transition is nonmonotonic for most observables, and there is a wide region in which the finite-size behavior is controlled by an effective exponent  $\nu_{\text{eff}} \approx 0.8$ . This occurs for  $L \lesssim \xi_s^{(c)}$ , where  $\xi_s^{(c)}$  is the spin correlation length at the chiral transition, which is usually large in these models; for example,  $\xi_s^{(c)} = 118(1)$  in the square-lattice FFXY model. This explains why many previous studies that considered smaller lattices always found  $\nu \approx 0.8$ . This universal behavior may be explained by the presence of a multicritical point, where chiral and spin modes are both critical. As far as its nature is concerned, our numerical data at the chiral transition suggest a zero-temperature multicritical point. In this case, a possible candidate is the O(4) multicritical point that is present in the  $\phi^4$  lattice model and controls the low-temperature phase of the 4-vector model.

This paper is organized as follows. In Sec. 2 we define the models investigated in this paper. The thermodynamic quantities considered in this study are introduced in Sec. 3. A brief presentation of our MC simulations is given in Sec. 4. Sec. 5 is dedicated to the study of the LT phase. In Sec. 6 we discuss the critical behavior of the square-lattice FFXY model. In Secs. 7 and 8 we investigate the phase diagram of the  $\phi^4$  model and of the IsXY model respectively. In Sec. 9 we discuss the crossover behavior at the

**Table 1.** Overview of results for the FFXY and related models. The shorthands used in the second and third column are explained in the text. The fourth column reports the number of transitions observed, and, in the case of two transitions, the relative difference between their temperatures, i.e.  $\delta \equiv (T_{\text{ch}} - T_{\text{sp}})/T_{\text{ch}}$ . The fifth column gives the estimates of the critical exponents associated with the chiral degrees of freedom.

Ref.	model	method	transitions	chiral exponents
[6] (1983)	FFXY <sub>sq</sub>	MC ( $L \leq 32$ )		consistent with Ising
[7] (1984)	FFXY <sub>tr</sub>	MC ( $L \leq 32$ )	2tr	
[8] (1984)	FFXY <sub>sq</sub>	MC ( $L \leq 45$ )	2tr, $\delta \approx 0.02$	
[10] (1985)	FFXY <sub>sq</sub>		$\delta \geq 0$	
[5] (1985)	FFXY <sub>sq</sub> , CG	RG	1tr	
[11] (1985)	2cXY	RG	1tr	
[13] (1986)	FFXY <sub>tr</sub>	MC ( $L \leq 72$ )	1-2tr, $\delta \lesssim 0.01$	consistent with Ising
[15] (1986)	FFXY <sub>tr</sub>	MC ( $L \leq 72$ )	1tr	
[16] (1986)	FFXY <sub>sq</sub>	MC ( $L \leq 100$ )	1tr	
[17] (1986)	2cXY	real-space RG	1tr	
[19] (1988)	CG	MC ( $L \leq 30$ )	1tr	
[21] (1989)	CG	MC ( $L \leq 50$ )	2tr, $\delta \approx 0.03$	
[22] (1989)	CG	MC ( $L \leq 48$ )	1tr	
[25] (1990)	FFXY <sub>sq</sub>	TM MC ( $L \leq 12$ )	1tr	$\nu \approx 1, \eta = 0.40(2)$
[26, 27] (1991)	FFXY <sub>sq</sub>	MC ( $L \leq 40$ )	1tr	$\nu = 0.85(3), \eta = 0.31(3)$
[26, 27] (1991)	FFXY <sub>tr</sub>	MC ( $L \leq 40$ )	1tr	$\nu = 0.83(4), \eta = 0.28(4)$
[28] (1991)	FFXY <sub>sq</sub>	MC ( $L \leq 128$ )	1-2tr	$\nu = 1.009(26)$
[29] (1991)	IsXY ( $C = -0.2885$ )	MC ( $L \leq 32$ )	1-2tr	$\nu = 0.84(3)$
[30] (1991)	FXY <sub><math>J_1, J_2</math></sub>	MC ( $L \leq 150$ )	1tr	$\nu = 0.9(2), \eta = 0.4(1)$
[31] (1992)	19-vertex-Is	TM ( $L \leq 7$ )	1tr	$\nu = 1.0(1), \eta = 0.26(1)$
[33] (1992)	FFXY <sub>sq</sub>	MC ( $L \leq 240$ )	1-2tr, $\delta \gtrsim -0.07$	$\nu = 0.875(35)$
[35, 45] (1992)	QLJJ ( $E_x/E_y = 1$ )	TM QMC		$\nu = 0.81(4), \eta = 0.47(4)$
[35, 45] (1992)	QLJJ ( $E_x/E_y = 3$ )	TM QMC		$\nu = 1.05(6), \eta = 0.27(3)$
[36] (1993)	FFXY <sub>sq</sub>	TM MC ( $L \leq 14$ )	1tr	$\nu = 0.80(5), \eta = 0.38(2)$
[37] (1994)	CG	MC ( $L \leq 30$ )	2tr, $\delta \approx 0.04$	$\nu = 0.84(3), \eta = 0.26(4)$
[38] (1994)	FFXY <sub>sq</sub>	MC ( $L \leq 48$ )	2tr, $\delta \approx 0.03$	$\nu = 0.813(5), \beta = 0.089(8)$
[39] (1994)	19-vertex model	TM ( $L \leq 15$ )	1tr	$\nu = 0.81(3), \eta = 0.28(2)$
[40] (1995)	FFXY <sub>sq</sub>	MC ( $L \leq 128$ )	2tr, $\delta \approx 0.013$	consistent with Ising
[42, 45] (1995)	IsXY ( $C = -0.2885$ )	TM MC ( $L \leq 30$ )	1tr	$\nu = 0.79, \eta = 0.40$
[43] (1996)	FFXY <sub>sq</sub>	MC ( $L \leq 128$ )		$\nu = 0.898(3)$
[44] (1996)	FFXY <sub>tr</sub>	MC ( $L \leq 144$ )	2tr, $\delta \approx 0.02$	$\gamma = 1.6(3), \beta = 0.11(3)$
[47] (1997)	Villain FFXYS <sub>sq</sub>	MC ( $L \leq 256$ )	2tr, $\delta \approx 0.014$	consistent with Ising
[48] (1997)	Villain FFXYS <sub>sq</sub>	spin waves, LT phase	1tr	
[49] (1997)	FXY <sub>zz</sub> ( $\rho = 0.7$ )	MC ( $L \leq 36$ )	1tr	$\nu = 0.78(2), \eta = 0.32(4)$
[49] (1997)	FXY <sub>zz</sub> ( $\rho = 1.5$ )	MC ( $L \leq 36$ )	1tr	$\nu = 0.80(1), \eta = 0.29(2)$
[50] (1997)	FFXY, 2cXY, CG	position-space RG	2tr, $\delta \approx 0.0005$	different from Ising
[51] (1997)	SOS-Is	MC ( $L \leq 22$ )	2tr	consistent with Ising
[52] (1997)	FXY <sub><math>J_1, J_2</math></sub> , CG	RG	1tr	
[56] (1998)	FFXY <sub>sq</sub>	NER <sub>std</sub> MC ( $L \leq 256$ )		$\nu = 0.81(2), \eta = 0.261(5)$
[57] (1998)	FFXY <sub>tr</sub>	MC ( $L \leq 60$ )	2tr, $\delta \approx 0.012$	$\nu = 0.833(7), \eta = 0.25(2)$
[58] (1998)	FFXXZ <sub>tr</sub>	MC ( $L \leq 120$ )	2tr, $\delta \lesssim 0.01$	consistent with Ising
[59] (1998)	FFXY <sub>sq</sub>	MC ( $L \leq 140$ )	1tr	$\nu = 0.852(2), \eta = 0.203(6)$
[61] (2000)	FXY <sub><math>J_1, J_2</math></sub>	MC ( $L \leq 150$ )	2tr, $\delta \approx 0.003$	$\nu = 0.795(20), \eta = 0.25(1)$
[62] (2000)	FXY <sub><math>nm+nnn</math></sub>	MC ( $L \leq 72$ )	2tr, $\delta \lesssim 0.01$	$\nu = 1.0(1)$
[63] (2001)	FFXY <sub>sq</sub>	NER <sub>std</sub> MC ( $L \leq 256$ )		$\nu = 0.80(2), \eta = 0.276(7)$
[63] (2001)	FXY <sub><math>nm+nnn</math></sub>	NER <sub>std</sub> MC ( $L \leq 256$ )		$\nu = 0.80(3), \eta = 0.282(8)$
[67] (2002)	FA6SC	MC ( $L \leq 192$ )	2tr, $\delta \approx 0.003$	consistent with Ising
[68] (2002)	FFXY		2tr, $\delta > 0$	
[70, 65] (2003)	LGW $\phi^4$	five-loop FT	stable FP	
[71] (2003)	FFXY <sub>sq</sub>	NER MC ( $L \leq 2000$ )	2tr, $\delta \approx 0.010$	$\nu = 0.82(2), \eta = 0.272(15)$
[71] (2003)	FFXY <sub>tr</sub>	NER MC ( $L \leq 2000$ )	2tr, $\delta \approx 0.008$	$\nu = 0.84(2), \eta = 0.250(10)$
[73] (2005)	FFXY <sub>sq</sub>	ED MC ( $L \leq 180$ )	1tr	$\nu = 0.9(1)$
[74] (2005)	FFXY <sub>sq</sub>	MC ( $L \leq 128$ )	2tr, $\delta > 0$	
this work	FFXY <sub>sq</sub>	MC ( $L \leq 1000$ )	2tr, $\delta = 0.0159(2)$	Ising
this work	IsXY ( $C = 0$ )	MC ( $L \leq 360$ )	2tr, $\delta = 0.0167(7)$	Ising
this work	$\phi^4$ ( $U = 1, D = 1/2$ )	MC ( $L \leq 1200$ )	2tr, $\delta = 0.0025(2)$	Ising

chiral transition. Finally, in Sec. 10 we summarize the main results of the paper and draw our conclusions. In Appendix A we provide some details on the algorithms used in the MC simulations. In Appendix B we report some results for the LT phase of the 2- $d$  XY model which are used in the paper.

## 2. Models

The Hamiltonian of the square-lattice FFXXY model is

$$\mathcal{H}_{\text{FFXY}} = -J \sum_{\langle xy \rangle} j_{xy} \vec{s}_x \cdot \vec{s}_y, \quad (3)$$

where the two-component spins  $\vec{s}_x$  satisfy  $\vec{s}_x \cdot \vec{s}_x = 1$ ,  $j_{xy} = 1$  along all horizontal lines, while along vertical lines ferromagnetic  $j_{xy} = 1$  and antiferromagnetic  $j_{xy} = -1$  couplings alternate. Here (as in the following models)  $J$  plays the role of inverse temperature, the Gibbs probability being simply proportional to  $e^{-\mathcal{H}_{\text{FFXY}}}$ .

We also consider the  $\phi^4$  model on a square lattice. The Hamiltonian is

$$\begin{aligned} \mathcal{H}_\phi = & -J \sum_{\langle xy \rangle, i} \vec{\phi}_{i,x} \cdot \vec{\phi}_{i,y} + \sum_{i,x} [\phi_{i,x}^2 + U(\phi_{i,x}^2 - 1)^2] \\ & + 2(U + D) \sum_x \phi_{1,x}^2 \phi_{2,x}^2, \end{aligned} \quad (4)$$

where  $i = 1, 2$ ,  $\vec{\phi}_{i,x}$  is a real two-component variable, the first sum goes over all nearest-neighbor pairs, and  $\phi_i^2 \equiv \vec{\phi}_i \cdot \vec{\phi}_i$ . Hamiltonian  $\mathcal{H}_\phi$  describes two identical O(2)-symmetric models coupled by an energy-energy term. This model is a straightforward lattice discretization of the LGW Hamiltonian

$$\mathcal{H}_{\text{LGW}} = \int d^d x \left\{ \frac{1}{2} \sum_{a=1,2} [(\partial_\mu \phi_a)^2 + r \phi_a^2] + \frac{1}{4!} u_0 \left( \sum_{a=1,2} \phi_a^2 \right)^2 + \frac{1}{4} v_0 \phi_1^2 \phi_2^2 \right\} \quad (5)$$

( $\phi_a$ ,  $a = 1, 2$ , is a two-component vector), which can be obtained by applying a Hubbard-Stratonovich transformation to the FFXXY model, dropping terms of order higher than four [29, 9, 5]. Therefore, the lattice  $\phi^4$  model (4) represents an effective ferromagnetic theory that is expected to describe the critical modes of the FFXXY model. This approach was already used to investigate the critical behavior of antiferromagnets on a stacked triangular lattice [79].

It is interesting to note that the symmetry of Hamiltonian (4) is larger than that of the FFXXY model. Indeed, the Hamiltonian is symmetric under separate rotations of the two fields and under the  $\mathbb{Z}_2$  transformation  $\phi_1 \leftrightarrow \phi_2$ . Therefore, the overall symmetry is  $[\text{O}(2) \oplus \text{O}(2)] \otimes \mathbb{Z}_2$ . For  $D > 0$  the ground state corresponds to  $\phi_1^2 = 0$  and  $\phi_2^2 \neq 0$  or the opposite, and thus it has the same degeneracy as the ground state of the FFXXY model. Indeed, the lowest-energy configurations are determined once one fixes which field does not vanish—thereby breaking the  $\mathbb{Z}_2$  interchange symmetry—and the direction of the nonvanishing one. Thus, the relation between the FFXXY model and the  $\phi^4$  Hamiltonian is not fixed by the symmetry of the original Hamiltonian but rather by the ground-state degeneracy group, which is the quotient of the symmetry

groups of the model and of the ground state. This is consistent with the paradigm that relates the universality class to the symmetry breaking pattern. Note that the extended symmetry of the LGW Hamiltonian is related to the truncation of the Hamiltonian to fourth order in the fields and it is lost if higher-order terms are added. More precisely, the Hubbard-Stratonovich calculation gives rise to  $\phi^6$  and  $\phi^8$  terms on the triangular and square lattice respectively, which break the  $O(2)\oplus O(2)$  symmetry down to  $O(2)$  [5]. These terms are irrelevant close to four dimensions but it is far from clear that the same holds in two dimensions. In any case, they do not change the relevant symmetry breaking pattern.

Due to the ground-state structure, for  $J \rightarrow \infty$  the field-interchange symmetry  $\phi_1 \leftrightarrow \phi_2$  is broken and thus this symmetry is the analog of the  $\mathbb{Z}_2$  chiral symmetry of the FFX model. The corresponding order parameter is

$$C_x = \phi_{1,x}^2 - \phi_{2,x}^2. \quad (6)$$

For  $D = 0$  model (4) is  $O(4)$  symmetric. Therefore, it does not have any transition at finite temperature. Criticality is observed only for  $J \rightarrow \infty$ . In this limit the correlation length  $\xi$  increases exponentially, i.e.  $\xi \sim e^{cJ}$ ; see, e.g., Ref. [80].

We also consider the Ising-XY (IsXY) model [26]

$$\mathcal{H}_{\text{IsXY}} = - \sum_{\langle xy \rangle} \left[ \frac{J}{2} (1 + \sigma_x \sigma_y) \vec{s}_x \cdot \vec{s}_y + C \sigma_x \sigma_y \right], \quad (7)$$

where  $\sigma_x = \pm 1$  and the two-component spins  $\vec{s}_x$  satisfy  $\vec{s}_x \cdot \vec{s}_x = 1$ . Here  $\vec{s}_x$  and  $\sigma_x$  correspond to spin and chiral variables, respectively. Note that, by performing the limit  $U \rightarrow \infty$  and then  $D \rightarrow \infty$  in the  $\phi^4$  model (4), one recovers the IsXY model for  $C = 0$ . In this case, the variables  $\sigma_x$  and  $\vec{s}_x$  are related with those of the  $\phi^4$  model by

$$\vec{\phi}_{1,x} = \frac{1}{2}(1 + \sigma_x)\vec{s}_x, \quad \vec{\phi}_{2,x} = \frac{1}{2}(1 - \sigma_x)\vec{s}_x. \quad (8)$$

Models with  $C \neq 0$  can also be recovered from a  $\phi^4$  Hamiltonian. It is enough to add an energy-energy nearest-neighbor hopping term  $\sum_{\langle xy \rangle} (\phi_{1,x}^2 \phi_{1,y}^2 + \phi_{2,x}^2 \phi_{2,y}^2)$ .

Apparently, the IsXY model is only invariant under the group  $O(2)\otimes\mathbb{Z}_2$ . However, its relation with the  $\phi^4$  model indicates that the symmetry is larger. Indeed, for any value of  $C$ , the model is invariant under the  $O(2)\oplus O(2)$  nonlinear transformations

$$\begin{aligned} \vec{s}'_x &= \left[ \frac{1}{2}(1 + \sigma_x)R^{(1)} + \frac{1}{2}(1 - \sigma_x)R^{(2)} \right] \vec{s}_x, \\ \sigma'_x &= \sigma_x, \end{aligned} \quad (9)$$

where  $R^{(1)}$  and  $R^{(2)}$  are  $O(2)$  rotation matrices.

It is possible to argue that in the IsXY model chiral and spin modes cannot be critical at the same value of  $J$  and  $C$ , see, e.g., Ref. [68]. Let us assume that, for fixed  $C$ , the model undergoes a continuous phase transition at  $J = J_{\text{ch}}$ , where the chiral correlation length is infinite, i.e. where  $\sigma$  correlations are critical. Let us consider first the dynamics of the spins  $\vec{s}_x$  for a fixed Ising  $\{\sigma_x\}$  configuration. Spins  $\sigma$  with the same sign form geometrical clusters and spins  $\vec{s}_x$  belonging to different geometrical (not Fortuin-Kasteleyn) clusters do not interact (either directly or indirectly) because of the

prefactor  $(1 + \sigma_x \sigma_y)$  in the hopping term of the spin variables. Thus, the behavior of the spins  $\vec{s}_x$  is completely determined by their behavior on each single cluster. It is easy to convince oneself that  $J = J_{\text{ch}}$  is the percolation threshold of the clusters. Indeed, if the clusters percolate at  $J^* < J_{\text{ch}}$ , for  $J = J^*$  Ising spins would already be critical, since in two dimensions percolation of the geometrical clusters implies Ising criticality. Now, at the percolation threshold we expect the clusters to have a fractal dimension that is smaller than 2. This is true for the Ising transition [81, 82]; we assume here that it holds in general. Thus, fields  $\vec{s}_x$  interact as on a system with  $d < 2$  and thus cannot be critical. Therefore, at the chiral transition the spin correlation length must be finite, and, moreover,  $J_{\text{ch}} < J_{\text{sp}}$ . As we shall see, the MC results that we shall present provide support to this argument.

### 3. Definitions and notations

#### 3.1. The fully frustrated XY model

In the square-lattice FFXXY model the ground state is only invariant under translations of two lattice spacings. Therefore, we divide the lattice into four sublattices, so that the four sites of each plaquette belong to different sublattices. Then, we define the spin correlation function  $G_s(x) \equiv \langle \vec{s}_0 \cdot \vec{s}_x \rangle$  only for  $x = (2n, 2m)$ ,  $n, m$  integers, and its Fourier transform as  $\tilde{G}_s(q) = \sum_x e^{iq \cdot x} G_s(x)$  where the sum goes over  $x \equiv (2n, 2m)$ . The corresponding susceptibility  $\chi_s$  and second-moment correlation length  $\xi_s$  are given by

$$\chi_s \equiv \sum_{x=(2n,2m)} G_s(x), \quad (10)$$

$$\xi_s^2 \equiv \frac{1}{4 \sin^2(q_{\text{min}}/2)} \frac{\tilde{G}_s(0) - \tilde{G}_s(q)}{\tilde{G}_s(q)}, \quad (11)$$

where  $q = (q_{\text{min}}, 0)$ , and  $q_{\text{min}} \equiv 2\pi/(L/2)$ . We shall consider two RG invariant ratios related to the continuous spin modes:

$$R_s \equiv \frac{\xi_s}{L}, \quad B_s \equiv \frac{\langle (\mu^2)^2 \rangle}{\langle \mu^2 \rangle^2}, \quad (12)$$

where  $\vec{\mu}$  is the magnetization corresponding to one of the four sublattices, i.e.

$$\vec{\mu} \equiv \frac{4}{V} \sum_{x=(2n,2m)} \vec{s}_x, \quad (13)$$

$V \equiv L^2$  is the volume, and  $\mu^2 \equiv \vec{\mu} \cdot \vec{\mu}$ . We also define the helicity modulus  $\Upsilon$ . For this purpose we introduce a twisted term in the Hamiltonian. More precisely, we consider the nearest-neighbor sites  $(x, y)$  with  $x_1 = L$ ,  $y_1 = 1$ , and  $x_2 = y_2$ , and replace the term  $\vec{s}_x \cdot \vec{s}_y$  in Hamiltonian (3) with

$$\vec{s}_x \cdot R_\varphi \vec{s}_y = s_x^{(1)} (s_y^{(1)} \cos \varphi + s_y^{(2)} \sin \varphi) + s_x^{(2)} (s_y^{(2)} \cos \varphi - s_y^{(1)} \sin \varphi), \quad (14)$$

where  $R_\varphi$  is a rotation of an angle  $\varphi$ . The helicity modulus is defined as the second derivative of the free energy with respect to  $\varphi$  at  $\varphi = 0$ :

$$\Upsilon \equiv - \left. \frac{\partial^2 \ln Z(\varphi)}{\partial \varphi^2} \right|_{\varphi=0}. \quad (15)$$

Chiral modes are related to the  $\mathbb{Z}_2$  symmetry that is broken by the ground state. As discussed in the introduction, a good order parameter is (we have dropped the sign here and thus  $C_n$  is no longer a “spin” susceptibility; this is of course irrelevant)

$$C_n \equiv \sum_{\langle xy \rangle \in \Pi_n} j_{xy} \sin(\theta_x - \theta_y), \quad (16)$$

where  $n$  is the dual lattice site at the center of  $\Pi_n$ . We consider the staggered correlation function

$$G_c(n) \equiv (-1)^{n_1+n_2} \langle C_0 C_n \rangle_c, \quad (17)$$

the chiral susceptibility  $\chi_c$ , and the second-moment correlation length  $\xi_c$ . They are defined as in Eqs. (10) and (11), though in this case sums are extended over the whole dual lattice and  $q_{\min} \equiv 2\pi/L$ . Analogously, we define the RG invariant quantities

$$R_c \equiv \frac{\xi_c}{L}, \quad B_c \equiv \frac{\langle \mu_c^4 \rangle}{\langle \mu_c^2 \rangle^2}, \quad (18)$$

where the staggered magnetization is defined as

$$\mu_c \equiv \frac{1}{V} \sum_{n=(n_1, n_2)} (-1)^{n_1+n_2} C_n. \quad (19)$$

### 3.2. The $\phi^4$ model

In the  $\phi^4$  model we define the hopping energy density and specific heat as

$$E \equiv \frac{1}{V} \langle \mathcal{H}_h \rangle, \quad C \equiv \frac{1}{V} (\langle \mathcal{H}_h^2 \rangle - \langle \mathcal{H}_h \rangle^2), \quad (20)$$

where

$$\mathcal{H}_h = \sum_{\langle xy \rangle} \vec{\phi}_{1,x} \cdot \vec{\phi}_{1,y} + \vec{\phi}_{2,x} \cdot \vec{\phi}_{2,y}. \quad (21)$$

The spin two-point correlation function  $G_s(x)$  is defined as

$$G_s(x) \equiv \langle \vec{\phi}_{1,0} \cdot \vec{\phi}_{1,x} + \vec{\phi}_{2,0} \cdot \vec{\phi}_{2,x} \rangle. \quad (22)$$

The corresponding susceptibility  $\chi_s$  and second-moment correlation length  $\xi_s$  are given by

$$\chi_s \equiv \sum_x G_s(x), \quad \xi_s^2 \equiv \frac{1}{4 \sin^2(q_{\min}/2)} \frac{\tilde{G}_s(0) - \tilde{G}_s(q)}{\tilde{G}_s(q)}, \quad (23)$$

where  $\tilde{G}_s(q)$  is the Fourier transform of  $G_s(x)$ ,  $q = (q_{\min}, 0)$ , and  $q_{\min} \equiv 2\pi/L$ . We shall consider two RG invariant ratios related to the continuous spin modes:

$$R_s \equiv \frac{\xi_s}{L}, \quad B_{s\phi} \equiv \frac{\langle (\sum_i \mu_i^2)^2 \rangle}{\langle \sum_i \mu_i^2 \rangle^2}, \quad (24)$$

where

$$\vec{\mu}_i \equiv \frac{1}{V} \sum_x \vec{\phi}_{i,x}, \quad \mu_i^2 \equiv \vec{\mu}_i \cdot \vec{\mu}_i. \quad (25)$$

As before, we consider the helicity modulus  $\Upsilon_i$  associated with each variable  $\vec{\phi}_{i,x} = (\phi_{i,x}^{(1)}, \phi_{i,x}^{(2)})$ , defined analogously to Eqs. (14) and (15). The total helicity modulus is given by  $\Upsilon \equiv \Upsilon_1 + \Upsilon_2$ .

The ‘‘chiral’’ modes related to the  $\mathbb{Z}_2$  field-interchange symmetry are associated with the quadratic operator defined in Eq. (6). We consider the corresponding connected two-point correlation function

$$G_c(x) \equiv \langle C_0 C_x \rangle_c, \quad (26)$$

the chiral susceptibility  $\chi_c$ , the second-moment correlation length  $\xi_c$  defined as in Eq. (23), and the ratios

$$R_c \equiv \frac{\xi_c}{L}, \quad B_c \equiv \frac{\langle \mu_c^4 \rangle}{\langle \mu_c^2 \rangle^2}, \quad \mu_c \equiv \frac{1}{V} \sum_x C_x. \quad (27)$$

### 3.3. The Ising-XY model

In the case of the IsXY model (7) we consider the correlation functions  $G_s(x) \equiv \langle \vec{s}_0 \cdot \vec{s}_x \rangle$  and  $G_c(x) \equiv \langle \sigma_0 \cdot \sigma_x \rangle$  and the corresponding observables that are defined as in the  $\phi^4$  model. For  $C = 0$  it is easy to verify that  $G_s(x)$  and  $G_c(x)$  exactly correspond to the correlation functions in the  $\phi^4$  model. Indeed, using mapping (8),  $C_x = \sigma_x$ , so that chiral correlations correspond to correlations of the Ising variables. On the other hand, mapping (8) gives

$$G_s(x) = \frac{1}{2} \langle (1 + \sigma_x \sigma_y) \vec{s}_x \cdot \vec{s}_y \rangle. \quad (28)$$

However, since Hamiltonian (7) is invariant under the transformations  $\vec{s}_x \rightarrow \sigma_x \vec{s}_x$ , we have

$$\langle \sigma_x \sigma_y \vec{s}_x \cdot \vec{s}_y \rangle = \langle \vec{s}_x \cdot \vec{s}_y \rangle. \quad (29)$$

Therefore,

$$G_s(x) = \langle \vec{s}_x \cdot \vec{s}_y \rangle. \quad (30)$$

Note that the Binder parameter  $B_{s\phi}$ , defined as in Eq. (24) using the mapping (8), is not the natural one in terms of the spin variables  $\vec{s}_x$ . Indeed, mapping (8) gives

$$B_{s\phi} = \frac{1}{4} \frac{\langle (\mu_s^2)^2 + 2\mu_s^2 \mu_{\sigma s}^2 + (\mu_{\sigma s}^2)^2 \rangle}{\langle \mu_s^2 \rangle^2}, \quad (31)$$

where

$$\vec{\mu}_s = \frac{1}{V} \sum_x \vec{s}_x, \quad \vec{\mu}_{\sigma s} = \frac{1}{V} \sum_x \sigma_x \vec{s}_x. \quad (32)$$

The conventional Binder parameter is instead $\ddagger$

$$B_s = \langle (\mu_s^2)^2 \rangle / \langle \mu_s^2 \rangle^2. \quad (33)$$

In the HT phase we have  $B_{s\phi} = 3/2$  and  $B_s = 2$  in the thermodynamic limit.

$\ddagger$  In terms of the original  $\phi$  variables, we have  $B_s = B_{s\phi} + 2\langle \mu_1^2 \mu_2^2 \rangle / (\sum_i \langle \mu_i^2 \rangle)^2$ . Note that  $B_s > B_{s\phi}$ .

#### 4. Monte Carlo simulations

We performed MC simulations of the FFXY model (1), of the  $\phi^4$  model (4) for  $U = 1$  and  $D$  in the range  $1/20 \leq D \leq 99$ , and of the IsXY model for  $-8 \leq C \leq 0.3$ . We considered  $L \times L$  square lattices with periodic boundary conditions, up to  $L = O(10^3)$ . The phase diagram and critical behavior is investigated by analyzing the FSS behavior of several quantities. The total CPU time used in this study was approximately 10 CPU years of a single 64-bit Opteron 246 (2GHz) processor.

In the MC simulations of the FFXY model, we used a local algorithm based on a mixture of Metropolis and overrelaxed (microcanonical) updates, as suggested in Ref. [60]. In the case of the IsXY and  $\phi^4$  model the updating algorithm was based on mixtures of Metropolis, overrelaxed (microcanonical), and single-cluster [83] updates. More details on the MC algorithms are reported in Appendix A. At the chiral transition, single-cluster updates have little influence on the autocorrelation times, while the overrelaxation updates are only able to speed up the simulation but do not change the dynamic critical exponent. This is always approximately equal to 2, as it is expected in the case of a purely local dynamics. This means that very long simulations are needed to obtain reliable statistics. For instance, in order to obtain approximately 2500 independent configurations for the FFXY model on a lattice with  $L = 1000$ , we used approximately 800 days of a single 64-bit Opteron 246 processor. Analogously, the runs on the largest lattices for the IsXY model ( $C = 0$ ,  $L = 360$ , 4000 independent configurations) and for the  $\phi^4$  model ( $D = 1/2$ ,  $L = 1200$ , 150 independent configurations) took approximately 100 days in both cases. A substantial reduction of the critical slowing down is achieved at the spin transition and in the LT phase, because the overrelaxed and the cluster algorithm are very effective in dealing with the spin modes.

#### 5. The low-temperature phase

In the high-temperature (HT) phase, in which symmetry is not broken, the spin and chiral correlation functions  $G_s(x)$  and  $G_c(x)$  decay exponentially at large distances. In the LT phase ( $J$  large) instead, the spin correlation function  $G_s(x)$  is expected to decay with a power law, giving rise to quasi-long-range order. Indeed, according to the Mermin-Wagner theorem [84], any magnetization breaking a continuous symmetry is forbidden in two dimensions. On the other hand, the discrete  $\mathbb{Z}_2$  symmetry may be broken with a nonvanishing chiral magnetization. In this section we study the main features of the LT phase. We shall see that  $\mathbb{Z}_2$  symmetry is broken and that  $O(2)$  quasi-long-range order is realized in the whole LT phase. The critical behavior of the spin variables is controlled by a line of Gaussian fixed points that are exactly those that control the LT phase of the standard XY model.

Direct evidence for the breaking of the  $\mathbb{Z}_2$  chiral symmetry in the LT phase is provided by the finite-size behavior of the chiral Binder parameter  $B_c$ . In the LT phase

**Table 2.** Results for  $B_c$ ,  $R_s$ ,  $\Upsilon$ ,  $\chi_s$ , and  $\eta_{\text{eff}}$  in the LT phase. In the case of the  $\phi^4$  model we report  $\xi_{\text{la}}/L$ ,  $\Upsilon_{\text{la}}$ , and  $\chi_{\text{la}}$  that converge to  $R_s$ ,  $\Upsilon$ , and  $\chi_s$  as  $L \rightarrow \infty$ . The exponent  $\eta_{\text{eff}}$  corresponds to  $\eta(L, 2L)$  defined in Eq. (34).

	$J$	$L$	$B_c$	$R_s$	$\Upsilon$	$\chi_s$	$\eta_{\text{eff}}$
FFXY	2.4	64	1.00232(2)	0.9886(12)	1.0800(10)	508.9(2)	0.1495(6)
		128	1.000598(3)	0.9992(12)	1.0749(9)	1835.2(5)	0.1480(5)
		256	1.0001503(8)	1.0020(13)	1.0771(8)	6625(2)	
FFXY	2.3	64	1.00712(9)	0.8945(12)	0.9123(13)	445.8(2)	0.1817(8)
		128	1.001882(12)	0.9048(9)	0.9066(14)	1572.0(5)	0.1775(7)
		256	1.000478(3)	0.9104(12)	0.9029(12)	5562(2)	0.1760(7)
		512	1.0001207(6)	0.9133(12)	0.9059(13)	19686(6)	0.1746(7)
		1024	1.0000302(3)	0.9149(14)	0.9052(13)	69766(27)	
FFXY	2.26	128	1.00447(5)	0.8374(10)	0.7985(16)	1399.4(7)	0.2053(9)
		256	1.001165(8)	0.8431(9)	0.7926(16)	4855(2)	0.2038(7)
		512	1.000291(2)	0.8447(10)	0.7904(16)	16862(6)	0.2031(9)
		1024	1.0000739(3)	0.8461(15)	0.7888(14)	58594(30)	
$\phi^4, D = 1/2$	1.50	32	1.0435(5)	1.0236(13)	1.2079(14)	730.2(6)	0.1431(14)
		64	1.01275(14)	1.0420(14)	1.1923(12)	2645.0(1.4)	0.1389(10)
		128	1.00342(3)	1.0473(17)	1.1867(10)	9609(4)	0.1353(8)
		256	1.000873(8)	1.0528(17)	1.1878(10)	34996(12)	0.1339(7)
		512	1.000216(2)	1.0521(16)	1.1850(10)	127579(39)	0.1341(6)
		1024	1.0000548(4)	1.0536(16)	1.1855(10)	465026(150)	
$\phi^4, D = 1/2$	1.48	32	1.0922(13)	0.9194(15)	1.0232(19)	634.1(9)	0.195(3)
		64	1.0382(9)	0.9207(15)	0.9810(19)	2215(3)	0.180(2)
		128	1.0123(3)	0.9275(14)	0.9635(16)	7824(7)	0.1718(15)
		256	1.0034(2)	0.9337(15)	0.9570(13)	27782(17)	0.1682(11)
		512	1.000832(10)	0.9341(15)	0.9539(12)	98897(46)	0.1669(11)
		1024	1.000216(5)	0.9386(26)	0.954(2)	352383(220)	0.1675(16)
		2048	1.0000530(9)	0.9377(28)	0.953(2)	1254983(1100)	

we should have  $B_c \rightarrow 1 + O(1/V)$  when  $L \rightarrow \infty$ . MC simulations (see Table 2) show this behavior in all models that we have considered.

Let us discuss the  $\phi^4$  model in more detail. We distinguish the fields  $\phi_{i,x}$  from the size of the corresponding quantity  $Q_i \equiv \sum_x \phi_{i,x}^2$ . For each configuration, we define the large (small) field  $\phi_{\text{la},x}$  ( $\phi_{\text{sm},x}$ ) to be the field  $\phi_{i,x}$  that has the maximum (minimum) value of  $Q_i$ . Then, we define the corresponding two-point functions  $G_{\text{la}}(x) = \langle \vec{\phi}_{\text{la},0} \cdot \vec{\phi}_{\text{la},x} \rangle$  and  $G_{\text{sm}}(x) = \langle \vec{\phi}_{\text{sm},0} \cdot \vec{\phi}_{\text{sm},x} \rangle$ , the magnetic susceptibilities  $\chi_{\text{la}}$  and  $\chi_{\text{sm}}$ , and the second-moment correlation lengths  $\xi_{\text{la}}$  and  $\xi_{\text{sm}}$ , defined according to Eq. (23). Our numerical results show that, as  $L$  increases, small and large fields effectively decouple. Indeed,  $\chi_{\text{sm}}$  converges to a constant, while  $\chi_{\text{la}}$  diverges as  $L^{2-\eta}$ . Therefore, in the large- $L$  limit, since  $\chi_s = \chi_{\text{la}} + \chi_{\text{sm}}$ , we have  $\chi_{\text{la}}/\chi_s = 1 + O(L^{-2+\eta})$ . Fig. 1 shows estimates of  $\chi_s$ ,  $\chi_{\text{sm}}$ , and  $\chi_{\text{la}}$  for  $U = 1$ ,  $D = 1/2$ , and  $J = 1.48$  in the LT phase [as we shall see, for  $D = 1/2$  there are two very close transitions, an Ising transition at  $J_{\text{ch}} = 1.4668(1)$  and a KT transition at  $J_{\text{sp}} = 1.4704(2)$ ]. It is evident that the large field is critical for any  $J$ , unlike the small one. We also checked the behavior of the correlation lengths: while  $\xi_{\text{la}}$  diverges as  $L$ , the small component  $\xi_{\text{sm}}$  remains finite. As a consequence  $\xi_{\text{la}}/\xi_s = 1 + O(L^{-2+\eta})$ ,

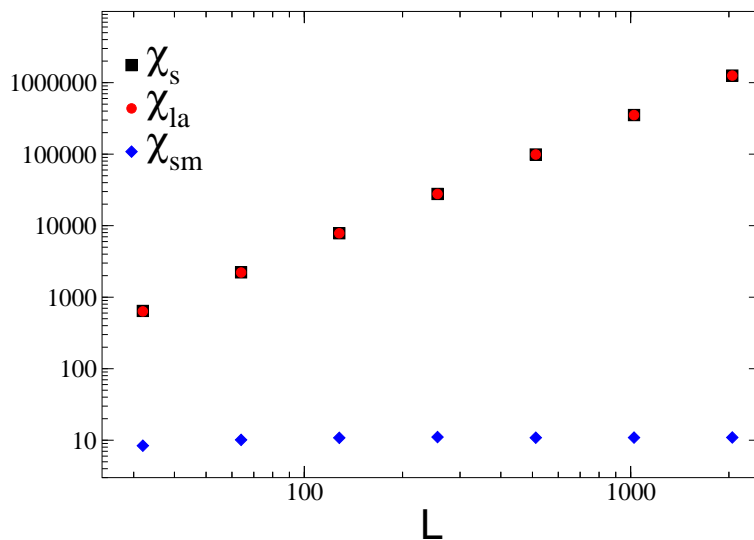


**Figure 1.** Magnetic susceptibilities  $\chi_s$ ,  $\chi_{1a}$ , and  $\chi_{sm}$  for  $U = 1$ ,  $D = 1/2$ , and  $J = 1.48$ . The data for  $\chi_s$  and  $\chi_{1a}$  can hardly be distinguished on the scale of the figure since differences are very small.

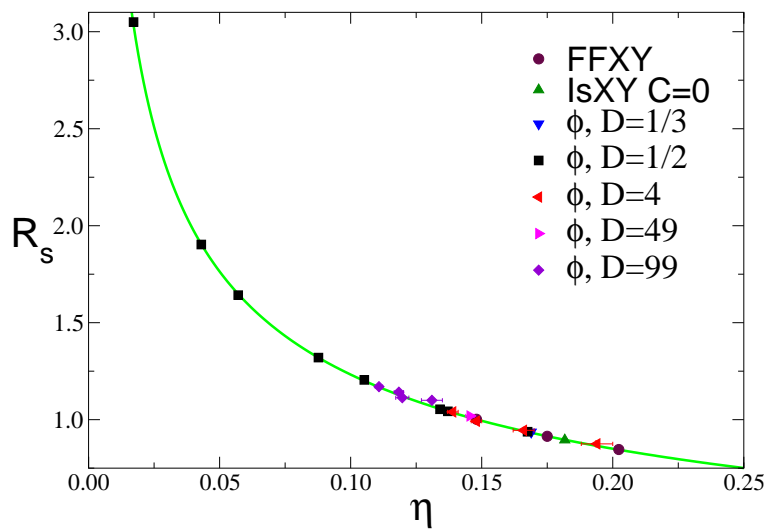


**Figure 2.** Estimates of  $R_s$  vs  $\eta$  in the LT phase. The continuous line represents the prediction obtained by assuming that the LT phase is described by the same Gaussian line of fixed points as the XY model; see Appendix B.

as it was the case for the magnetic susceptibility. Finally, we computed the helicity moduli  $\Upsilon_{1a}$  and  $\Upsilon_{sm}$ . The helicity modulus of the small field vanishes within error bars starting from relatively small lattice sizes (for example, for  $L \geq 64$  for  $J = 1.48$  and  $D = 1/2$ ). Therefore, also for this quantity we have  $\Upsilon \equiv \Upsilon_1 + \Upsilon_2 \approx \Upsilon_{1a}$ . These results show convincingly that the large-distance behavior in the LT phase of the  $\phi^4$  model is effectively determined by only one of the two fields  $\phi_i$ , with a complete decoupling of the other one. This reflects the fact that the  $\mathbb{Z}_2$  chiral symmetry is broken with a spontaneous magnetization  $M_C \neq 0$ .

**Table 3.** Estimates of  $R_s \equiv \xi_s/L$ ,  $\Upsilon$ , and  $\eta$  in the LT phase. The column  $L_{\max}$  reports the size of the largest lattice used. The estimate of  $\eta$  that appears in the fifth column is obtained by using the finite-size behavior of  $\chi_s \sim L^{2-\eta}$ . Those given in the last two columns are obtained by using the estimates of  $R_s$  and  $\Upsilon$  and the relations among these variables that are obtained in the XY model.

	$J$	$L_{\max}$	$R_s$	$\Upsilon$	$\eta$ [ $\chi$ ]	$\eta$ [ $R_s$ ]	$\eta$ [ $\Upsilon$ ]
FFXY	2.4	256	1.0020(13)	1.0771(8)	0.1480(5)	0.1478(4)	0.14776(11)
	2.3	1024	0.9141(12)	0.9052(13)	0.1750(5)	0.1752(4)	0.1758(3)
	2.26	1024	0.847(2)	0.7872(13)	0.2023(11)	0.2015(7)	0.2021(5)
IsXY $C = 0$	1.52	512	0.8951(11)	0.8750(6)	0.1817(7)	0.1821(4)	0.18190(13)
$\phi^4$ , $D = 4/3$	1.49	500	0.936(4)		0.1689(13)	0.1677(13)	
$\phi^4$ , $D = 1/2$	3	300	3.050(10)		0.01717(10)	0.01698(11)	
	2	400	1.903(5)		0.04301(9)	0.0431(2)	
	1.8	400	1.642(4)		0.0571(4)	0.0575(3)	
	1.6	400	1.320(3)		0.0877(4)	0.0877(4)	
	1.5	1024	1.0536(16)	1.1855(10)	0.1341(6)	0.1346(4)	0.13425(12)
	1.48	2048	0.938(3)	0.953(2)	0.1675(16)	0.1672(10)	0.1670(4)
	1.51	200	1.04(10)		0.139(2)	0.138(3)	
$\phi^4$ , $D = 4$	1.505	300	1.002(10)		0.148(2)	0.148(3)	
	1.50	200	0.945(6)		0.166(4)	0.165(2)	
	1.495	400	0.875(15)		0.194(6)	0.190(6)	
	1.578	512	1.020(2)	1.221(3)	0.146(2)	0.1433(5)	0.1420(4)
$\phi^4$ , $D = 49$	1.577	1024	0.867(7)	0.849(14)	0.183(14)	0.193(4)	0.188(3)
	1.602	256	1.170(4)	1.434(5)	0.1108(14)	0.1105(7)	0.1110(4)
	1.601	512	1.142(5)	1.372(4)	0.1184(18)	0.1156(9)	0.1160(5)
	1.6005	512	1.113(3)	1.324(6)	0.120(3)	0.1214(6)	0.1202(5)
	1.6003	512	1.100(5)	1.288(5)	0.131(4)	0.1241(10)	0.1235(5)

We now prove that the long-distance behavior of the spin correlation function is analogous to the one of the standard XY model, i.e. it is controlled by the same line of Gaussian fixed points with varying critical exponent  $\eta$ . For this purpose, we show that, in the large- $L$  limit, the exponent  $\eta$  (computed from  $\chi_s \sim L^{2-\eta}$ ),  $R_s \equiv \xi_s/L$ , and  $\Upsilon$  satisfy the same universal FSS relations as the corresponding quantities in the XY model. These relations, that are reported in Appendix B, are universal once the shape of the lattice and the boundary conditions are fixed: in our case we consider a  $L \times L$  square lattice with periodic boundary conditions.

In order to verify these relations, for each  $L$  we compute  $R_s$ ,  $\Upsilon$ , and an effective estimate of  $\eta$ . Since the susceptibility behaves as  $\chi_s \sim L^{2-\eta}$ , we define

$$\eta(L_1, L_2) \equiv 2 - \ln[\chi(L_1)/\chi(L_2)]/\ln(L_1/L_2). \quad (34)$$

In the  $\phi^4$  and IsXY models we use the results for  $\chi_{1a}$ ,  $\xi_{1a}/L$ , and  $\Upsilon_{1a}$  because they have smaller scaling corrections with respect to the analogous quantities  $\chi$ ,  $\xi_s/L$ , and  $\Upsilon$ . Some results are reported in Table 2. In most of the cases, as  $L$  increases, all quantities approach a constant within error bars, indicating that we have reached the infinite-volume limit within errors. When convergence is not clearly observed within errors, we extrapolate the data assuming the scaling corrections that are expected in the LT phase

of the XY model: we perform an extrapolation of the form  $a + bL^{-\zeta}$ , with  $\zeta = 1/\eta - 4$  for  $\Upsilon$  and  $\zeta = \text{Min}(2 - \eta, 1/\eta - 4)$  for  $\chi_s$  and  $R_s$ , see Appendix B.

Infinite-volume estimates of  $\eta$  are reported in Table 3. Beside the values obtained from the magnetic susceptibility, we also report the estimates obtained from  $R_s$  and  $\Upsilon$  using the XY relations. In all cases the estimates are in good agreement. In Fig. 2 we plot  $\xi_s/L$  versus  $\eta$  as obtained from the susceptibility, for several models in the LT phase. The results agree quite precisely with the curve obtained in the standard XY model, see Appendix B. Thus, we conclude that the LT phase of the FFXY,  $\phi^4$ , and IsXY models is controlled by the same line of Gaussian fixed points that are relevant for the XY model.

In the XY model the LT phase becomes unstable against dissociation of vortices when  $\eta = 1/4$ , and [85]  $\xi_s/L = R_{\text{KT}} = 0.750691\dots$ ,  $\Upsilon = \Upsilon_{\text{KT}} = 0.636508\dots$ . At these values, a KT transition occurs and the system becomes disordered. We expect that a similar mechanism is realized in the models considered here, as long as the chiral  $\mathbb{Z}_2$  symmetry is broken. With decreasing  $J$ ,  $\eta$  increases. If  $\eta = 1/4$  is reached, vortices disorder the system and thus we expect a phase transition. If the transition is continuous and the chiral  $\mathbb{Z}_2$  magnetization does not vanish at the transition, then the phase transition is expected to be of KT type. An Ising or first-order transition should then occur at a smaller value of  $J$ , where also chiral variables disorder. Otherwise, if the  $\mathbb{Z}_2$  magnetization vanishes, the transition should belong to a new universality class. Note that this possibility is excluded in the IsXY model by the argument reported in Sec. 2. If a transition occurs for  $\eta < 1/4$ , it cannot be a KT one. Thus, it must be of first order or a continuous transition belonging to a new universality class. In the latter case, however, we expect a single transition, since a new type of transition can only be due to the interaction of spin and chiral modes that become critical at the same value of  $J$ .

## 6. Phase transitions in the fully frustrated XY model

In this section we investigate the phase diagram of the square-lattice FFXY model. We show that there are two very close but separate transitions, a KT transition at  $J = J_{\text{sp}}$  involving the spin degrees of freedom and an Ising transition at  $J_{\text{ch}} < J_{\text{sp}}$  associated with the breaking of the chiral  $\mathbb{Z}_2$  symmetry.

### 6.1. Finite-size scaling at the chiral transition

We perform a FSS analysis using the method proposed in Ref. [86] and also discussed in Ref. [87]. Instead of computing the various quantities at fixed Hamiltonian parameters, we compute them at a fixed value of a chiral—this guarantees that we are observing the chiral transition—RG invariant quantity; in our specific case we choose  $R_c \equiv \xi_c/L$ . This means that, given a MC sample generated at  $J = J_{\text{run}}$ , we determine, using standard reweighting techniques, the value  $J_{R_c}$  such that  $R_c(J = J_{R_c}) = R_{c,\text{fix}}$ . All interesting

**Table 4.** Results at fixed  $R_c = R_{\text{Is}}$  for the FFXY model. Estimates of the pseudocritical coupling  $J_{R_c}$ , the chiral magnetic susceptibility  $\chi_c$ , the chiral Binder parameter  $B_c$ , the derivatives of  $R_c$  and  $B_c$  with respect to  $J$ , the spin correlation length  $\xi_s$ , the derivative of  $R_s$  with respect to  $J$ , and the helicity modulus  $\Upsilon$ .

$L$	$J_{R_c}$	$\chi_c$	$B_c$	$dR_c/dJ$	$-dB_c/dJ$	$\xi_s$	$dR_s/dJ$	$\Upsilon$
8	2.1642(16)	28.38(3)	1.1913(7)	2.099(10)	0.903(8)	5.430(8)	0.805(5)	0.8628(14)
12	2.1735(11)	56.99(7)	1.1820(6)	3.14(2)	1.323(12)	8.051(12)	1.179(8)	0.7833(15)
16	2.1797(8)	93.09(11)	1.1839(7)	4.34(2)	1.885(2)	10.533(14)	1.653(12)	0.730(2)
24	2.1849(6)	185.7(3)	1.1854(8)	6.98(4)	3.06(3)	15.26(2)	2.53(2)	0.649(2)
32	2.1887(3)	303.4(3)	1.1872(6)	9.79(4)	4.39(3)	19.72(2)	3.45(2)	0.591(2)
48	2.1931(4)	607.1(9)	1.1934(8)	16.08(10)	7.43(8)	28.00(4)	5.43(4)	0.514(2)
64	2.1968(3)	1004(2)	1.1952(10)	23.1(2)	10.77(14)	35.75(7)	7.48(7)	0.457(3)
96	2.2004(2)	2038(4)	1.2009(10)	38.7(3)	18.4(2)	49.75(9)	11.61(8)	0.384(3)
128	2.20242(8)	3385(4)	1.2007(6)	54.8(3)	25.6(2)	61.92(8)	15.67(8)	0.325(2)
192	2.20451(8)	6932(14)	1.2002(9)	88.6(6)	40.2(5)	81.9(2)	22.8(2)	0.235(4)
256	2.20529(4)	11469(20)	1.1962(8)	120.5(9)	53.0(6)	96.0(3)	27.8(3)	0.173(4)
384	2.20610(5)	23414(61)	1.1853(11)	178(2)	72.8(1.3)	112.6(5)	31.8(5)	0.083(5)
512	2.20623(5)	38450(152)	1.1793(13)	232(3)	94(2)	117.8(7)	31.1(6)	0.031(6)
800	2.20630(6)	83390(573)	1.172(2)	346(8)	133(5)	118.0(1.2)	22.7(1.1)	0.003(8)
1000	2.20630(4)	123208(659)	1.171(2)	445(8)	171(5)	118.3(9)	18.0(1.3)	-0.005(6)

observables are then measured at  $J = J_{R_c}$ ; their errors at fixed  $R_c$  are determined by a standard jackknife analysis. The pseudocritical temperature  $J_{R_c}$  converges to  $J_{\text{ch}}$  as  $L \rightarrow \infty$ . This method has the advantage that it does not require a precise knowledge of the critical value  $J_{\text{ch}}$  (an estimate is only needed to fix  $J_{\text{run}}$  that should be close to  $J_{\text{ch}}$ ). Moreover, for some observables the statistical errors at fixed  $R_c$  are smaller than those at fixed  $J$  (close to  $J_{\text{ch}}$ ). This is due to cross correlations and to a reduction of the effective autocorrelation times. The ratio  $E/E_{\text{fix}R_c}$  of the errors at  $J_{R_c}$  computed at fixed  $J$  and at fixed  $R_c$  turns out to be roughly independent of  $L$ :  $E/E_{\text{fix}R_c} \approx 1.6, 4.3, 1.9, 1.0$  respectively for  $\chi_c, B_c, dB_c/dJ$  and  $\Upsilon$ .

The value  $R_{c,\text{fix}}$  can be specified at will as long as it is positive,§ though  $R_{c,\text{fix}} = \bar{R}_c$  ( $\bar{R}_c$  is the critical-point value) improves the convergence for  $L \rightarrow \infty$  [86, 87]. Since in the two-transition scenario the chiral transition is predicted to be in the Ising universality class, we choose  $R_{c,\text{fix}} = R_{\text{Is}}$  where  $R_{\text{Is}} = 0.9050488292(4)$  is the universal value of  $\xi/L$  at the critical point in the 2- $d$  Ising universality class [88]. This choice does not bias our analysis in favor of the Ising nature of the chiral transition. For any chosen value (as long as it is positive) and whatever the universality class of the chiral transition is (it may also coincide with the spin transition),  $J_{R_c}(L)$  converges to  $J_{\text{ch}}$  for  $L \rightarrow \infty$ . Indeed, in the FSS limit  $R_c = f_R[L^{1/\nu}(J - J_{\text{ch}})]$ , where  $\nu$  and  $f_R(x)$  depend on the universality class of the transition. Therefore, fixing  $R_c$  is equivalent to fixing  $X \equiv L^{1/\nu}[J_{R_c}(L) - J_{\text{ch}}]$ . Critical exponents determined by using FSS do not depend on the chosen value  $R_{c,\text{fix}}$ , while other finite-size quantities do. For instance, the Binder cumulant satisfies the

§ The method can be used with any RG invariant quantity. For instance, one could also use the Binder parameter. The fixed value can be taken arbitrarily between the corresponding HT and LT values.

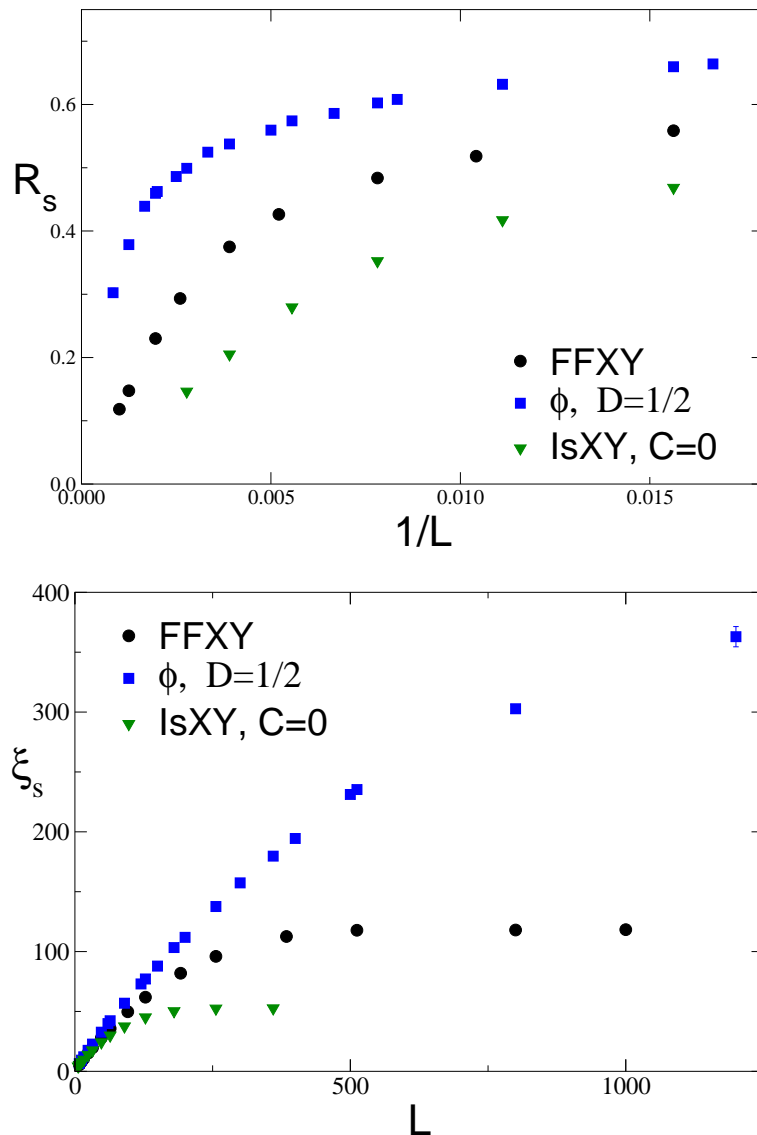


**Figure 3.**  $R_s \equiv \xi_s/L$  (above) and  $\xi_s$  (below) at fixed  $R_c$  versus  $1/L$  and  $L$  respectively, for the FFXY model, the  $\phi^4$  model at  $D = 1/2$ , and the IsXY model at  $C = 0$ .

analogous relation  $B_c = f_B[L^{1/\nu}(J - J_{\text{ch}})]$ , so that  $B_c$  converges to  $f_B(X)$  in the limit  $L \rightarrow \infty$  at fixed  $R_c$ . By fixing  $R_c$  to the critical Ising value, we will be able to perform an additional consistency check. If the chiral transition belongs to the Ising universality class, then  $X = 0$  (apart from scaling corrections) and we should find that any RG-invariant quantity converges to its critical-point value in the Ising model.

If the transition is unique also spin variables should have a finite nontrivial limit: for instance,  $R_s$  at fixed  $R_c$  should converge to a nonvanishing constant. On the other hand, if the chiral transition occurs in a region in which the spin variables are still disordered, the spin correlation length should be finite and thus  $R_s$  at fixed  $R_c$  should converge to zero as  $1/L$ .

We performed simulations on quite large lattices, up to  $L = 1000$ . Results are

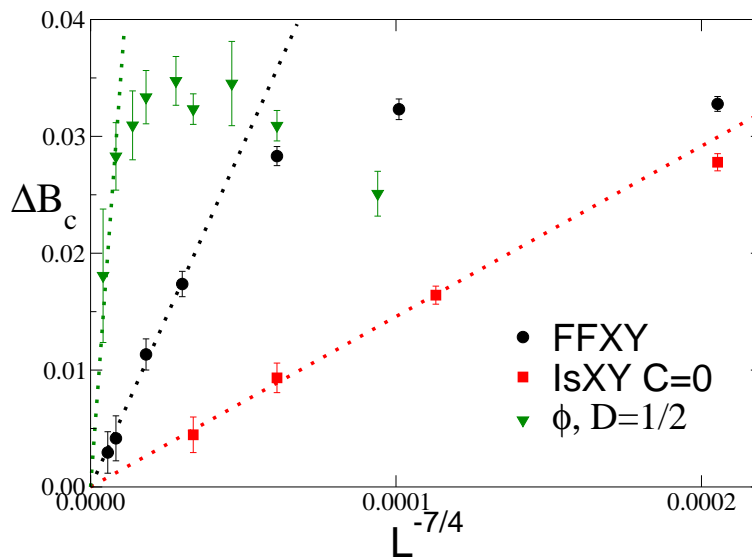


**Figure 4.**  $\Delta B_c \equiv B_c - B_{\text{Is}}$  at fixed  $R_c = R_{\text{Is}}$  vs  $L^{-7/4}$ , for the FFXY model, the  $\phi^4$  model at  $D = 1/2$ , and the IsXY model at  $C = 0$ .  $B_{\text{Is}} = 1.167923(5)$  is the value of the Binder parameter at the critical point in the Ising model [88]. The dotted lines correspond to a linear fit of the data for the largest available lattices.

reported in Table 4. In Fig. 3 we show the spin correlation length  $\xi_s$  as a function of  $L$ . It clearly converges to a constant as  $L \rightarrow \infty$ . We can thus estimate the infinite-volume spin correlation length  $\xi_s^{(c)}$  at the chiral transition:  $\xi_s^{(c)} = 118(1)$ . Moreover, the helicity modulus  $\Upsilon$  at the chiral transition appears to vanish in the large- $L$  limit, see Table 4, consistently with the fact that spin variables are disordered. These results definitely show that spin modes are not critical at the chiral transition, and therefore that, for  $J > J_{\text{ch}}$ , there is a phase in which the chiral  $\mathbb{Z}_2$  symmetry is broken while spins remain paramagnetic.

If spin and chiral modes decouple, the chiral transition should belong to the Ising universality class. The best evidence for that is provided by the finite-size behavior of the chiral Binder cumulant  $B_c$ . In the case of an Ising transition, the asymptotic behavior of  $B_c$  is expected to be [88, 89, 90]

$$B_c = B_{\text{Is}} + O(L^{-\omega}) + O(L^{-2+\eta}), \quad (35)$$

where [88]  $B_{\text{Is}} = 1.167923(5)$ . The first correction is due to the leading irrelevant operator, the second one to the analytic background terms. Since for unitary Ising models [89, 90]  $\omega = 2$  and  $2 - \eta = 7/4$ , the dominant scaling corrections are those related to the analytic background. The estimates of  $B_c$  reported in Table 4 show a peculiar intermediate nonmonotonic crossover: for  $L \lesssim \xi_s^{(c)} \approx 118$ ,  $B_c$  is approximately constant and equal to 1.19-1.20, while the asymptotic regime given by Eq. (35) is observed only when  $L \gg \xi_s^{(c)}$ . In Fig. 4 we plot  $\Delta B_c \equiv B_c - B_{\text{Is}}$  versus  $L^{-7/4}$ . The data clearly approach the Ising value as  $L$  increases. A linear fit to  $a + bL^{-7/4}$  of the data with  $L \geq 384$  gives  $B_c = 1.1678(16)$ . We also mention that a linear fit of  $\Delta B_c$  to  $bL^{-7/4}$  for  $L \geq 384$  gives  $b = 585(32)$  with  $\chi^2/\text{d.o.f.} \approx 0.2$ , where d.o.f. is the number of degrees

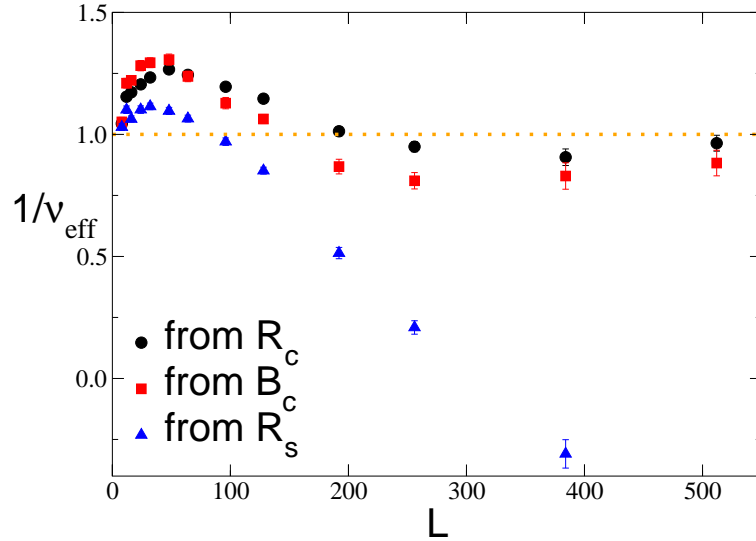


**Figure 5.** Effective exponent  $1/\nu_{\text{eff}}$  as obtained from the derivatives of  $R_c$ ,  $B_c$ , and  $R_s$ , for the FFXY model. The dotted line corresponds to the Ising value  $\nu = 1$ .

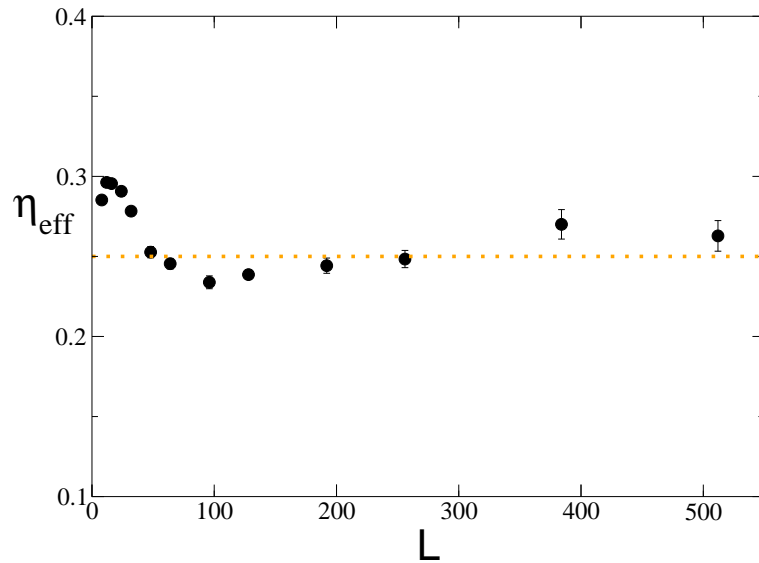


**Figure 6.** Effective exponent  $\eta_{\text{eff}}$  as obtained from  $\chi_c$ , for the FFXY model. The dotted line corresponds to the Ising value  $\eta = 1/4$ .

of freedom of the fit. These results provide a rather strong evidence of the Ising nature of the critical behavior.

In order to determine the critical exponents, we consider the derivatives of  $R_c$  and  $B_c$  with respect to  $J$  at fixed  $R_c$ . In the large- $L$  limit, they behave as

$$\frac{dR_c}{dJ} \sim \frac{dB_c}{dJ} \sim L^{1/\nu}, \quad (36)$$

where  $\nu$  is the chiral exponent associated with the correlation length. Then, given an interval  $L_1 \leq L \leq L_2$ , with  $L_2/L_1 \approx 2$ , we compute an effective chiral exponent  $1/\nu_{\text{eff}}(L_1)$  by fitting the available data for  $dR_c/dJ$  and  $dB_c/dJ$  in the interval. In some

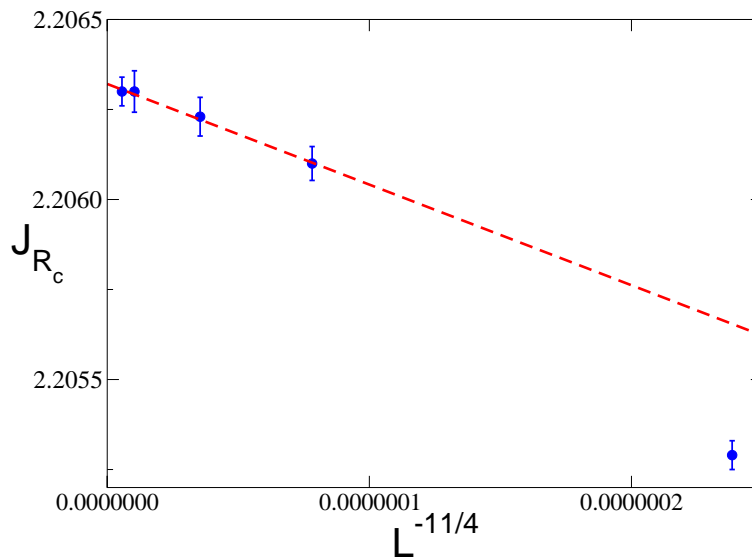


**Figure 7.**  $J_{R_c}$  versus  $L^{-11/4}$  for the FFXY model. The dashed line corresponds to a linear fit of the data for the largest available lattices.

cases, only two results are available and we use

$$1/\nu_{\text{eff}}(L_1) \equiv \frac{\ln dS/dJ|_{L_2} - \ln dS/dJ|_{L_1}}{\ln(L_2/L_1)}, \quad (37)$$

where  $S$  is either  $R_c$  or  $B_c$ . The results are shown in Fig. 5. The exponents  $1/\nu_{\text{eff}}(L)$  obtained from  $R_c$  and  $B_c$  show a similar behavior. They are nonmonotonic and, for  $20 \lesssim L \lesssim 70$ , they are approximately constant and equal to 1.3, which corresponds to  $\nu_{\text{eff}} \approx 0.8$ . This is consistent with the result  $\nu \approx 0.8$  obtained in previous studies that considered lattice sizes in this range [25, 26, 27, 36, 38]. For  $L \gtrsim \xi_s^{(c)} = 118$ , the effective exponent  $1/\nu_{\text{eff}}(L)$  decreases rapidly, undershoots the Ising value  $\nu = 1$ , which is then approached from below. In Fig. 5 we also report  $1/\nu_{\text{eff}}(L)$  computed by using  $R_s$ . For small values of  $L$ , we find  $\nu_{\text{eff}}(L) \approx 0.9$ —this explains why spin modes have sometimes been thought to be critical at the Ising transition—while for  $L \gtrsim \xi_s^{(c)}$  it starts to decrease towards the asymptotic value  $-1$ , corresponding to a finite  $\xi_s^{(c)}$  at the chiral transition. In Fig. 6 we show the effective chiral exponent  $\eta_{\text{eff}}$  defined analogously to  $\nu_{\text{eff}}$  in terms of  $\chi_c$ , which should behave as  $L^{2-\eta}$ . The exponent is first larger than the Ising value, then becomes smaller, and only for  $L \gtrsim 500$  appears to approach the Ising value  $\eta = 1/4$ .

The critical value  $J_{\text{ch}}$  of the hopping coupling at the chiral transition can be determined from the finite-size behavior of  $J_{R_c}$ . Assuming that the transition is of Ising type, the large-volume behavior of  $J_{R_c}$  is given by

$$J_{R_c} = J_{\text{ch}} + O(L^{-1/\nu-\omega}) + O(L^{-1/\nu-2+\eta}), \quad (38)$$

where the first correction is due to the leading irrelevant operators, while the second correction is due to the analytic background [89, 90]. Note that in Eq. (38) we use the fact that the fixed value  $R_{c,\text{fix}}$  is the critical Ising value  $R_{\text{Is}}$ . If  $R_{c,\text{fix}} \neq R_{\text{Is}}$ , the leading

**Table 5.** Results for  $J_{\text{sp}}$  in the FFXY model.

$L_1$	$L_2$	from $R_s$	from $\Upsilon$
128	256	2.236(5)	2.2405(12)
256	512	2.2400(10)	2.2415(5)
512	1024	2.2409(3)	2.2415(5)

corrections are of order  $L^{-1/\nu}$  [86, 87]. According to Eq. (38), since  $\omega = 2$  and  $\eta = 1/4$ , the leading corrections to the infinite-volume limit are of order  $L^{-11/4}$ . In Fig. 7 we plot  $J_{R_c}$  versus  $L^{-11/4}$ . In analogy with what is observed for the other chiral quantities, the asymptotic behavior sets in only for  $L \gg \xi_s^{(c)}$ . A linear fit of the data with  $L \geq 384$  gives  $J_{\text{ch}} = 2.20632(5)$ . This estimate is significantly more precise than earlier results:  $J_{\text{ch}} = 2.2051(24)$  (Ref. [71]),  $J_{\text{ch}} = 2.2002(10)$  (Ref. [63]),  $J_{\text{ch}} = 2.212(5)$  (Ref. [40]), and  $J_{\text{ch}} = 2.203(10)$  (Ref. [38]).

In conclusion, a careful FSS analysis on lattice sizes up to  $L = 1000$  is consistent with an asymptotic critical behavior belonging to the Ising universality class, as expected within the two-transition scenario. However, before observing the asymptotic Ising behavior, we find a peculiar nonmonotonic crossover behavior. This is related to the fact that the spin correlation length  $\xi_s^{(c)}$  is large at the chiral transition. For  $L \lesssim \xi_s^{(c)}$  spin modes appear as being critical, as also indicated by the effective exponent  $\nu_{\text{eff}}$  that is obtained from  $dR_s/dJ$ , which, for  $L \lesssim \xi_s^{(c)}$ , behaves as the exponent obtained from chiral observables, see Fig. 5. We will further discuss these crossover behaviors in Sec. 9.

## 6.2. The spin transition

Since spins are paramagnetic at the chiral transition, the quasi-long-range order that characterizes the LT phase requires a spin transition at a larger value of  $J$ . Since the LT phase is controlled by the same line of fixed points that are relevant for the XY model, and chiral modes do not play any role at the transition, it is natural to conjecture that it belongs to the KT universality class.

In order to determine the critical hopping parameter  $J_{\text{sp}}$  of the spin transition, we exploit the predicted asymptotic behavior of the helicity modulus  $\Upsilon$  and of the ratio  $R \equiv \xi/L$  at the KT transition. On a square lattice  $L \times L$  at the critical temperature we have for  $L \rightarrow \infty$  [85]

$$\Upsilon = 0.63650817819\dots + \frac{0.318899454\dots}{\ln L + C_\Upsilon} + \dots, \quad (39)$$

$$R = 0.7506912\dots + \frac{0.212430\dots}{\ln L + C_R} + \dots, \quad (40)$$

where  $C_R$  and  $C_\Upsilon$  are nonuniversal constants and the neglected corrections are of order  $\ln \ln L / \ln^2 L$ .

The critical point  $J_{\text{sp}}$  is obtained by determining the value of  $J$  where the behavior of  $\Upsilon$  and  $R_s$  is given by Eqs. (39) and (40). In practice, we first obtain an approximate estimate of  $J_{\text{sp}}$  by looking for the value of  $J$  at which  $\Upsilon$  and  $R_s$  are both close to the

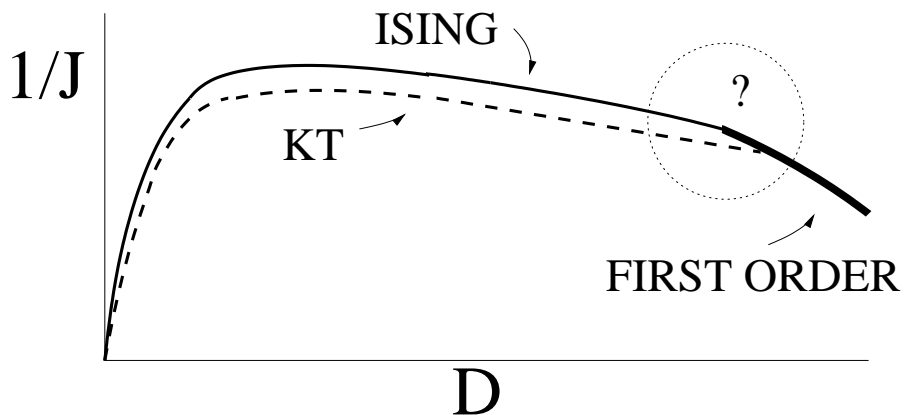


**Figure 8.** Sketch of the phase diagram of the  $\phi^4$  model (4) for  $U = 1$  and  $D > 0$  in the plane  $J^{-1}$ - $D$ . The continuous, dashed, and thick continuous lines represent Ising, KT, and first-order transition lines. The distance between the Ising and KT lines is amplified; otherwise, the two transitions could not be distinguished on the scale of the figure. The phase diagram within the circled region is unknown. In the figure we show one possibility, in which the two continuous transitions connect to the unique first-order line.

theoretical large- $L$  value. Then, we perform simulations at two values of  $J$ ,  $J_1$  and  $J_2$ , that are close to the estimated  $J_{\text{sp}}$ , and determine  $\Upsilon$  and  $R_s$  for  $J_1 < J < J_2$  by linear interpolation. Finally, for each pair of sizes  $L_1$  and  $L_2$ , we require  $\Upsilon$  and  $R_s$  at  $J = J_{\text{sp}}$  to be exactly given by the previous expressions. In this way we obtain two nonlinear equations for two free parameters: the critical value  $J_{\text{sp}}$  and the constant  $C$ . Table 5 shows the results for several pairs of lattices with  $L_2/L_1 = 2$ . In spite of the expected slow convergence, the results obtained from  $R_s$  and  $\Upsilon$  are consistent. This provides a nontrivial check of the KT nature of the transition. The helicity modulus  $\Upsilon$  shows the least  $L$  dependence and provides our final estimate:  $J_{\text{sp}} = 2.2415(5)$ . Previous estimates of  $J_{\text{sp}}$  are:  $J_{\text{sp}} = 2.227(5)$  (Ref. [71]),  $J_{\text{sp}} = 2.2422(5)$  (Ref. [40]), and  $J_{\text{sp}} = 2.273(10)$  (Ref. [38]). We also estimate the infinite-volume chiral second-moment correlation length  $\xi_c^{(s)}$  at the spin transition:  $\xi_c^{(s)} = 8.0(5)$ . The Ising and KT transitions are very close: we have

$$\delta \equiv \frac{J_{\text{sp}} - J_{\text{ch}}}{J_{\text{ch}}} = 0.0159(2). \quad (41)$$

## 7. Phase transitions in the $\phi^4$ model

In this section we study the phase diagram of the  $\phi^4$  model for  $U = 1$ . We only consider the case  $D > 0$ , since only in this case is the ground-state degeneracy the same as in the FFXY model. We show that there is a unique first-order transition for  $D > D^*$ ,  $34 < D^* \lesssim 49$ . On the other hand, for sufficiently small  $D$ , we provide evidence of two very close transitions, a KT transition at  $J = J_{\text{sp}}$  associated with the breaking of the continuous degrees of freedom and an Ising transition at  $J_{\text{ch}} < J_{\text{sp}}$  associated with the breaking of the interchange (chiral)  $\mathbb{Z}_2$  symmetry. In Fig. 8 we show the phase diagram

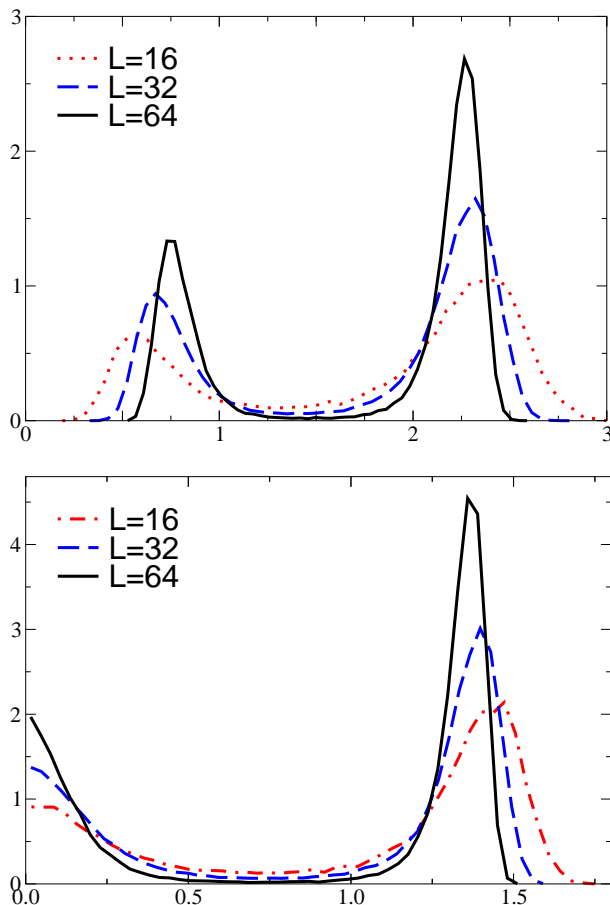


**Figure 9.** Distributions of the hopping-energy density (above) and of the chiral magnetization (below) for  $D = 99$  ( $\phi^4$  model) at the pseudocritical transition point  $J_{pc}(L)$ .

of the  $\phi^4$  model for  $U = 1$  and  $D > 0$ , which emerges from the MC results we shall present in this section. We do not know how the two continuous transition lines connect to the unique first-order one. There are several possibilities. Under the hypothesis that no unique continuous transition occurs, as expected in the IsXY model (see Sec. 2), we may have: (i) the Ising line becomes of first order at  $D = D_{ch} < D^*$ , and then the KT line meets the first-order line at  $D^*$  (this possibility is presented in Fig. 8); (ii) as before, but interchanging Ising and KT lines; (iii) both the Ising and KT lines become of first order at  $D = D_{ch}$  and  $D = D_{sp}$  respectively, with  $D_{ch}, D_{sp} < D^*$ , and then they meet at  $D = D^*$ . Our data suggest that the intermediate region between the one characterized by two continuous transitions and the one with a unique first-order transition should be relatively small, i.e.  $D_{ch}, D_{sp}, D^*$  are close to 49 and larger than 34. However, we cannot exclude that the system undergoes a unique continuous transition at some value of  $D$  or in some interval of  $D$  in this intermediate region. In this case two further possibilities may be realized: the Ising and KT line meet and then, a single transition line starts, which can be either of first order or of second order (turning eventually to first order).

**Table 6.** Results for  $D = 99$  and  $49$ . Here  $J_{\text{pc}}(L)$  is the pseudocritical  $J$  obtained by using the equal-weight method,  $P(E_{\text{min}})$  is the minimum of the normalized energy distribution between the two peaks,  $J_{\text{max}}(L)$  is the value of  $J$  corresponding to the maximum of the specific heat, and  $C_{\text{max}}$  the maximum of the specific heat.

	$L$	$J_{\text{pc}}(L)$	$P(E_{\text{min}})$	$J_{\text{max}}(L)$	$C_{\text{max}}/V$
$D = 99$	16	1.5975(3)	0.120(10)	1.5956(4)	0.663(5)
	24	1.59840(14)	0.069(23)	1.59766(13)	0.600(4)
	32	1.59942(7)	0.053(5)	1.59898(7)	0.569(2)
	48	1.59994(4)	0.032(5)	1.59973(4)	0.539(2)
	64	1.60018(4)	0.018(3)	1.60006(4)	0.522(2)
$D = 49$	48	1.57636(6)	0.152(13)	1.57608(6)	0.283(2)
	64	1.57661(2)	0.181(8)	1.57643(2)	0.2523(13)
	96	1.576771(15)	0.174(14)	1.576692(15)	0.2145(13)
	128	1.576853(11)	0.151(23)	1.576801(11)	0.196(2)

### 7.1. First-order transition for large $D$

For sufficiently large values of  $D$  there is a unique first-order transition from the disordered phase to the LT phase. Evidence for a first-order transition is provided by the presence of two peaks in the distribution  $P(E)$  of the hopping-energy density  $E$  defined in Eq. (20). We determine the position of the transition by using the equal-weight method for the two phases applied to the energy density. In practice, for each lattice size we compute  $E_{\text{min}}$ , the energy corresponding to the minimum between the peaks of the histogram. Then, a given configuration is considered as a LT configuration if  $E > E_{\text{min}}$ , a HT configuration otherwise. Finally, for each lattice size we determine a pseudo-critical value  $J_{\text{pc}}(L)$  by requiring that for  $J = J_{\text{pc}}(L)$  the ratio of the probabilities of LT and HT configurations is some fixed number  $w$ . In our case the value  $w = 2$  seems the most appropriate one, since the LT phase is expected to be twofold degenerate. Note that  $J_{\text{pc}}(L)$  converges to the infinite-volume transition value  $J_c$  for any chosen value  $w$ , with corrections that are generically of order  $1/V$ . The position of the transition point can also be identified by considering the value  $J_{\text{max}}(L)$  where the specific heat  $C$  takes its maximum value. Also  $J_{\text{max}}(L)$  is expected to converge to  $J_c$  with corrections of order  $1/V$ .

To identify the first-order transition region, we have performed simulations for  $D = 34, 49$ , and  $99$ . The distributions of the hopping energy and of the chiral magnetization for  $D = 99$  shown in Fig. 9 clearly indicate that the transition is of first order. They have a deep minimum between the two peaks which decreases exponentially as  $L \rightarrow \infty$ , consistently with a first-order transition. For instance, the minimum of the energy distribution,  $P(E_{\text{min}})$ , is expected to behave as  $e^{-2\sigma L}$ , where  $\sigma$  is the interface tension. Fitting the estimates of  $P(E_{\text{min}})$  reported in Table 6 to  $ce^{-2\sigma L}$ , where  $\sigma$  is the interface tension, we obtain the estimate  $\sigma = 0.017(2)$ , which is rather small. The critical value  $J_c$  can be estimated by fitting the results for  $J_{\text{pc}}$  and  $J_{\text{max}}$  reported in Table 6 to  $J_c + a/V$ . We obtain  $J_c = 1.60042(5)$  from  $J_{\text{pc}}$  and  $J_c = 1.60040(6)$  from  $J_{\text{max}}$ . Finally, from the maximum value of  $C$  one can also estimate the latent heat

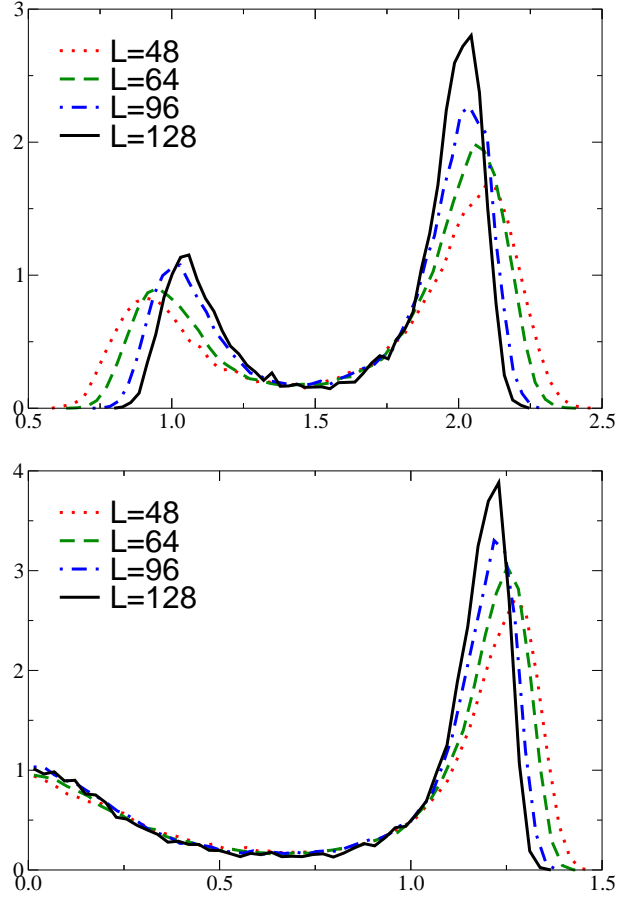


**Figure 10.** Distributions of the hopping energy density (above) and of the chiral magnetization (below) for  $D = 49$  and several lattice sizes at the corresponding  $J_{pc}$ .

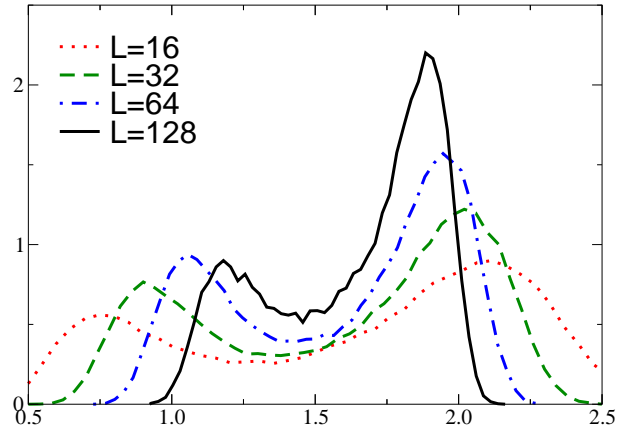


**Figure 11.** Hopping-energy distribution for  $D = 34$  and several lattice sizes at the corresponding  $J_{pc}$ .

$\Delta \equiv E_+ - E_-$ , where  $E_{\pm}$  are the values of the hopping energy  $E_h$  at the peaks of the energy distribution. Using  $\Delta^2 = 4C_{\max}/V + O(1/V)$ , we obtain  $\Delta \approx 1.4$ .

The analysis of the chiral and spin degrees of freedom does not provide evidence of other transitions. On the LT side of the first-order transition, i.e. for  $J \rightarrow J_c \approx 1.6004$

from above, the data for  $D = 99$  reported in Table 3 give  $\eta \approx 0.12$ , which is much below the value  $\eta = 1/4$  where vortex dissociation destabilizes the LT XY phase. In Table 3 we also report a result for  $J = 1.6003$ . This value of  $J$  is on the HT side. On the other hand, the MC run started from a LT configuration and no drastic change of the thermodynamic variables was observed during the run. Thus, the result corresponds to an average taken in the metastable phase. Finally, we mention that also the finite-size behavior of the derivative of the chiral Binder parameter with respect to  $J$  at  $J_{pc}$  is consistent with the behavior expected at a first-order transition [91]. Indeed, we find  $dB_c(L)/dJ \sim L^{1/\nu_{\text{eff}}}$  with  $1/\nu_{\text{eff}} = 2.0(1)$ , in agreement with  $1/\nu_{\text{eff}} = d = 2$ , which is valid in the FSS limit at a first-order transition.

With decreasing  $D$ , the first-order transition becomes weaker and weaker and eventually disappears. The results for  $D = 49$  reported in Table 6 and the distributions shown in Fig. 10 suggest that this occurs for  $D \approx 49$ . Although two peaks are still present,  $P(E_{\min})$  is roughly constant with  $L$  and does not show the exponential decrease expected at a first-order transition. This is the typical behavior of energy distributions close to a tricritical point where the first-order transition line ends; see, e.g., Ref. [92]. An analogous behavior is observed in the distributions of the chiral magnetization shown in Fig. 10. It is interesting to observe that two peaks in the energy and chiral-magnetization distributions are also observed for smaller values of  $D$  on lattice sizes of order  $L \sim 10^2$ . However, in this case the minimum value of the energy distribution increases. This is clearly observed for  $D = 34$ , see Fig. 11. For  $D = 49$  the analysis of the finite-size behavior of the derivative of the chiral Binder parameter gives  $1/\nu = 1.84(16)$ . This estimate suggests a value smaller than 2, the value expected at a first-order transition, and it is consistent with the corresponding value at the tricritical Ising point, which is  $1/\nu = 9/5$  [95]. We do not find evidence of other transitions for  $D = 49$ .

## 7.2. Continuous transitions

*7.2.1. Standard finite-size scaling analysis.* Let us first discuss the results for  $D = 1/2$ . In Fig. 12 we plot  $R_s \equiv \xi_s/L$  and  $R_c \equiv \xi_c/L$  versus  $J$  for  $L \leq 500$  in the critical region. The crossing points correspond to different, though very close values of  $J$ :  $J_{\text{cross}} \approx 1.4688$  for  $R_s$  and  $J_{\text{cross}} \approx 1.4668$  for  $R_c$ . Apparently, chiral and spin variables have different crossing points, as also confirmed by the analysis of the Binder parameters:  $J_{\text{cross}} \approx 1.4680$  for  $B_{s\phi}$ , and  $J_{\text{cross}} \approx 1.4668$  for  $B_c$ . This difference may be due to scaling corrections or to the presence of two different transitions. In order to investigate this issue we perform a scaling analysis. We fit the data for  $\mathcal{R} = R_s, B_{s\phi}, R_c$ , and  $B_c$  with

$$\mathcal{R}(L, J) = f[(J - J_c)L^{1/\nu}], \quad (42)$$

where  $f(x)$  is approximated by a polynomial. Fits of the chiral variables  $R_c$  and  $B_c$  for  $L \geq 200$  give  $\nu = 0.78(2)$  and  $\nu = 0.80(3)$  with a reasonable, though not good,  $\chi^2$ , i.e.  $\chi^2/\text{d.o.f.} \approx 2$ . The analysis of the spin variables is much less stable. We obtain  $\nu = 0.9$ – $1.2$  from  $B_{s\phi}$  and  $\nu \approx 1.5$  for  $R_s$ . These results suggest that spin and chiral variables undergo two different, though close transitions. Indeed, if the transition is unique, all

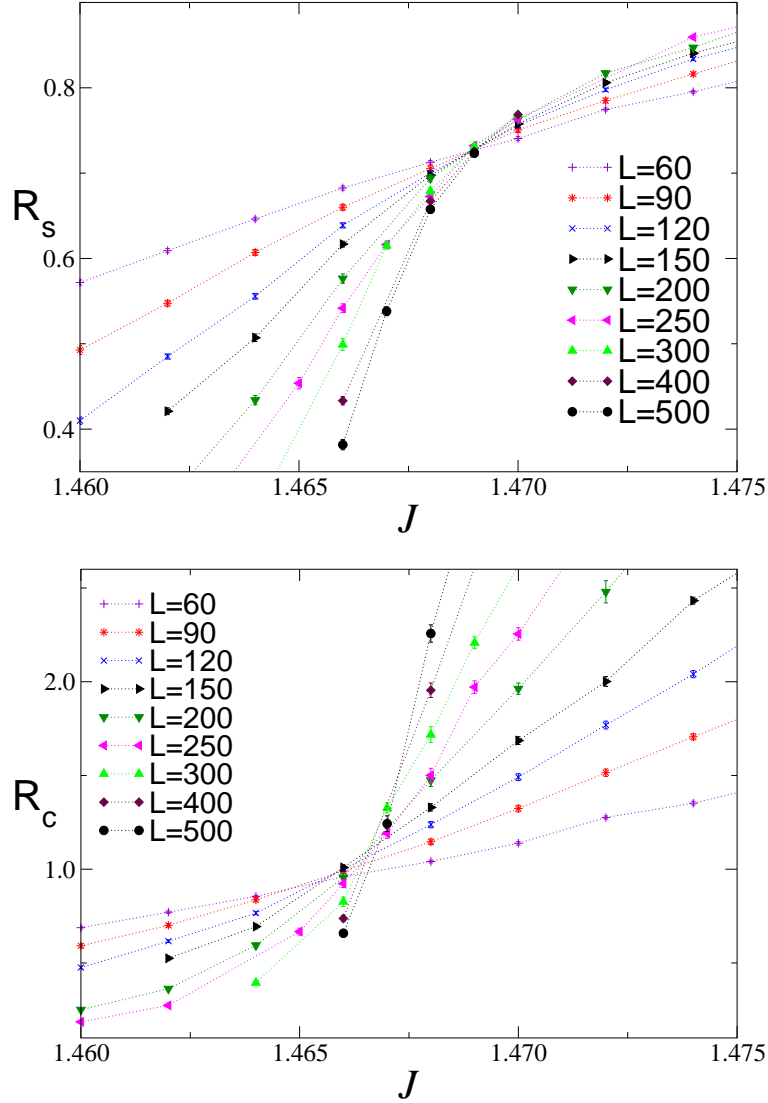


**Figure 12.**  $R_s \equiv \xi_s/L$  (above) and  $R_c \equiv \xi_c/L$  (below) versus  $J$  for  $D = 1/2$ . The dotted lines connecting different sets of data are drawn to guide the eye.

observables have a FSS behavior with the same exponent  $\nu$ . Moreover, the numerical results apparently exclude that the chiral transition is in the Ising universality class. Indeed, the exponent  $\nu$  appears to be different from the Ising one  $\nu_{\text{Is}} = 1$  and, at the crossing point,  $R_c$  and  $B_c$  take the values  $\bar{R}_c = 1.15(3)$  and  $\bar{B}_c = 1.116(5)$ , that differ from the Ising values [88]  $R_{\text{Is}} = 0.9050488292(4)$ ,  $B_{\text{Is}} = 1.167923(5)$ .

Similar results are also obtained for other values of  $D$ . For example, the same FSS analysis of the data at  $D = 1/3$  up to  $L = 600$  gives  $J_{\text{cross}} \approx 1.4768$  (chiral observables),  $\nu = 0.79(1)$  (from  $R_c$ ),  $\nu = 0.80(1)$  (from  $B_c$ ), and  $\bar{R}_c = 1.11(2)$  and  $\bar{B}_c = 1.116(5)$ ;  $R_s$  and  $B_{s\phi}$  have crossing points at  $J \approx 1.4791$  and  $J \approx 1.4785$ , with exponent  $\nu = 0.9-1.2$ . For  $D = 1$ ,  $R_c$  and  $B_c$  have a crossing point at  $J \approx 1.4610$ , with exponents  $\nu = 0.78(2)$  and  $\nu = 0.80(2)$  respectively, and  $\bar{R}_c = 1.17(3)$  and  $\bar{B}_c = 1.132(8)$ ;  $R_s$  and  $B_{s\phi}$  have crossing points at  $J \approx 1.4632$  and  $J \approx 1.4625$ , with exponents  $\nu = 1.2-1.4$ .

**Table 7.** Estimates at fixed  $R_c = R_{\text{Is}}$  of the pseudocritical coupling  $J_{R_c}$ , the chiral magnetic susceptibility  $\chi_c$ , the chiral Binder parameter  $B_c$ , the derivatives of  $R_c$  and  $B_c$  with respect to  $J$ , the ratio  $R_s$  and its derivative with respect to  $J$ , and the total helicity modulus  $\Upsilon$ . They refer to the  $\phi^4$  model with  $D = 1/2$ .

$L$	$J_{R_c}$	$\chi_c$	$B_c$	$dR_c/dJ$	$-dB_c/dJ$	$R_s$	$dR_s/dJ$	$\Upsilon$
8	1.5320(9)	63.76(15)	1.185(2)	4.10(7)	0.185(8)	0.8124(9)	1.93(3)	1.470(2)
12	1.4976(4)	107.7(2)	1.1687(9)	6.45(6)	0.340(8)	0.7798(7)	2.89(2)	1.269(2)
16	1.4824(3)	158.8(2)	1.1659(11)	9.05(9)	0.572(10)	0.7578(7)	3.94(4)	1.119(2)
24	1.4717(2)	283.6(5)	1.1633(8)	14.48(13)	1.12(2)	0.7303(7)	6.04(5)	0.968(2)
32	1.46766(15)	437.5(6)	1.1658(8)	20.7(2)	1.90(3)	0.7107(7)	8.28(8)	0.878(2)
48	1.46539(8)	827.1(1.1)	1.1694(7)	33.8(3)	3.95(7)	0.6810(8)	13.07(11)	0.769(2)
60	1.46499(11)	1188(3)	1.1726(8)	44.8(4)	5.98(10)	0.6641(7)	16.87(15)	
64	1.46498(9)	1320(3)	1.1743(9)	49.1(5)	6.87(12)	0.6597(8)	18.3(2)	0.696(2)
90	1.46490(10)	2323(8)	1.1811(11)	76.2(9)	13.2(3)	0.6319(12)	27.5(3)	
120	1.46523(7)	3790(11)	1.1829(11)	107.4(1.0)	21.6(4)	0.6080(10)	37.1(4)	
128	1.46528(5)	4223(9)	1.1855(9)	117.6(1.0)	24.7(4)	0.6024(9)	40.3(4)	0.555(3)
150	1.46546(7)	5539(19)	1.1906(14)	147(2)	33.4(7)	0.5859(14)	49.7(6)	
180	1.46568(5)	7622(23)	1.1910(15)	185(2)	45.0(1.0)	0.5741(12)	60.2(8)	0.497(3)
200	1.46579(6)	9132(40)	1.193(2)	208(3)	55.5(1.4)	0.559(2)	67.9(1.2)	
256	1.46601(3)	14046(37)	1.1988(13)	289(3)	87.3(1.4)	0.5376(11)	90.5(9)	0.421(3)
300	1.46624(8)	18742(148)	1.202(4)	364(9)	119(5)	0.525(3)	109(3)	
360	1.46625(3)	25534(100)	1.2002(13)	438(5)	159(3)	0.499(2)	129.9(1.2)	0.352(4)
400	1.46636(3)	30907(139)	1.203(2)	514(8)	192(5)	0.486(2)	145(2)	
500	1.46646(3)	45794(283)	1.208(3)	682(13)	279(9)	0.462(3)	183(4)	
512	1.46651(3)	48282(338)	1.201(2)	696(13)	283(5)	0.459(3)	186(3)	0.280(6)
600	1.46664(6)	64317(882)	1.199(3)	834(30)	379(18)	0.439(6)	209(4)	0.252(8)
800	1.46666(2)	104255(603)	1.196(3)	1095(25)	564(15)	0.379(2)	252(3)	0.176(5)
1200	1.46675(4)	214664(3746)	1.186(6)	1630(91)	967(57)	0.302(7)	317(17)	0.097(7)

In conclusion, the analysis presented here apparently favors the presence of two transitions. The first one is associated with the chiral degrees of freedom with an exponent  $\nu \approx 0.8$ . This is similar to what has been observed in the past in similar systems, see Table 1. In the next Section, we shall show that the result  $\nu \approx 0.8$  is a crossover effect: The chiral transition belongs to the Ising universality class.

*7.2.2. Finite-size scaling at fixed  $R_c$ .* In order to check whether the appearance of two very close transitions is just due to uncontrolled systematic errors, or the value  $\nu \approx 0.8$  of the chiral exponent is an effective exponent associated with a preasymptotic regime, we performed additional simulations on larger lattices. We follow here the same strategy used in Sec. 6.1 for the FFXY model, i.e. we perform a FSS analysis at fixed  $R_c = R_{\text{Is}}$ .

In Table 7 we report the data for  $D = 1/2$  up to  $L = 1200$ . The results for  $R_s$  and  $\Upsilon$  at fixed  $R_c$ , which are also plotted in Fig. 3 and 13 respectively, strongly favor the two-transition picture:  $R_s$  and  $\Upsilon$  are clearly decreasing and do not show any evidence of convergence to a nonzero value. Note that the spin correlation length  $\xi_s^{(c)}$  at the chiral transition is rather large. The results for the largest lattices suggest  $\xi_s^{(c)} \gtrsim 360$ , explaining the strong crossover effects. The large correlation length  $\xi_s^{(c)}$  also suggests

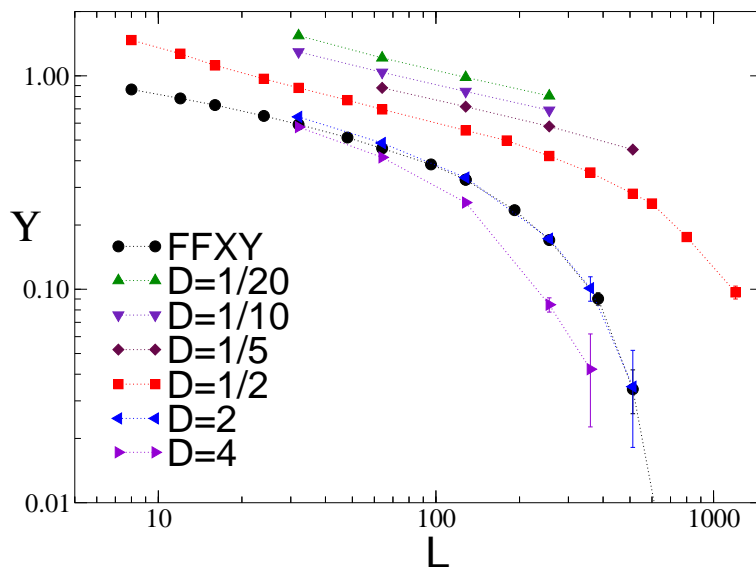


**Figure 13.** Helicity modulus  $\Upsilon$  at fixed  $R_c$  for several values of  $D$  in the  $\phi^4$  model. For comparison, we also show the data for the FFXY model. The dotted lines connecting different sets of data are drawn to guide the eye. Note that the data for  $D = 2$  overlap with those for the FFXY model.

that the spin transition should occur at values of  $J$  that are very close to  $J_{\text{ch}}$ . This will be confirmed in Sec. 7.2.4.

Similar results are obtained for other values of  $D$ ,  $D = 1/20, 1/10, 1/5, 1/3, 1, 2, 4$ , performing the same FSS analysis for lattices with  $L \leq 600$ . In Fig. 13 we show the helicity modulus  $\Upsilon$  for several values of  $D$ . In all cases  $\Upsilon$  appears to decrease, consistently with the fact that it should eventually vanish in the large- $L$  limit.

*7.2.3. Ising critical behavior at the chiral transition.* We now analyze the critical behavior at the chiral transition. In particular, we wish to understand whether the results of the FSS analysis of Sec. 7.2.1, indicating a critical behavior different from the Ising one, are confirmed by a FSS analysis that includes larger lattices. As in Sec. 6.1, we consider the chiral effective exponents  $1/\nu_{\text{eff}}$  obtained from  $R_c$  and  $B_c$ . The results for  $D = 1/2$  are shown in Fig. 14. The curves for  $1/\nu_{\text{eff}}(L)$  show first an extended region, corresponding approximately to  $50 \lesssim L \lesssim 300$ , in which  $\nu_{\text{eff}} \approx 0.8$ . Then, the FSS curves decrease rapidly towards values which are substantially consistent with the Ising exponent  $\nu = 1$ . In Fig. 15 we show the results for the effective chiral exponent  $\eta_{\text{eff}}$  defined by using  $\chi_c \sim L^{2-\eta}$ , in analogy with the definition of  $\nu_{\text{eff}}$ . The exponent approaches the Ising value  $\eta = 1/4$  as  $L$  increases. Analogous crossovers are observed in other quantities, in the Binder cumulant  $B_c$ , see Fig. 4, and in the pseudocritical  $J_{R_c}$ . The Ising regime, in which  $B_c \approx B_{\text{Is}} + cL^{-7/4}$  and  $J_{R_c} = J_{\text{ch}} + aL^{-11/4}$ , cf. Eqs. (35) and (38), is observed only when  $L \gtrsim 600$ . From linear fits of the data for the largest available lattice sizes, we obtain the estimate  $J_{\text{ch}} = 1.4668(1)$ .

In Figs. 16 and 17 we show the chiral Binder cumulant and the effective exponents

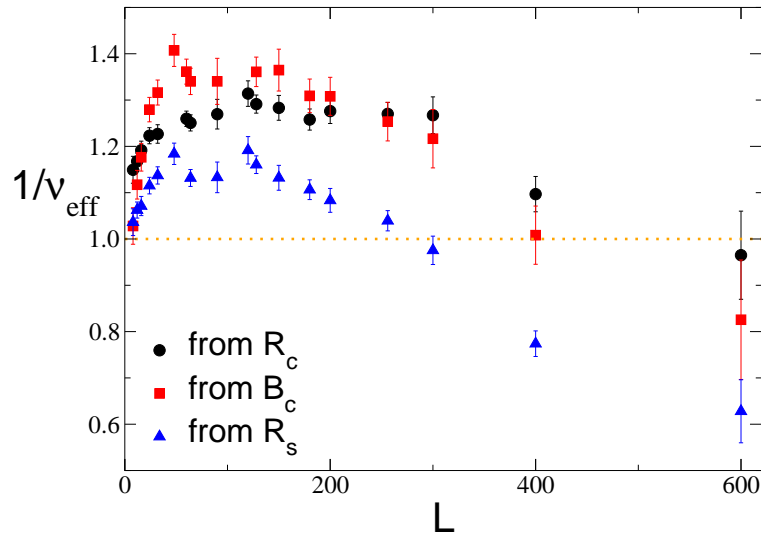


**Figure 14.** Effective exponents  $1/\nu_{\text{eff}}$  as obtained from the derivatives of  $R_c$ ,  $B_c$ , and  $R_s$ , for  $D = 1/2$ . The dotted line corresponds to the Ising value  $\nu = 1$ .

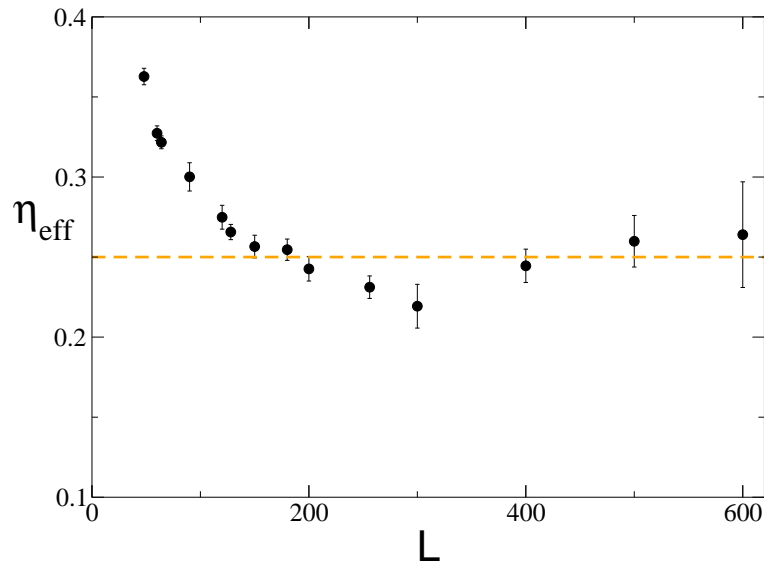


**Figure 15.** Effective exponent  $\eta_{\text{eff}}$  as obtained from  $\chi_c$ , for  $D = 1/2$ . The dotted line corresponds to the Ising value  $\eta = 1/4$ .

$1/\nu_{\text{eff}}$  derived from  $R_c$  and  $B_c$  for other values of  $D$ . For  $0 < D \lesssim 2$  the behavior is similar to that observed for  $D = 1/2$  and in the FFXY model. In particular, also here  $B_c$  and the exponent  $\nu_{\text{eff}}$  are respectively approximately equal to 1.19-1.20 and 0.8 in a quite large range of values of  $L$ . For these values of  $D$  we do not observe the approach to the Ising value. This is not surprising since, as we shall show in Sec. 9,  $\xi_s^{(c)}$  increases as  $D \rightarrow 0$  and thus our data do not satisfy the condition  $L \gg \xi_s^{(c)}$ . For  $D \gtrsim 2$  the approach appears qualitatively different and, in particular, no plateau at  $\nu \approx 0.8$  appears. In Table 8, see also Fig. 18, we give the values of  $J_{\text{ch}}$  for several values of  $D$ .

In conclusion, a careful FSS analysis on lattice sizes up to  $L = 1200$  shows that the

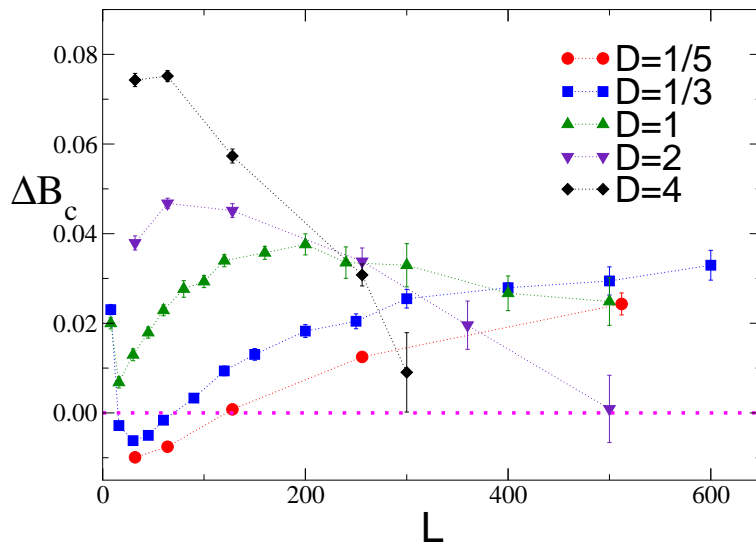


**Figure 16.**  $\Delta B_c \equiv B_c - B_{\text{Is}}$  at fixed  $R_c = R_{\text{Is}}$  for several values of  $D$  in the  $\phi^4$  model.  $B_{\text{Is}} = 1.167923(5)$  is the value of the Binder parameter at the critical point in the Ising model [88].

**Table 8.** Critical values of  $J$  at the chiral and KT transitions, as explained in the text.

	$J_{\text{ch}}$	$J_{\text{sp}}$	$J_{\text{sp,low}}$ from $R_s$	$\delta$
$\phi^4, D = 1/3$	1.4765(1)		1.4792(1) [ $L = 600$ ]	$\gtrsim 0.0018$
$\phi^4, D = 1/2$	1.4668(1)	1.4704(2)	1.46971(2) [ $L = 1024$ ]	0.0025(2)
$\phi^4, D = 1$	1.4609(1)		1.4642(1) [ $L = 400$ ]	$\gtrsim 0.0023$
$\phi^4, D = 2$	1.4696(1)		1.4736(1) [ $L = 400$ ]	$\gtrsim 0.0027$
$\phi^4, D = 4$	1.4884(1)		1.4918(1) [ $L = 300$ ]	$\gtrsim 0.0023$
IsXY, $C = 0$	1.4684(1)	1.493(1)	1.4888(2) [ $L = 512$ ]	0.0167(7)
FFXY	2.20632(5)	2.2415(5)	2.2348(4) [ $L = 1024$ ]	0.0159(2)

behavior close to the chiral transition in the  $\phi^4$  model with  $D = 1/2$  is similar to what has been observed in the FFX model. Also in this case the chiral transition should belong to the Ising universality class, as expected within the two-transition scenario. We expect that, as in the FFX model, Ising behavior can be clearly observed only when  $L \gg \xi_s^{(c)}$ . Since,  $\xi_s^{(c)} \gtrsim 360$  in this case, much larger lattices would be needed to obtain a result as reliable as that of the FFX model. Similar results are obtained for other values of  $D$ . In particular, for  $0 < D \lesssim 2$  we observe a rather extended region in which  $\nu_{\text{eff}} \approx 0.8$ , as it was already observed in the FFX model. We will discuss again this issue in Sec. 9.

*7.2.4. The spin transition.* In order to determine the critical hopping parameter  $J_{\text{sp}}$  of the spin transition for  $D = 1/2$ , we use the same method applied to the FFX model in Sec. 6.2. We assume that the transition belongs to the KT universality class and exploit the predicted asymptotic behavior of  $\Upsilon$  and  $R_s \equiv \xi_s/L$  at the KT transition, cf. Eqs. (39) and (40). Effective estimates are reported in Table 9. They allow us to obtain

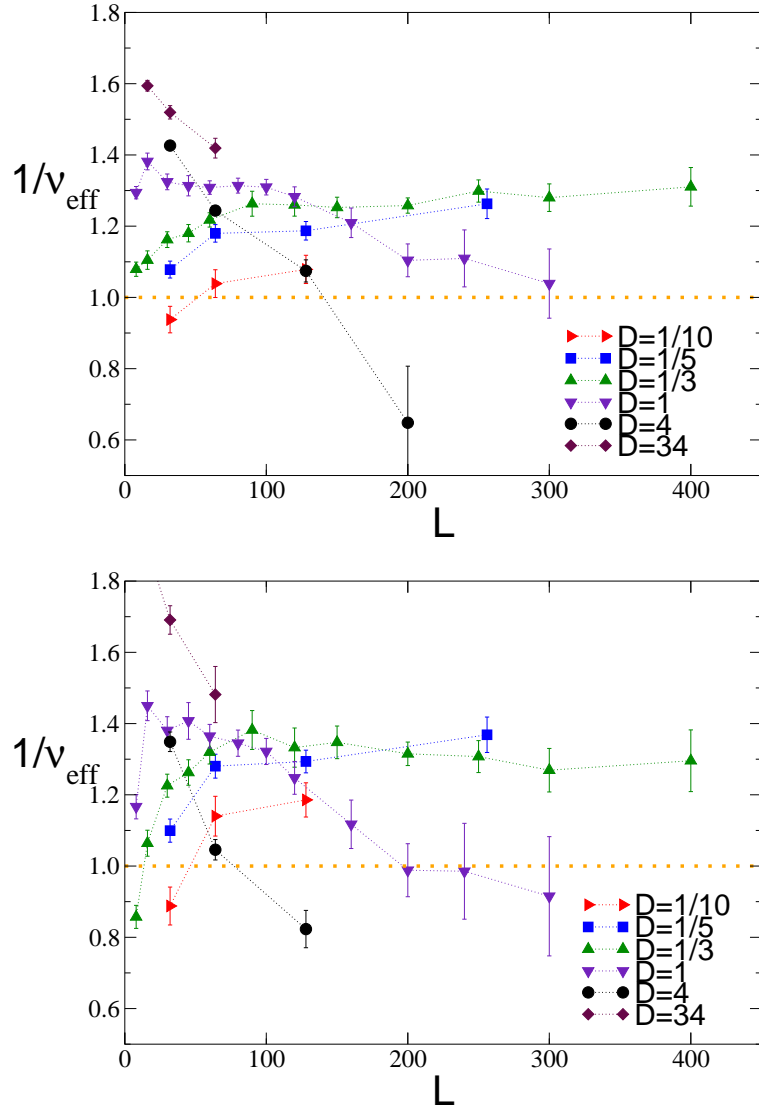


**Figure 17.**  $1/\nu_{\text{eff}}$  for several values of  $D$  in the  $\phi^4$  model, from  $R_c$  (above) and  $B_c$  (below).

the final estimate  $J_{\text{sp}} = 1.4704(2)$ . We also mention that the chiral second-moment correlation length  $\xi_c^{(s)}$  [which can be obtained from the chiral connected correlation function (26)] is  $\xi_c^{(s)} = 22(3)$  at the KT transition. As expected, the Ising and KT transitions are very close, indeed  $\delta \equiv J_{\text{sp}}/J_{\text{ch}} - 1 = 0.0025(2)$ .

For other values of  $D$  we do not have enough data to perform the previous analysis. Nonetheless, we are still able to obtain a lower bound for  $J_{\text{sp}}$ . We assume only that, in the limit  $L \rightarrow \infty$ ,  $R_s = 0.7506912\dots$  and  $\Upsilon = 0.63650817819\dots$  for  $J = J_{\text{sp}}$ , and that  $R$  and  $\Upsilon$  decrease with  $L$ , as suggested by Eqs. (40) and (39) and confirmed by our data. Then, for each  $L$ , we determine, using the results for  $\xi_s/L$  and  $\Upsilon$ , the value  $J$  for which  $R_s$  and  $\Upsilon$  are equal to the theoretical infinite-volume predictions. These results provide lower bounds on the correct critical  $J_{\text{sp}}$ . If we apply this procedure to the data with  $D = 1/2$  and  $L = 1024$  we obtain  $J_{\text{sp,low}} = 1.46971(2)$  from  $\xi_s/L$ , and  $J_{\text{sp,low}} = 1.46957(2)$  from

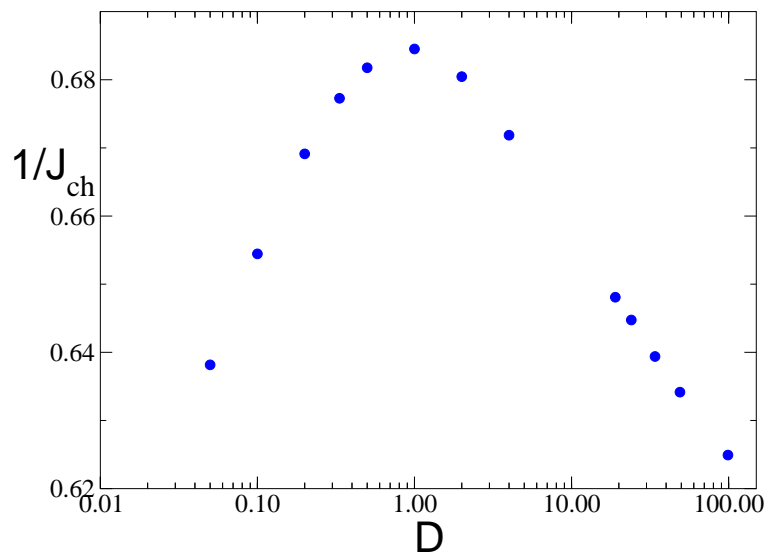


**Figure 18.** Critical values of the hopping parameter at the chiral transition for several values of  $D$ .

**Table 9.** Critical values of  $J$  at the KT transition for the  $\phi^4$  model with  $D = 1/2$ .

$L_1$	$L_2$	from $R_s$	from $\Upsilon$
128	256	1.4696(1)	1.4709(3)
256	512	1.4700(1)	1.4704(1)
512	1024	1.4705(2)	1.4704(1)

$\Upsilon$ , that are not far from the result obtained above,  $J_{\text{sp}} = 1.4704(2)$ . In Table 8 we report lower bounds for other values of  $D$  and estimates of the relative difference  $\delta \equiv J_{\text{sp}}/J_{\text{ch}} - 1$ . In all cases  $\delta$  is of the order of  $10^{-3}$ .

### 7.3. The phase diagram for small values of $D$

Our numerical simulations provide evidence of two transitions for  $D = 1/3, 1/2, 1, 2, 4$ . In addition, relatively short MC simulations at  $D = 1/20, 1/10, 1/5$ , and 34 appear consistent with the two-transition scenario, although the evidence is less robust since our simulations used smaller lattice sizes. A natural conjecture is that the two-transition scenario extends from  $D \lesssim D^*$ ,  $34 < D^* \lesssim 49$ , down to  $D \rightarrow 0$ . For  $D = 0$  Hamiltonian  $\mathcal{H}_\phi$  is  $O(4)$  symmetric. According to the Mermin-Wagner theorem [84], it does not have any transition at finite temperature, and criticality is observed only for  $J \rightarrow \infty$ . Therefore, the Ising and KT transition lines should meet at  $D = 0, 1/J = 0$ , which is a multicritical point.

At a generic multicritical point with two even relevant parameters, such as the reduced temperature  $t \equiv T/T_{\text{mc}} - 1$  and a generic scaling field  $g$  (where  $T = T_{\text{mc}}$  and  $g = 0$  is the position of the multicritical point), the singular part of the free energy is given by [96, 95]

$$\mathcal{F}_{\text{sing}} \sim t^{2-\alpha} B(X), \quad X = gt^{-\phi}, \quad (43)$$

where  $\alpha$  and  $\phi$  are the specific-heat and crossover exponents. This expression is not very useful in our case, since  $T_{\text{mc}} \equiv 1/J_{\text{mc}} = 0$  and  $\xi \sim e^{cJ}$ . However, it is easy to rewrite Eq. (43) in a different form that can be easily generalized. If  $\xi(t, g = 0)$  is the correlation length for  $g = 0$ , and  $\nu$  is the corresponding critical exponent so that  $\xi(t, g = 0) \sim t^{-\nu}$ , we can write

$$\mathcal{F}_{\text{sing}} \sim \xi(t, g = 0)^d A(Y), \quad Y = g\xi(t, g = 0)^\rho, \quad (44)$$

where  $\rho \equiv \phi/\nu$ . In this expression there is no explicit  $t$  dependence and thus we can use it for  $D \rightarrow 0$ .

In the theory described by  $\mathcal{H}_\phi$ ,  $g$  is essentially the parameter  $D$ . The crossover exponent  $\rho$  is related to the RG dimension of the perturbation  $\sum_x \phi_{1,x}^2 \phi_{2,x}^2$  at the O(4) fixed point. In two dimensions,  $\rho$  is equal to the engineering dimension of the operator, so that  $\rho = 2$ , with logarithmic corrections. The perturbative analysis is analogous to that presented in Ref. [93], in which the effect of a spin- $n$  perturbation in the 3-vector model is discussed. The correct scaling variable is  $Y \equiv D\xi^2(\ln \xi)^{-6}$ , or, using the fact that  $\xi \sim J^{-1/2}e^{cJ}$ ,

$$\hat{Y} \equiv D(cJ)^{-7} \exp(2cJ). \quad (45)$$

The power appearing in the logarithm, which is universal, has been determined by using the perturbative results of Ref. [94], which gives the anomalous dimension of any dimension-zero spin- $n$  perturbation of the  $N$ -vector model. In the limit  $U \rightarrow \infty$ , in which the  $\phi^4$  model reduces to the 4-vector model with a spin-4 perturbation, we also have  $c = \pi$ .

A standard scaling assumption in multicritical theories [96, 95] is that, along the critical lines meeting at the multicritical point, the scaling variables  $Y$  and  $\hat{Y}$  are asymptotically constant. This implies that the Ising and KT critical lines, corresponding to  $J = J_{\text{ch}}(D)$  and  $J = J_{\text{sp}}(D)$ , approach the O(4) multicritical point according to

$$D(cJ_{\text{ch,sp}})^{-7} \exp(2cJ_{\text{ch,sp}}) = \hat{Y}_{\text{ch,sp}}, \quad (46)$$

where  $\hat{Y}_{\text{ch}}$  and  $\hat{Y}_{\text{sp}}$  are two different constants, with  $\hat{Y}_{\text{sp}} > \hat{Y}_{\text{ch}}$ . It follows

$$cJ_{\text{ch,sp}} \approx \frac{1}{2} \ln(\hat{Y}_{\text{ch,sp}}/D) + \frac{7}{2} \ln \left[ \frac{1}{2} \ln(\hat{Y}_{\text{ch,sp}}/D) \right], \quad (47)$$

and

$$\delta \equiv \frac{J_{\text{sp}}}{J_{\text{ch}}} - 1 \sim \frac{\ln(\hat{Y}_{\text{sp}}/\hat{Y}_{\text{ch}})}{\ln \hat{Y}_{\text{ch}}/D}. \quad (48)$$

We finally mention that for  $D < 0$  we expect only one KT transition line starting from  $1/J = 0, D = 0$ , where both fields  $\phi_{i,x}$  become critical simultaneously. The same RG arguments used above tell us that  $J_{\text{sp}, D < 0} \sim \ln(1/|D|)$ .

Unfortunately, we are not able to check numerically these predictions. Indeed, this requires to work in a regime in which  $J_{\text{ch}}$  and  $J_{\text{sp}}$  are large and this happens only for very tiny values of  $D$ . But for very small values of  $D$  very large lattices are needed in order to observe the asymptotic behavior. For  $D \lesssim 1$ , the values of  $J_{\text{ch}}$  increase with

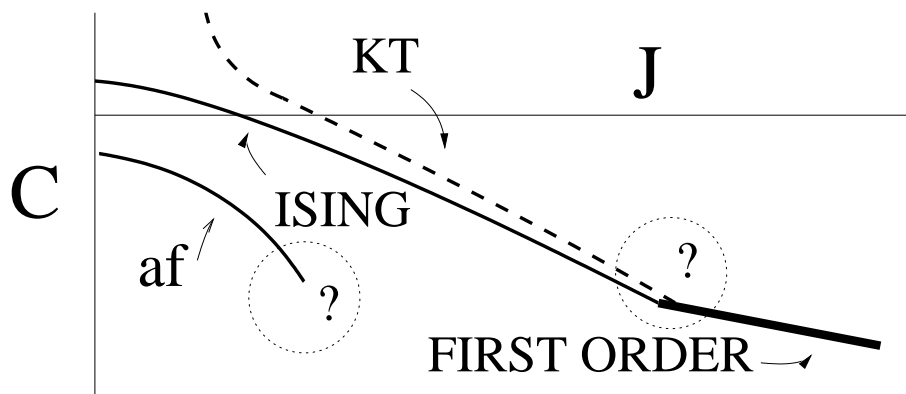


**Figure 19.** Sketch of the phase diagram of the Ising-XY model. The continuous, dashed, and thick continuous lines represent Ising, KT, and first-order transition lines. The distance between the Ising and KT lines is amplified to distinguish them. The phase diagram within the two circled regions is unknown.

decreasing  $D$ , see Fig. 18, but  $D \approx 0.1$  seems still far from the asymptotic regime in which Eq. (47) holds. Note that the presence of the  $O(4)$  point influences the values of  $\nu_{\text{eff}}$  for the lowest values of  $D$ . Indeed, see Fig. 17,  $\nu_{\text{eff}}$  is larger than one for small values of  $L$ . This is due to the influence of the  $O(4)$  multicritical point, for which  $1/\nu = 0$ .

Finally, we would like to point out that an  $O(4)$  zero-temperature multicritical behavior is also expected in the antiferromagnetic XXZ model on a triangular lattice. Its Hamiltonian is

$$\mathcal{H}_{\text{XXZ}} = J \sum_{\langle xy \rangle} s_x^1 s_y^1 + s_x^2 s_y^2 + A s_x^3 s_y^3, \quad (49)$$

where  $\vec{s}_x$  is a three-component vector satisfying  $\vec{s}_x \cdot \vec{s}_x = 1$ . In the easy-axis regime  $A < 1$ , the ground-state structure is analogous to that of the FFXY model [97, 58], and therefore two close Ising and KT transitions are expected. For  $A = 1$  one recovers the isotropic Heisenberg antiferromagnetic model, which is not expected to present any finite-temperature transition, but it should become critical only for  $J \rightarrow \infty$ , see, e.g., Refs. [98, 99]. Due to the effective enlargement of the symmetry from  $O(3) \otimes O(2)$  to  $O(4)$  [100], the asymptotic behavior for  $J \rightarrow \infty$  is expected to be the same as that of the  $O(4)$  vector model.

## 8. Phase transitions in the Ising-XY model

In this section we discuss the critical behavior of the IsXY model (7). Some features of its phase diagram can be easily determined, see Fig. 19. At  $J = 0$  we have an Ising transition at  $C = C_{\text{Is}} = \frac{1}{2} \log(1 + \sqrt{2}) = 0.4406868 \dots$ . An Ising transition line in the  $J$ - $C$  plane starts from this point. For  $C = \infty$  there is a KT transition at [101, 85]  $J \approx 1.1199$ , from which a KT line starts. As we shall see, with decreasing  $C < C_{\text{Is}}$  the KT and Ising transition lines get closer and closer. Another Ising transition occurs at  $J = 0$  and  $C = -C_{\text{Is}}$ , from which an Ising transition line should start and lie in the

**Table 10.** Estimates of several quantities computed at fixed  $R_c = R_{\text{Is}}$  in the IsXY model for  $C = 0$ .

$L$	$J_{R_c}$	$\chi_c$	$B_c$	$dR_c/dJ$	$-dB_c/dJ$	$\xi_s$	$dR_s/dJ$	$\Upsilon$
6	1.4339(7)	23.6(2)	1.1788(6)	4.74(2)	1.956(13)	4.143(4)	1.973(10)	0.7886(11)
8	1.4415(4)	38.83(3)	1.1842(5)	6.51(2)	2.822(16)	5.371(5)	2.638(10)	0.7264(9)
12	1.4498(3)	78.02(5)	1.1904(5)	10.37(4)	4.72(3)	7.680(6)	3.98(2)	0.6394(9)
16	1.4538(2)	127.68(12)	1.1958(7)	14.73(7)	6.94(6)	9.816(14)	5.42(3)	0.5780(13)
24	1.4589(2)	257.9(3)	1.2023(7)	24.49(12)	11.93(10)	13.85(2)	8.49(5)	0.4978(16)
32	1.46165(7)	426.7(4)	1.2043(8)	35.1(2)	17.13(14)	17.58(2)	11.59(7)	0.4427(16)
48	1.46445(4)	868.8(1.0)	1.2061(8)	58.0(3)	28.1(2)	24.25(4)	17.71(8)	0.360(2)
64	1.46586(4)	1441.7(1.6)	1.2062(7)	82.1(4)	39.2(3)	29.98(5)	23.38(12)	0.303(2)
90	1.46707(3)	2627(3)	1.2029(8)	121.1(6)	55.6(5)	37.55(7)	31.3(2)	0.223(2)
128	1.46782(3)	4865(7)	1.1957(7)	175.6(1.0)	76.2(8)	45.11(10)	38.9(3)	0.137(2)
180	1.46823(3)	8855(19)	1.1843(8)	240(2)	97.4(1.2)	50.29(17)	41.1(4)	0.069(2)
256	1.46834(3)	16247(50)	1.1773(13)	328(4)	131(3)	52.5(3)	38.7(7)	0.018(3)
360	1.46838(3)	29466(133)	1.1724(15)	463(8)	177(5)	52.7(4)	31.8(9)	0.005(4)

region  $C < -C_{\text{Is}}$ , bounding an antiferromagnetic phase. We have not investigated the behavior of the IsXY model along this antiferromagnetic transition line, although it is likely (but we have not numerically checked) that the second-order transition line turns into a first-order one as  $J$  increases, as it happens for the ferromagnetic case that we are going to discuss below.

The phase diagram of the IsXY model was already studied in Refs. [26, 29, 42]. They found an Ising and a KT transition for  $C_{\text{Is}} > C \gtrsim 0.1$  and a single first-order transition for  $C \lesssim -4$ . These works also claimed the existence of unique continuous transitions belonging to new universality classes for  $-4 \lesssim C \lesssim 0.1$ . Along this line critical exponents were found to depend on  $C$ . As we shall see, our results do not support the existence of a unique continuous transition in which spin and chiral modes become critical at the same  $J$ . We find two close KT and Ising continuous transitions for  $C \lesssim -5$ , and a single first-order transition beyond, in agreement with the argument reported in Sec. 2, which forbids a continuous transition where chiral and spin modes become critical.

We perform the same FSS analysis as described in Sec. 6.1. We first discuss in some detail the results for  $C = 0$ . In Table 10 we report data for  $C = 0$  up to  $L = 360$ , which turn out to be sufficient to infer the asymptotic critical behavior. As also shown in Fig. 3, the spin correlation length  $\xi_s^{(c)}$  at the chiral transition clearly converges to a finite value: we find  $\xi_s^{(c)} = 52.7(4)$ . Correspondingly, the helicity modulus vanishes in the large- $L$  limit. Again, the best evidence of an asymptotic Ising critical behavior is obtained from the analysis of the chiral Binder cumulant  $B_c$ . Fig. 4 shows the difference  $\Delta B_c \equiv B_c - B_{\text{Is}}$  that clearly converges to the Ising value as  $L$  increases. A linear fit to  $a + bL^{-7/4}$  of the data for the three largest lattices gives  $B_c = 1.1679(18)$ , to be compared with [88]  $B_{\text{Is}} = 1.167923(5)$ . A linear fit to  $bL^{-7/4}$  of  $\Delta B_c$  for the three largest lattices gives  $b = 146(6)$  with  $\chi^2/\text{d.o.f} \approx 0.1$ . The critical coupling  $J_{R_c}$  shows the expected rate of convergence. A linear fit to  $a + bL^{-11/4}$  of the results for the largest lattices gives

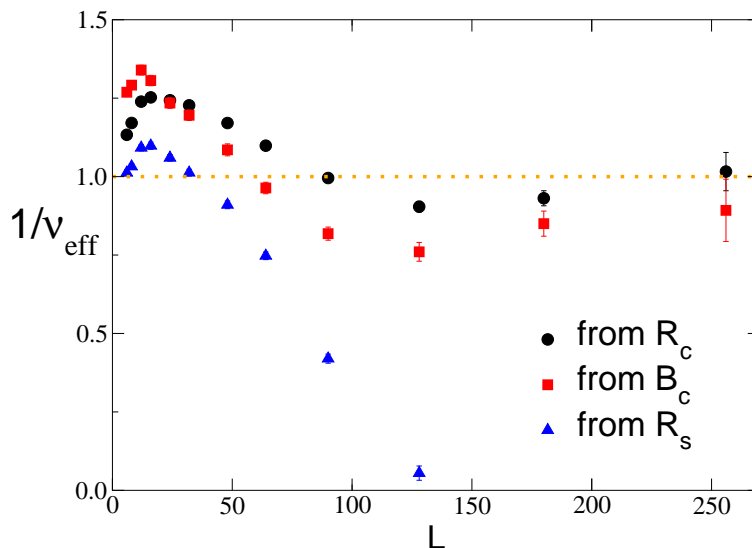


**Figure 20.** Effective exponents  $1/\nu_{\text{eff}}$  as obtained from the derivatives of  $R_c$ ,  $B_c$ , and  $R_s$ , for the IsXY model at  $C = 0$ . The dotted line corresponds to the Ising value  $\nu = 1$ .

$J_{\text{ch}} = 1.4684(1)$ . The effective exponents  $\nu_{\text{eff}}$  obtained from the derivative of  $R_c$ ,  $B_c$ ,  $R_s$ , see Fig. 20, and the exponent  $\eta_{\text{eff}}$  obtained from  $\chi_c$  behave as observed in the FFXY model and in the  $\phi^4$  model in the region  $0 < D \lesssim 2$ , see also Sec. 9. The values of  $1/\nu_{\text{eff}}$  obtained from  $R_c$  and  $B_c$  are first larger than the Ising value, then become significantly smaller, and eventually converge to 1 from below.

Estimates of the critical value of  $J$  at the KT transition have been obtained following the procedure described in Sec. 6.2, using the estimate of  $R_s$  and  $\Upsilon$  with  $L \leq 512$ . We obtain  $J_{\text{sp}} = 1.493(1)$ , see also Table 8. The chiral correlation length  $\xi_c^{(s)}$  at the KT transition is  $\xi_c^{(s)} = 4.3(5)$ . Again, the relative difference  $\delta \equiv J_{\text{sp}}/J_{\text{ch}} - 1$  of the critical couplings is very small, i.e.  $\delta = 0.0167(7)$ .

The results for the other values of  $C$  are similar. For example, in Figs. 21, 22, and 23 we show the helicity modulus  $\Upsilon$ , the chiral Binder parameter  $B_c$ , and the effective exponent  $1/\nu_{\text{eff}}$  for several values of  $C$ . Precise estimates of the spin correlation length at the chiral transition are obtained for  $C = 0.1, 0.2, 0.3$ :  $\xi_s^{(c)} = 26.6(2), 10.8(1), 3.70(2)$ , respectively. As expected  $\xi_s^{(c)}$  rapidly decreases with increasing  $C$ , indicating that the difference between the Ising and KT critical temperature becomes larger and larger up to  $C = C_{\text{Is}}$ . We also performed simulations for negative values of  $C$ ,  $C = -0.2, -0.5$  for lattice sizes up to  $L = 256$ ,  $C = -1, -2$  to  $L = 128$ , and  $C = -3$  to  $L = 192$ . The estimates of  $R_s$  and  $\Upsilon$  appear to decrease as in the  $C = 0$  case, suggesting that the spin modes are not critical at the chiral transition, thus favoring the two-transition picture. With decreasing  $C$ ,  $\xi_s^{(c)}$  apparently increases, but we have not been able to directly observe that  $\xi_s^{(c)}$  is finite on the lattice sizes that we considered. However, our results are not consistent with a unique transition. As we shall see in the next section, the results for  $C \geq -1$  can be explained in terms of an approximately universal crossover within the standard two-transition picture. For  $C = -2$  and  $C = -3$  the estimates of

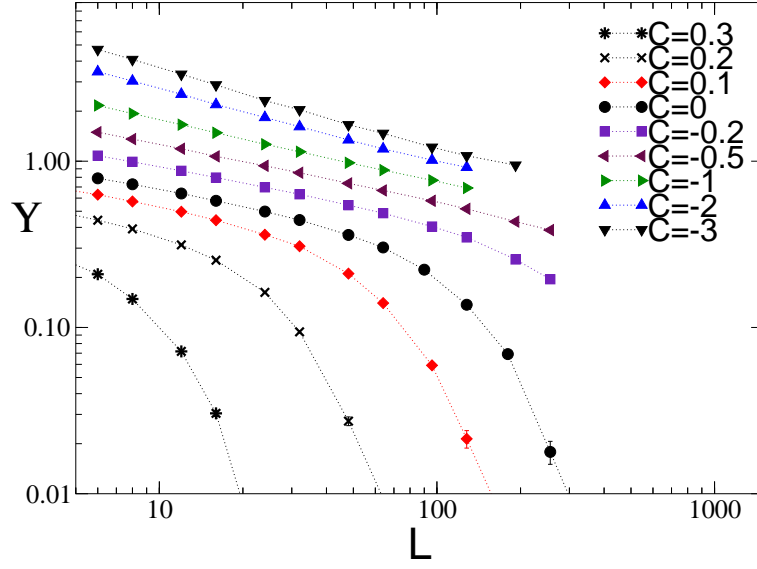


**Figure 21.** Helicity modulus at fixed  $R_c$  for several values of  $C$  in the IsXY model.

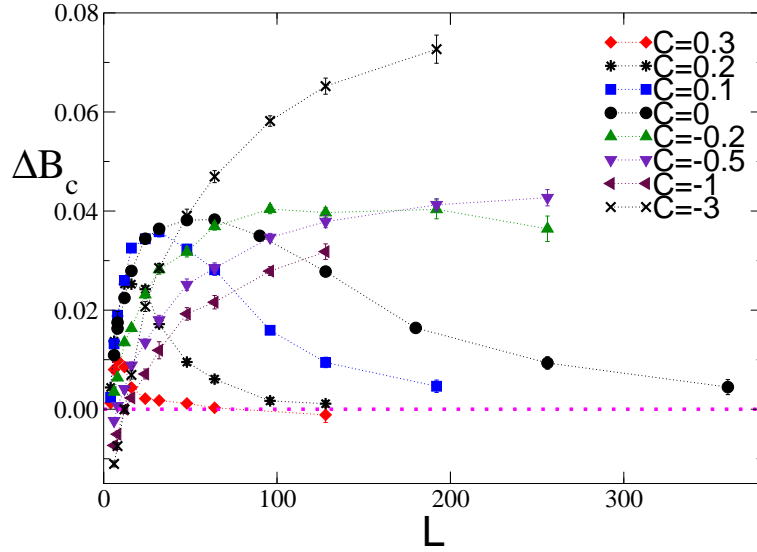


**Figure 22.**  $\Delta B_c \equiv B_c - B_{\text{Is}}$  at fixed  $R_c = R_{\text{Is}}$  for the IsXY at several values of  $C$ .  $B_{\text{Is}} = 1.167923(5)$  is the value of the Binder parameter at the critical point in the Ising model [88].

RG quantities (see, e.g., Fig. 23 for  $\nu_{\text{eff}}$ ) are apparently stable with  $L$ . For instance, the analysis of the derivatives of  $R_c$ ,  $B_c$ ,  $R_s$  with respect to  $J$  for  $C = -2$  up to  $L = 128$  gives  $1/\nu \approx 1.31, 1.40, 1.10$ . Each estimate appears quite stable with respect to  $L$  and thus it could be taken as evidence that the asymptotic limit has been reached and that the critical chiral behavior is not Ising but belongs to a new universality class. This interpretation is however not possible, since, if the transition is unique, the estimate of  $\nu$  should be independent of the observable. Analogously, for  $C = -3$  up to  $L = 192$  we obtain  $1/\nu \approx 1.42, 1.57, 1.23$  from  $R_c$ ,  $B_c$ ,  $R_s$ , which are again not consistent with the existence of a new universality class. Taking also into account the argument reported

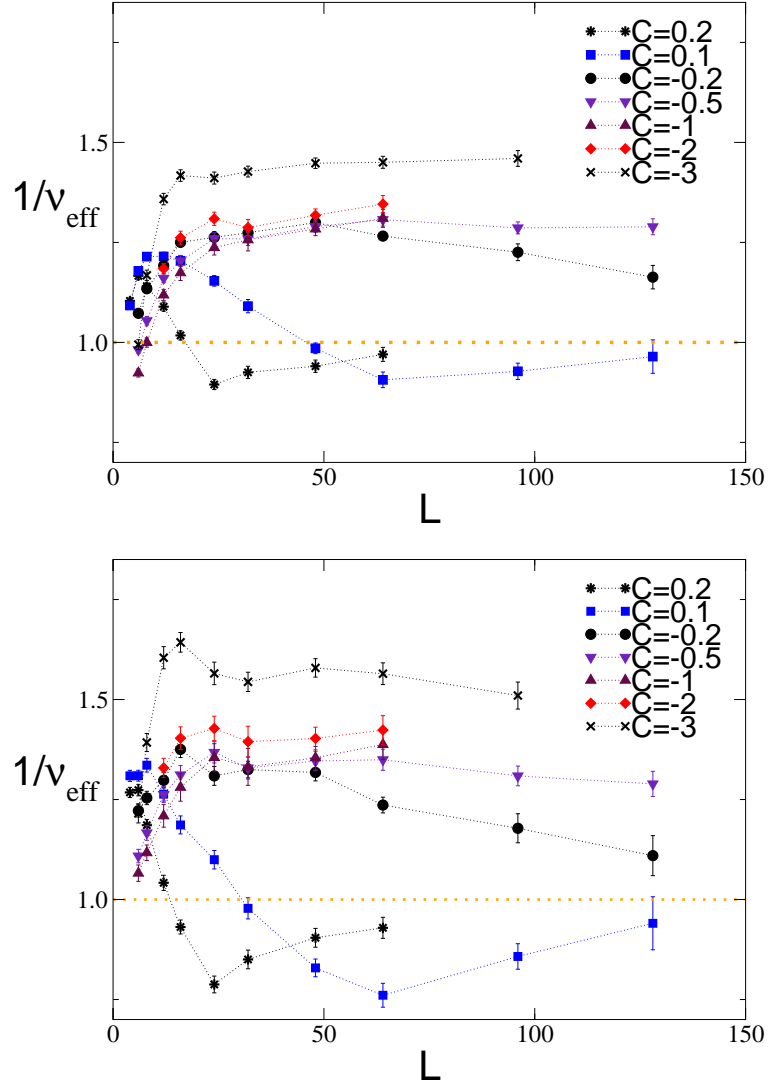


**Figure 23.** Effective exponent  $1/\nu_{\text{eff}}$  for several values of  $C$  in the IsXY model, from  $R_c$  (above) and  $B_c$  (below).

in Sec. 2, which forbids continuous transitions where chiral and spin modes become critical, we conclude that these results are better explained in terms of crossover effects.

The FSS behavior of the helicity modulus  $\Upsilon$  at the chiral transition and for lattice sizes  $L \ll \xi_s^{(c)}$  can be related to the fractal dimension of the geometrical Ising clusters. As already discussed in Sec. 2, at the chiral transition spins  $\vec{s}$  effectively live on geometrical Ising clusters. If  $L \ll \xi_s^{(c)}$ , XY spins are strongly correlated and thus we can use the spin-wave approximation, which leads to the prediction

$$\Upsilon \propto L^{-\epsilon} \quad (50)$$

where  $\epsilon = 2 - d_{\text{gc}} > 0$  and  $d_{\text{gc}}$  is the effective fractal dimension of the geometrical clusters in this range of lattice sizes. In the case chiral and spin modes are effectively decoupled, and therefore the properties of the geometrical clusters are not affected by the spin modes, one expects  $d_{\text{gc}}$  to be equal to the fractal dimension of the geometrical Ising

clusters which is predicted to be  $d_{\text{Igc}} = 187/96 = 1.9479\dots$  [81, 82], corresponding to  $\epsilon = 5/96 = 0.0521\dots$ . For  $L \lesssim \xi_s^{(c)}$  the data shown in Fig. 21 show a power-law behavior as in Eq. (50), but with a rather different exponent. For example, we find  $\epsilon \approx 0.35$  for  $0.2 \gtrsim C \gtrsim -1$ . This is due to the interaction between chiral and spin modes, which changes the effective fractal dimension of the geometrical clusters when  $L \lesssim \xi_s^{(c)}$ . Note that the power-law decay of the helicity modulus is another piece of evidence in favor of the argument presented in Sec. 2, which excludes a unique second-order transitions for any  $C$ , and therefore also for  $C = -2, -3$ .

For larger values of  $-C$ , first-order transitions separate the LT from the disordered phase. Our simulations indicate the presence of a unique first-order transition for  $C \lesssim -5$ . In particular, we obtain the estimates  $\sigma \approx 0.012, 0.006$  for the interface tension at  $C = -8, -7$ , respectively. Moreover, for  $C \leq -7$ , the absence of a continuous KT transition is rather clear from the analyses of the spin variables. On the LT side of the transition, which is at  $J_c = 15.4255(5)$  for  $C = -7$ , we definitely find  $\eta < 1/4$ :  $\eta \approx 0.035$  at  $J = 15.426$ , and  $\eta \approx 0.043$  at  $J = 15.425$  in the metastable LT phase. The presence of first-order transitions for  $C \lesssim -5$  may also explain the results for the effective exponent  $1/\nu_{\text{eff}}$  at  $C = -2, -3$ . The apparent increase of  $1/\nu_{\text{eff}}$  as  $|C|$  increases on small lattices can be interpreted as due to the presence of a nearby first-order transition.

In conclusion, the phase diagram of the IsXY model is characterized by an Ising and a KT transition for  $C_{\text{Is}} > C \gtrsim -5$ , and by a unique first-order transition for  $C < C^*$  with  $-5 \gtrsim C^* \gtrsim -7$ . A sketch of the phase diagram is shown in Fig. 19. Again we do not know how the two continuous transition lines connect to the first-order transition line. The discussion at the beginning of Sec. 7 applies also in this case, with the only difference that a unique continuous transition is excluded by the argument reported in Sec. 2. A possible scenario, consistent with our numerical results, is shown in Fig. 19. The crossover curves of the effective exponents are quite similar to those of the  $\phi^4$  model, at least for  $C$  not too negative, as we will further discuss in Sec. 9.

## 9. Crossover behavior

In the preceding sections we established that the FFXY model and the  $\phi^4$  and IsXY models in a large parameter region undergo two transitions that belong to the Ising and KT universality classes respectively. However, the eventual Ising critical regime at the chiral transition is reached after a crossover regime which is surprisingly similar in all models considered. For example, in most cases we find a rather extended preasymptotic region in which the effective correlation-length exponent  $\nu_{\text{eff}}$  is approximately equal to 0.8. Similar values have also been observed in other models related to the FFXY model, see Table 1. This suggests that this crossover is somewhat universal.

First, we consider the behavior at the chiral transition and show that any RG quantity scales approximately as

$$\mathcal{R} = f_{\mathcal{R}}(L/l), \tag{51}$$

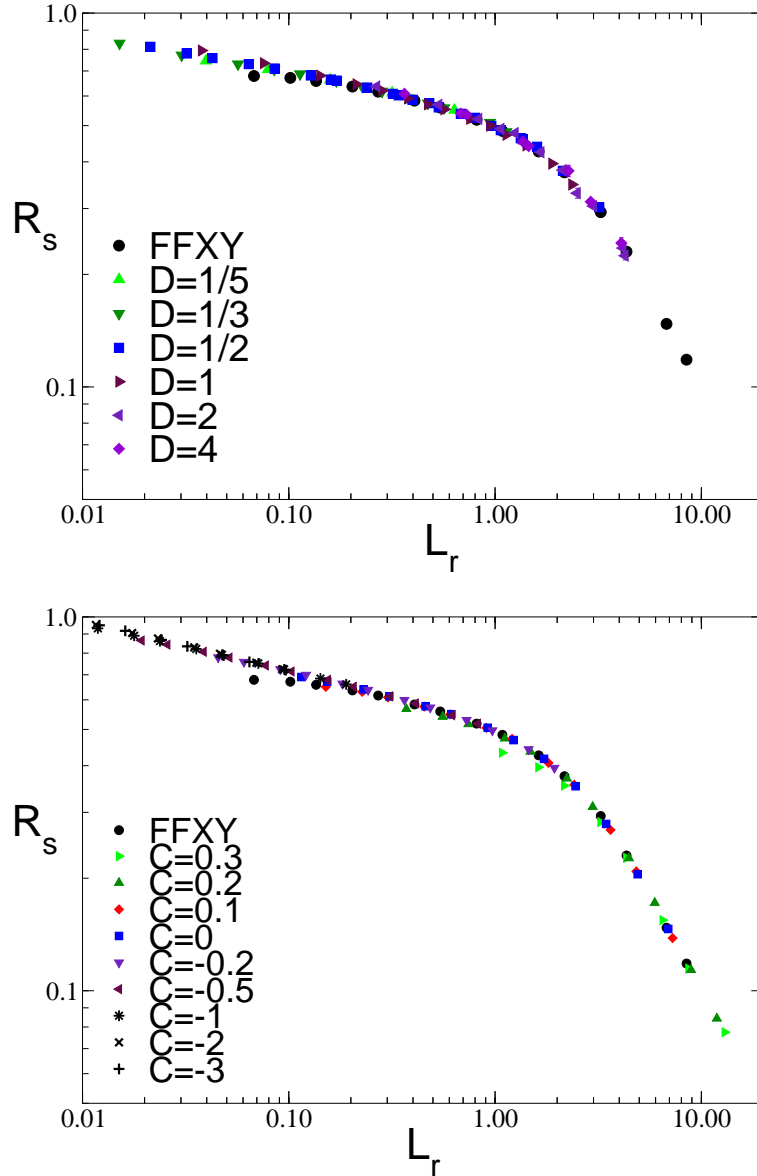


**Figure 24.** Correlation-length ratio  $R_s$  at fixed  $R_c$  vs  $L_r = L/l$  for the FFXY model and  $\phi^4$  (above) and IsXY (below) models. Note the logarithmic scale on both axes. We set  $l_{\text{FFXY}} = 118 \approx \xi_s^{(c)}$ .

where  $l$  is a model-dependent, but observable-independent length scale. To verify Eq. (51), we consider  $R_s$ , determining the factors  $l$  so as to obtain the best collapse of the data. The results are reported in Fig. 24. The data fall on a single curve with remarkable precision. The optimal data collapse is obtained for  $l/l_{\text{FFXY}} \approx 7.0, 4.5, 3.2, 1.8, 1.0, 0.75$  respectively for  $D = 1/5, 1/3, 1/2, 1, 2, 4$ , and  $l/l_{\text{FFXY}} = 0.031, 0.089, 0.22, 0.45, 1.11, 2.6, 5.7, 12, 17$  for

|| Note that our results have been obtained at fixed  $R_c$  and not at the chiral critical point. However, since we are dealing with an Ising transition and  $R_c$  has been fixed to the critical-point Ising value, this is irrelevant in the scaling limit. Had we fixed  $R_c$  to a different value, we would have still observed a universal crossover behavior, though the scaling curves would have been quantitatively different.

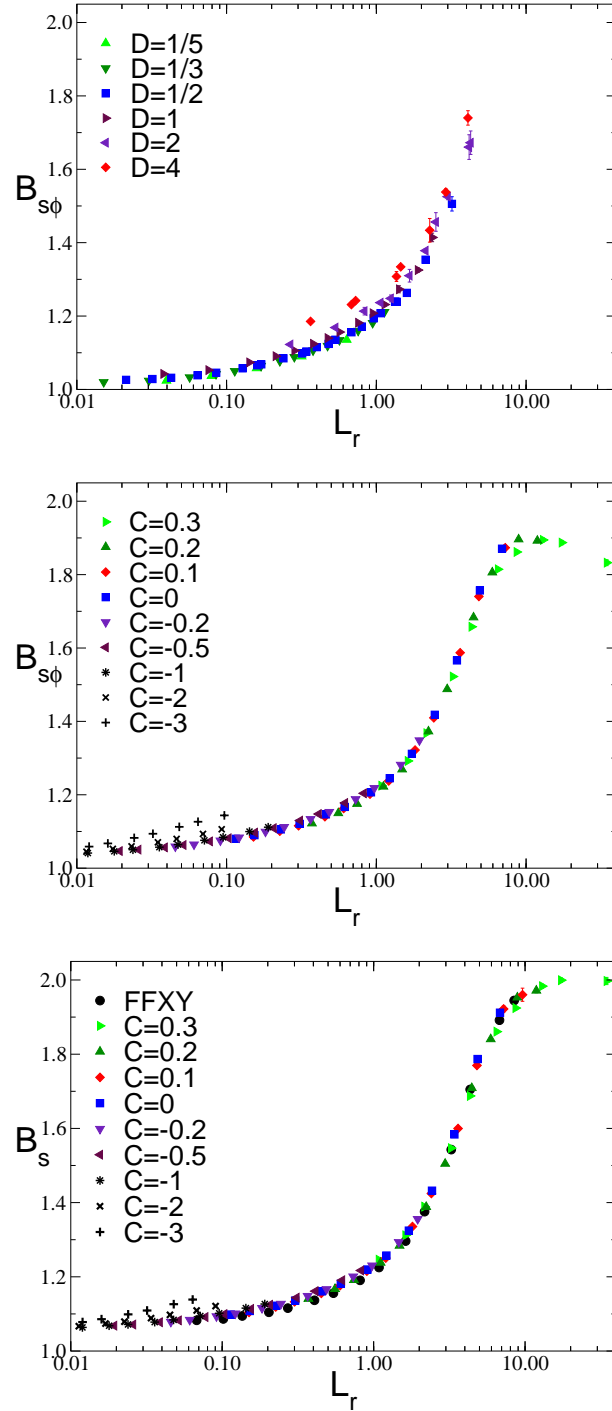


**Figure 25.** Binder parameters  $B_{s\phi}$  (top and middle) and  $B_s$  (bottom) at fixed  $R_c$ , versus  $L_r = L/l$ , for the FFXY,  $\phi^4$ , and IsXY models. The rescalings  $l$  are the same as in Fig. 24. For  $L_r \rightarrow \infty$ ,  $B_s \rightarrow 2$  and  $B_{s\phi} \rightarrow 3/2$ .

$C = 0.3, 0.2, 0.1, 0, -0.2, -0.5, -1, -2, -3$  in the case of the IsXY model.

In order to verify the universality of the scaling Ansatz (51) we have considered the spin Binder parameters  $B_s$  and  $B_{s\phi}$ . In Fig. 25 we plot these quantities in terms of  $L_r = L/l$ , using the rescaling factors determined in the analysis of  $R_s$ . Again we

observe a good universal behavior.¶ The quality of the data collapse worsens as  $D$  or  $-C$  increases. Indeed, while for  $R_s$  all data collapse on a single curve, except for a few FFXY points that correspond to small values of  $L$  ( $L \lesssim 10$ ), the data of  $B_{s\phi}$  for  $D = 4$  ( $\phi^4$  model) and  $C = -2, -3$  (IsXY model) show some systematic deviations. They apparently require a rescaling  $l$  that differs by approximately a factor of 2 for  $D = 4$  and by a factor of 5 for  $C = -3$  from that determined by using  $R_s$ . Note that these deviations are not due to small values of  $L$  and/or of  $\xi_s^{(c)}$ , since  $\xi_s^{(c)} \approx 88$  for the  $\phi^4$  model at  $D = 4$ , and  $\xi_s^{(c)} \gtrsim 200$  for the IsXY model at  $C = -2, -3$ . Most probably, the behavior is influenced by the first-order transition line that is present nearby in the phase diagram.

It is easy to realize that, given two different models,  $l_1/l_2$  corresponds to the ratio of the corresponding spin correlation lengths at the chiral transition. Indeed, since  $R_s = f_{R_s}(L/l)$  and  $\xi_s \rightarrow \xi_s^{(c)}$  for large  $L$ , we must have  $f_{R_s}(x) = a/x$  for  $x \rightarrow \infty$ , where  $a$  is model independent, and  $\xi_s^{(c)} = l/a$ . Thus, the scaling we observe implies that  $R_s$  is an approximately universal function of  $L/\xi_s^{(c)}$ . Assuming universality, this allows us to estimate the spin correlation length  $\xi_s^{(c)}$  at the chiral transition even in those cases in which our simulations did not probe the regime  $L \gg \xi_s^{(c)}$  that allows us to obtain a direct estimate of  $\xi_s^{(c)}$ . For example, using the above-reported estimates of the optimal ratio  $l/l_{\text{FFXY}}$  and  $\xi_s^{(c)} = 118(1)$  for the FFXY model, we infer that  $\xi_s^{(c)} \approx 830, 530, 380, 212, 118$  respectively for  $D = 1/5, 1/3, 1/2, 1, 2$  ( $\phi^4$  model) and  $\xi_s^{(c)} \approx 131, 310, 670$  respectively for  $C = -0.2, -0.5, -1$  (IsXY model). The result for the  $\phi^4$  model at  $D = 2$  is consistent with the estimate  $\xi_s^{(c)} = 116(3)$  obtained for  $L = 500$ . In Fig. 24 and in those we shall present below we have fixed  $l_{\text{FFXY}} = 118 \approx \xi_s^{(c)}$ , so that we are reporting the data in terms of  $L_r \equiv L/\xi_s^{(c)}$ .

In Fig. 26 we do the same analysis for the helicity modulus  $\Upsilon$ . Again, the collapse of the data is remarkable. In a quite large region, i.e. for  $L_r \lesssim 0.5$ ,  $\Upsilon$  decreases as  $L_r^{-\epsilon}$  with  $\epsilon \approx 0.33$ , with differences of at most 10%.<sup>+</sup> As already discussed in Sec. 8, a power-law decay is expected in the IsXY model for  $L \ll \xi_s^{(c)}$  and gives the effective fractal dimension of the geometrical clusters,  $d_{\text{gc}} = 2 - \epsilon$ . The universal behavior observed in Fig. 26 shows that a power-law decay also characterizes the FFXY and  $\phi^4$  models. It is interesting to note that the value  $\epsilon \approx 0.33$  is much larger than the value  $\epsilon = 5/96$  corresponding to the fractal dimension  $d_{\text{Igc}} = 187/96$  of Ising geometrical clusters: in the IsXY model, this is the dimension of the geometrical clusters only for  $L \gg \xi_s^{(c)}$ . This shows, once again, that chiral and spin modes are strongly coupled for  $L \lesssim \xi_s^{(c)}$ . A

¶ The Binder parameter  $B_{s\phi}$  is expected to converge to  $3/2$  for  $L_r \rightarrow \infty$  (a simple argument predicts:  $B_{s\phi} = 3/2 + aL_r^{-1/4}$ ,  $a > 0$ ). Nonetheless, for  $L_r \approx 10$ , such a quantity is still quite different from its asymptotic value.

<sup>+</sup> More precisely, fitting the available data for  $L \gtrsim 10$  and  $L_r \lesssim 0.5$  to  $\Upsilon = cL_r^{-\epsilon}$ , we find  $\epsilon = 0.335(8)$  ( $\chi^2/\text{d.o.f.} \approx 1.1$ ) for the FFXY model,  $\epsilon = 0.332(2)$  ( $\chi^2/\text{d.o.f.} \approx 0.5$ ) for the  $\phi^4$  model with  $D = 1/2$ ,  $\epsilon = 0.297(4)$  ( $\chi^2/\text{d.o.f.} \approx 0.5$ ) for the  $\phi^4$  model with  $D = 1/5$ ,  $\epsilon = 0.360(5)$  ( $\chi^2/\text{d.o.f.} \approx 1.1$ ) for the IsXY model with  $C = 0$ ,  $\epsilon = 0.352(3)$  ( $\chi^2/\text{d.o.f.} \approx 0.7$ ) for the IsXY model with  $C = -0.5$  (d.o.f. is the number of degrees of freedom of the fit). The small differences in the estimates of  $\epsilon$  can be easily accounted for by scaling corrections.

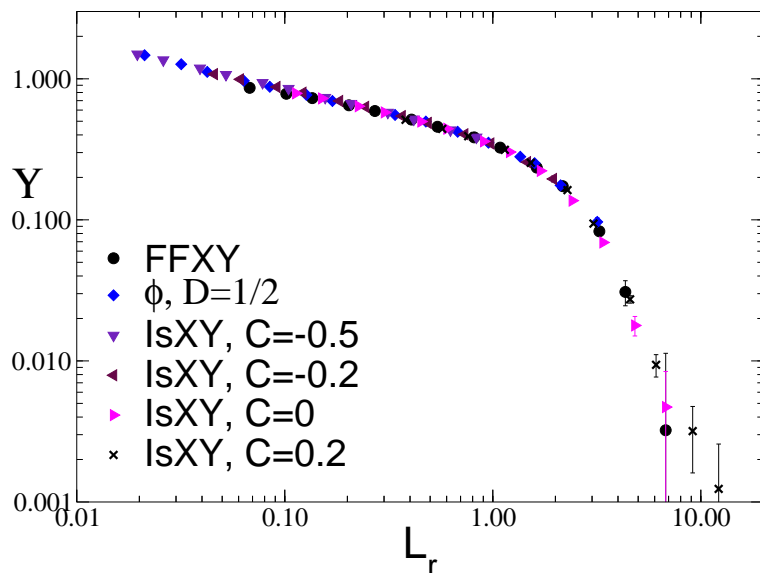


**Figure 26.** Helicity modulus  $\Upsilon$  at fixed  $R_c$ , versus  $L_r = L/l$ . The rescalings  $l$  are the same as in Fig. 24. Note the logarithmic scale on both axes.

power-law behavior is also observed in  $R_s$ . As it can be seen from Fig. 24, for  $L_r \lesssim 0.5$   $R_s$  scales as  $L_r^{-\epsilon}$ , although in this case  $\epsilon$  is much smaller,  $\epsilon \approx 0.1$ . Note that, if the behavior we observe for  $0.02 \lesssim L_r \lesssim 0.5$  holds up to  $L_r = 0$  we would obtain  $R_s, \Upsilon \rightarrow \infty$  for  $L_r \rightarrow 0$ .

In Fig. 27 we plot the effective exponents  $1/\nu_{\text{eff}}$ , defined as in Eq. (37), as obtained from the derivative of  $R_c$ ,  $B_c$ , and  $R_s$  with respect to  $J$ , versus the rescaled lattice size  $L_r = L/l = L/\xi_s^{(c)}$ . We use the same rescaling factors  $l$  as above. The agreement is quite good, although the quality of the collapse for the chiral exponent  $\nu_{\text{eff}}$  is not as impressive as what is observed for the spin-related quantities  $R_s$ ,  $B_s$ , and  $B_{s\phi}$ . These crossover curves show a quite interesting pattern. The effective exponents  $1/\nu_{\text{eff}}$  derived from  $R_c$  and  $B_c$  show first a rather flat region in which  $1/\nu_{\text{eff}} \approx 1.3$ , corresponding to  $\nu_{\text{eff}} \approx 0.8$ . Therefore, a FSS analysis limited to values  $L \lesssim \xi_s^{(c)}$  would apparently provide the estimate  $\nu \approx 0.8$  for the critical exponent associated with the chiral correlation length, as found in the FSS analysis of Sec. 7.2.1. Only by using larger lattices, i.e.  $L \gg \xi_s^{(c)}$ , can one observe the asymptotic Ising critical behavior. Note that, to make things worse, the asymptotic approach is nonmonotonic: for  $L \approx \xi_s^{(c)}$  the exponent  $\nu_{\text{eff}}$  starts to increase, becomes larger than the Ising value (the curves of  $1/\nu_{\text{eff}}$  have a minimum for  $L/\xi_s^{(c)} \approx 2$  corresponding to  $\nu_{\text{eff}} \approx 1.1$  for  $R_c$  and  $\nu_{\text{eff}} \approx 1.2$  for  $B_c$ ) and then eventually converges to the Ising value. The effective exponents  $1/\nu_{\text{eff}}$  associated with the spin variables show a similar crossover behavior. The exponent derived from  $R_s$  must converge to  $-1$  for  $L \gg \xi_s^{(c)}$ , since the spin correlation length is finite. However, for  $L \lesssim \xi_s^{(c)}$  the data of  $1/\nu_{\text{eff}}$  show a plateau at  $1/\nu_{\text{eff}} \approx 1.1$ , see Fig. 27. In the case of  $B_s$  and  $B_{s\phi}$  (not shown) we observe an analogous plateau, but at  $1/\nu_{\text{eff}} \approx 1.7$ . Substantial deviations from the above behaviors are observed for  $D = 4$  in the  $\phi^4$  model and for  $C = -2, -3$  in the IsXY model, as one can already see from Figs. 17 and 23 where  $1/\nu_{\text{eff}}$  is plotted versus

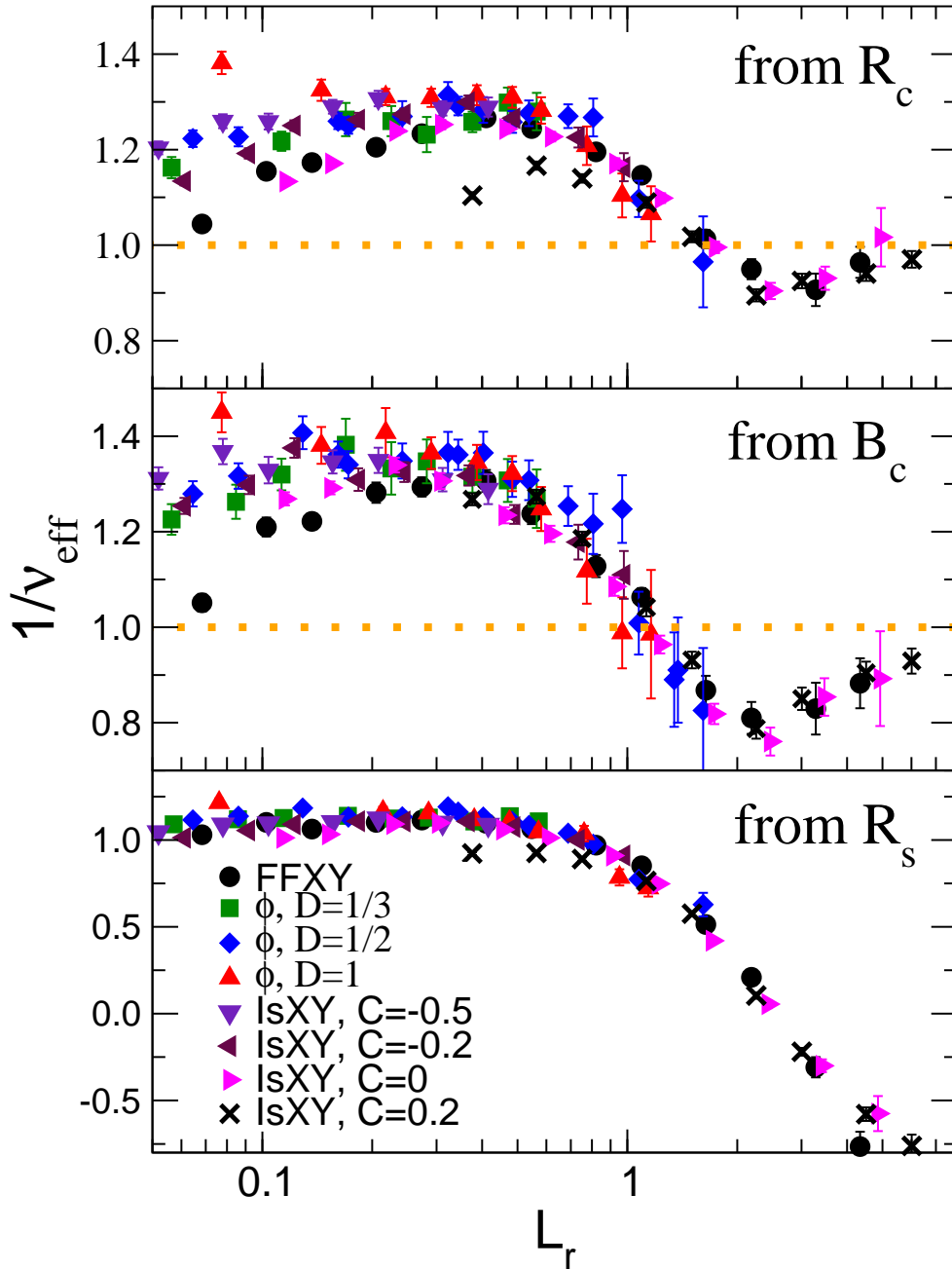


**Figure 27.** Effective exponent  $1/\nu_{\text{eff}}$  computed using  $R_c$ ,  $B_c$ , and  $R_s$ , versus  $L_r = L/l$ . The rescalings  $l$  are the same as in Fig. 24. For  $L_r \rightarrow \infty$ ,  $1/\nu_{\text{eff}}$  should converge to  $1/\nu_{\text{Is}} = 1$  for  $R_c$  and  $B_c$ , and  $-1$  for  $R_s$ .

$L$ .

It is impossible to estimate from the data the behavior of the effective exponent  $\nu_{\text{eff}}$  for  $L_r \rightarrow 0$ , since points are quite scattered. For small values of  $D$  in the  $\phi^4$  model  $1/\nu_{\text{eff}}$  is smaller than one for small lattice sizes, as expected from the influence of the close  $O(4)$  multicritical point, for which  $1/\nu = 0$ , see Sec. 7.3. On the other hand, for  $D \gtrsim 1$  and  $C \lesssim -1$ , the effective exponent approaches the plateau from above, a behavior that

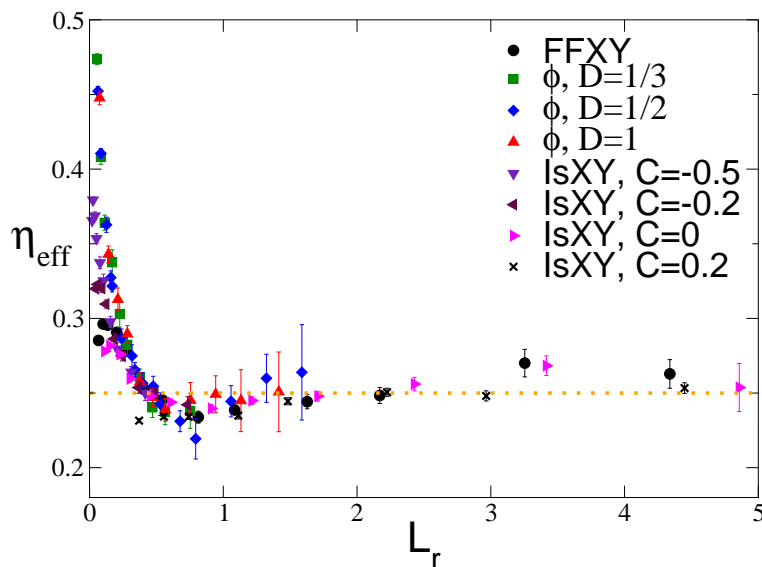


**Figure 28.** Effective exponent  $\eta_{\text{eff}}$  at fixed  $R_c$ , as obtained from  $\chi_c$ , versus  $L_r = L/l$ . The rescalings  $l$  are the same as in Fig. 24.

may be due to the presence of a first-order transition line for large  $D$  and  $-C$ .

In Figs. 28 and 29 we plot the effective exponent  $\eta_{\text{eff}}$  obtained from  $\chi_c$  and  $\Delta B_c \equiv B_c - B_{\text{Is}}$ . Again, we observe an approximate collapse of the data. A more quantitative check can be done by observing that the approximate universality implies for  $L \rightarrow \infty$

$$\Delta B_c = a(L/\xi_s^{(c)})^{-7/4}, \quad (52)$$

where  $a$  is model independent. If we define  $b \equiv a(\xi_s^{(c)})^{7/4}$ , the previous equation gives a relation between the ratio of the constants  $b$  in different models and the ratio of the spin correlation lengths. Using the estimates of  $b$  reported in Secs. 6.1 and 8 for the FFXY model and IsXY model with  $C = 0$ , we find  $b_{\text{FFXY}}/b_{\text{IsXY}, C=0} = 4.0(3)$ . This is in perfect agreement with the prediction  $b_{\text{FFXY}}/b_{\text{IsXY}, C=0} = (\xi_{s, \text{FFXY}}^{(c)}/\xi_{s, \text{IsXY}, C=0}^{(c)})^{7/4} = 4.1(1)$ .

The results reported above show that, in the FFXY model and in the  $\phi^4$  and IsXY models for a rather extended region of parameters (respectively for  $0 < D \lesssim 2$  and  $-1 \lesssim C \lesssim 0.2$ ), the finite-size behavior at the chiral transition is somewhat universal. A natural conjecture is that this universality is controlled by a *multicritical* point (or by a line of multicritical points of the same type) where chiral and spin degrees of freedom become both critical. If this conjecture is correct, one must observe a universal crossover behavior also at the spin transition, with the same rescaling factors.

In Fig. 30 we report  $R_s \equiv \xi_s/L$  and  $\Upsilon$  at the spin transitions for the three models for which we have a reliable estimate of  $J_{\text{sp}}$ . The rescaling factors  $l$  are those determined at the chiral transition. The agreement is again quite good. The existence of scaling at the two transitions with the same rescaling factors is another piece of evidence in favor of the multicritical origin of the universality we observe. This hypothesis is also supported by the fact that the ratio  $\xi_s^{(c)}/\xi_c^{(s)}$  is approximately constant. Indeed, we have  $\xi_c^{(s)} = 8.0(5)$ ,

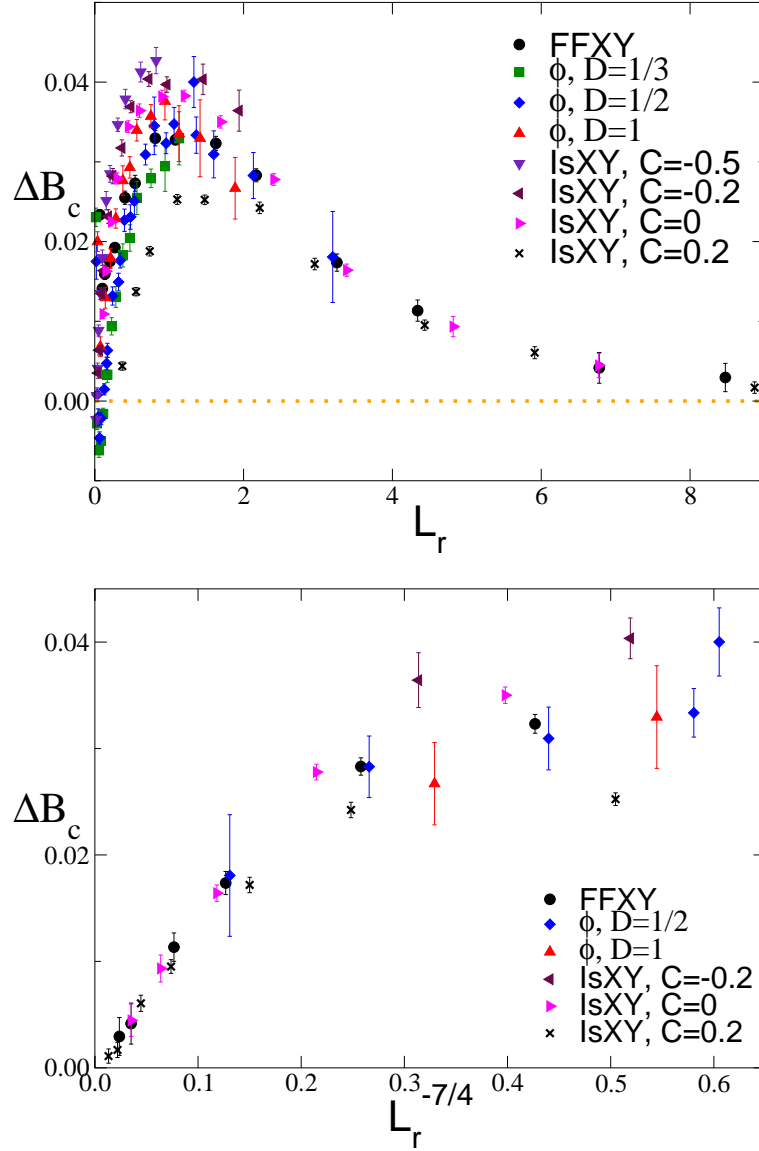


**Figure 29.** Binder parameter  $B_c$  at fixed  $R_c$ , versus  $L_r = L/l$ . The rescalings  $l$  are the same as in Fig. 24. We plot  $\Delta B_c = B_c - B_{\text{Is}}$ , where  $B_{\text{Is}} = 1.167923(5)$  is the value of the Binder parameter at the critical point in the Ising model [88].

$\xi_s^{(c)} = 118(1)$ , thus  $\xi_s^{(c)}/\xi_c^{(s)} = 15(1)$ , for the FFXY model;  $\xi_c^{(s)} = 22(3)$ ,  $\xi_s^{(c)} \approx 380$ , thus  $\xi_s^{(c)}/\xi_c^{(s)} = 17(3)$  (assuming an uncertainty of approximately 10% on  $\xi_s^{(c)}$ ), for the  $\phi^4$  model for  $D = 1/2$ ;  $\xi_c^{(s)} = 4.3(5)$ ,  $\xi_s^{(c)} = 52.7(4)$ , thus  $\xi_s^{(c)}/\xi_c^{(s)} = 12(2)$ , for the IsXY model at  $C = 0$ . These results are consistent with a constant ratio  $\xi_s^{(c)}/\xi_c^{(s)} \approx 15$ .

While for  $L_r \rightarrow \infty$  one observes Ising and KT behavior, in the opposite limit  $L_r \rightarrow 0$ , the scaling functions converge to the value of the corresponding observable at the multicritical point (assuming it exists, of course). The relevant scales are  $\xi_s^{(c)}$  and  $\xi_c^{(s)}$  at the two transitions and thus information on the nature of the multicritical point can be obtained by studying the crossover curves in the regimes  $L \ll \xi_s^{(c)}$  (chiral transition) and  $L \ll \xi_c^{(s)}$  (spin transition). Unfortunately, in the models in which we

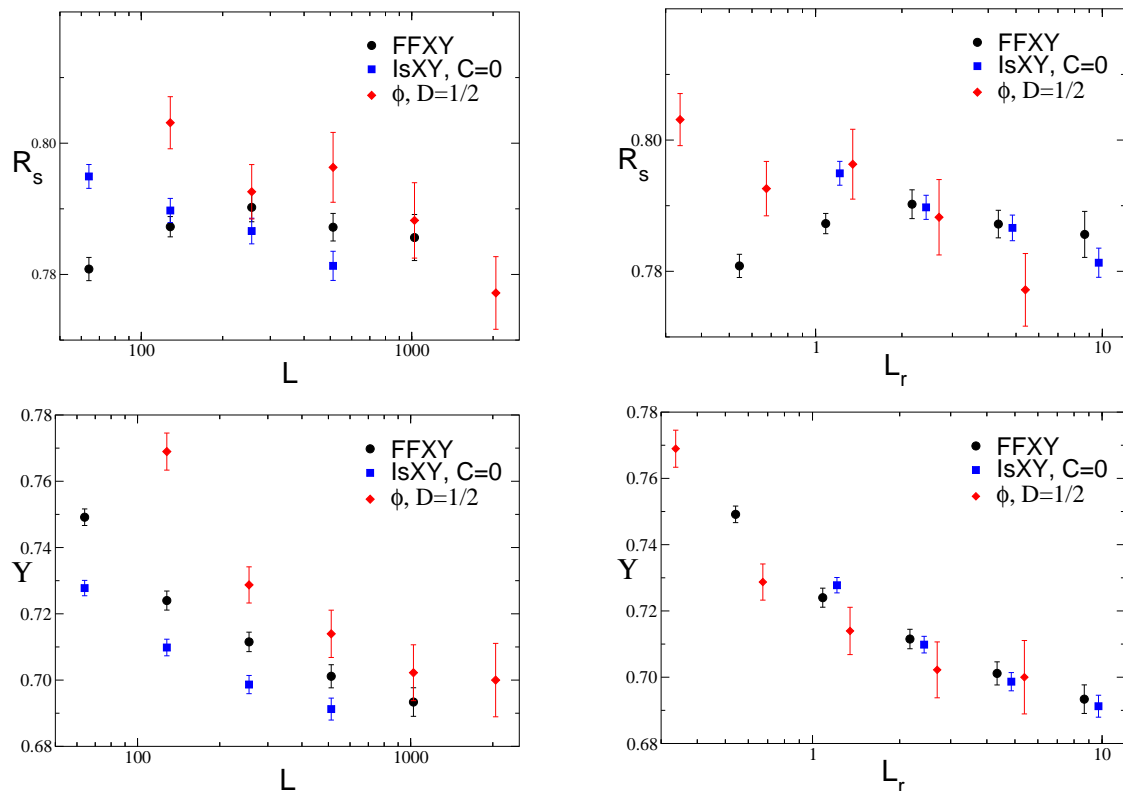


**Figure 30.** Ratio  $R_s \equiv \xi_s/L$  (above) and helicity modulus (below) at the spin transition. On the left we plot the data versus  $L$ , on the right versus  $L_r = L/l$ . The rescalings  $l$  are the same as in Fig. 24.

have a precise knowledge of  $J_{\text{sp}}$ ,  $\xi_c^{(s)}$  is quite small and thus we are not able to probe the multicritical regime at the spin transition. On the other hand, since  $\xi_s^{(c)}$  is quite large, the behavior at the chiral transition gives us some indications on the multicritical point.

From the data we can certainly exclude an Ising-XY decoupled multicritical point. Indeed, see Fig. 26, the helicity modulus is clearly larger than the XY value  $\Upsilon_{XY} \approx 0.6365$ . A more likely possibility is that the behavior for  $L_r$  small is controlled by a zero-temperature transition point. Indeed, as we already discussed, our data are compatible with  $R_s, \Upsilon \rightarrow \infty$  for  $L_r \rightarrow 0$ . In Fig. 31 we report the results for  $B_{s\phi}$  using a double logarithmic scale in order to make the region of small  $L_r$  more visible. Even though scaling corrections are present, it is quite plausible that  $B_{s\phi} \rightarrow 1$  for  $L_r \rightarrow 0$ , as expected in the case of a zero-temperature transition.

## 10. Conclusions

In this paper we investigated the phase diagram of the square-lattice FFXY model and of two related models, a lattice discretization of the LGW Hamiltonian for the critical modes of the FFXY model, cf. Eq. (4), and the IsXY model (7). For this purpose we presented a FSS analysis of the numerical results obtained by high-statistics MC simulations on square lattices  $L^2$ , for quite large values of  $L$ , up to  $L = O(10^3)$ . Our

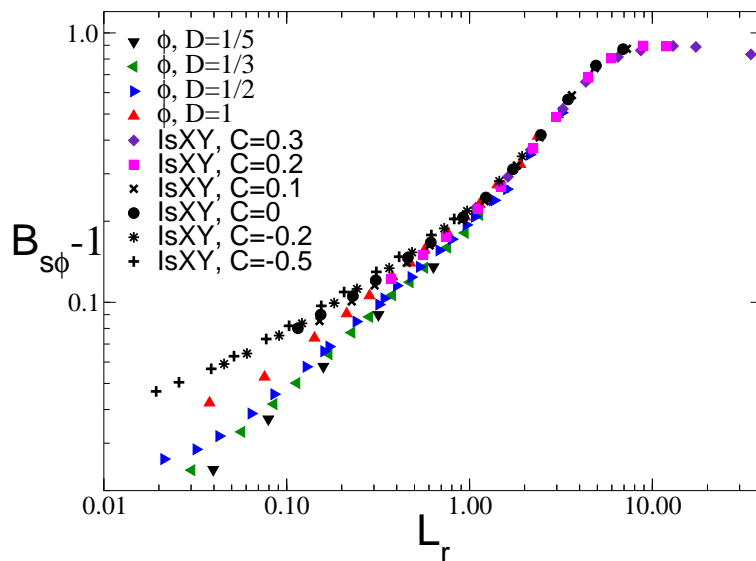


**Figure 31.** Binder cumulant  $B_{s\phi}$  at fixed  $R_c$ , versus  $L_r = L/l$ . The rescalings  $l$  are the same as in Fig. 24. Note the logarithmic scale on both axes.

main results can be summarized as follows.

(i) In all models the LT phase is characterized by the breaking of the  $\mathbb{Z}_2$  symmetry with a chiral magnetization, and by quasi-long-range order associated with the breaking of the  $O(2)$  rotational symmetry. We find that the critical behavior of the spin modes is controlled by the same line of Gaussian fixed points as in the standard XY model. Indeed, we verify that the spin correlation length, the helicity modulus, and the exponent  $\eta$  satisfy the same universal finite-size relations that hold in the LT phase of the XY model.

(ii) We conclusively show that the square-lattice FFXY model undergoes two very close transitions, respectively at  $J_{sp}$  and  $J_{ch}$ , with  $J_{sp} > J_{ch}$ . The transition at  $J_{sp}$  is a KT transition associated with the spin modes, while for  $J = J_{ch}$  there is an Ising transition where the chiral  $\mathbb{Z}_2$  symmetry is restored. For  $J_{ch} < J < J_{sp}$ , spins are paramagnetic but chiral symmetry is broken. The Ising and KT transitions are very close:  $\delta \equiv (J_{sp} - J_{ch})/J_{ch} = 0.0159(2)$ .

(iii) The phase diagram of the  $\phi^4$  model for  $U = 1$  is shown in Fig. 8. It presents two qualitatively different regions. There is a region in which the behavior is analogous to that of the FFXY model, with an Ising and a KT transition at  $J_{ch} < J_{sp}$ . These transitions are very close: we find  $\delta \equiv (J_{sp} - J_{ch})/J_{ch} \lesssim 0.003$  for all values of  $D$  in the two-transition region ( $\delta = 0.0025(2)$  for  $D = 1/2$ ). For  $D > D^*$  with  $34 < D^* \approx 49$ , we find instead a single first-order transition. We do not know how the two continuous transition lines connect to the unique first-order one (see the discussion at the beginning of Sec. 7). A possibility is shown in Fig. 8: the Ising line ends at a tricritical Ising point, which is the endpoint of the first-order transition line; then the KT line meets the first-order one. Since for  $D = 0$  there is no finite- $J$  transition, it is natural to assume that the two transition lines get closer and closer as  $D \rightarrow 0$  and meet at  $1/J = 0, D = 0$ ,

which thus acts as an  $O(4)$ -symmetric multicritical point. The critical lines approach the multicritical point according to  $J_{\text{ch}} \sim \ln D^{-1}$  and  $\delta \sim 1/\ln D^{-1}$  for  $D \rightarrow 0$ .

(iv) The phase diagram of the IsXY model (7) is shown in Fig. 19. In Sec. 2 we argue that the IsXY model cannot undergo a continuous transition in which chiral and spin modes become both critical. Our MC results support this fact. As in the  $\phi^4$  model, there is a rather extended region in which there is an Ising and a KT transition with  $J_{\text{ch}} > J_{\text{sp}}$ . The Ising and KT transitions are close in most of the cases. For example, we find  $\delta \equiv (J_{\text{sp}} - J_{\text{ch}})/J_{\text{ch}} = 0.0167(7)$  for  $C = 0$ . For  $C < C^*$ ,  $-7 \lesssim C^* \lesssim -5$ , we find a single first-order transition. Again, we do not know how the two continuous transition lines connect to the unique first-order one. A possibility is shown in Fig. 19.

(v) We do not find evidence of continuous transitions—but we cannot completely exclude their presence—where chiral and spin modes become both critical, giving rise to a new universality class. Thus, our results do not support the field-theoretical results of Refs. [70, 65], which provided some evidence for the existence of a stable fixed point in the RG flow of the LGW continuous theory (5). However, they are not necessarily in contradiction, since the lattice models considered here may be outside the attraction domain of the stable fixed point found in Refs. [70, 65]. Note also that the existence of two continuous transitions at fixed bare parameters (i.e., at fixed  $D$  and  $U$ , or  $C$ ) means that the critical modes are not appropriately described by the LGW theory, at least in the cases considered in this paper. Actually, it suggests that a field theory with an Ising and an XY field, for instance the multicritical theory of Refs. [96, 102], might be more appropriate.

(vi) In most cases the spin correlation length  $\xi_s^{(c)}$  at the chiral transition is quite large. For example,  $\xi_s^{(c)} \approx 118$  in the FFXY model,  $\xi_s^{(c)} \approx 53$  in the IsXY model for  $C = 0$ , and  $\xi_s^{(c)} \approx 380$  in the  $\phi^4$  model for  $D = 1/2$ . The presence of this additional length scale makes the observation of the expected Ising behavior quite problematic. We find that Ising behavior is observed only for  $L \gg \xi_s^{(c)}$ , which in turn requires very large lattices.

(vii) At the chiral and spin transitions we observe a preasymptotic regime that is universal to some extent. Indeed, in the FFXY model, in the  $\phi^4$  model with  $U = 1$  and  $0 < D \lesssim 2$ , and in the IsXY model with  $-1 \lesssim C \lesssim 0.2$ , we find that RG quantities at the transitions scale approximately as

$$\mathcal{R}(L) \approx f_{\mathcal{R}}(L/l), \quad (53)$$

where  $f_{\mathcal{R}}(x)$  is a model-independent function that is of course different at the two transitions. The rescalings  $l$  are model dependent and set the length scale. Given two different models,  $l_1/l_2$  is equal to the ratios  $\xi_{s,1}^{(c)}/\xi_{s,2}^{(c)}$  or  $\xi_{c,1}^{(s)}/\xi_{c,2}^{(s)}$ . One might expect scaling (53) to be valid for  $L \rightarrow \infty$ ,  $l \rightarrow \infty$  (or, equivalently,  $\xi_s^{(c)}, \xi_c^{(s)} \rightarrow \infty$ ) at fixed ratio. However, these conditions are not sufficient to observe this universal behavior. Substantial deviations are observed in other parameter regions, e.g., for  $D = 4$  in the  $\phi^4$  model and for  $C = -2, -3$  in the IsXY, even though  $\xi_s^{(c)}$  is large. This may be due to the influence of the first-order transition present for large values of  $D$  and  $-C$ . Note that,

at the chiral transition, the effective chiral exponent  $\nu$  shows an intermediate region in which it is approximately equal to 0.8. This explains earlier results obtained by using smaller lattices. By using only data with  $L \lesssim \xi_s^{(c)}$  one would obtain  $\nu = 0.8$  instead of the Ising value. Scaling (53) may be due to a multicritical point where chiral and spin modes are both critical. The analysis of the crossover curves for  $L/l \rightarrow 0$  allows us to exclude a decoupled Ising-XY multicritical transition. A zero-temperature point is instead compatible with the numerical data. Note that the universal behavior we have observed here concerns the finite-size behavior at criticality, but of course similar phenomena are expected in the thermodynamic limit close to the critical points. If  $t_{\text{ch}}$  and  $t_{\text{sp}}$  are the reduced temperatures and  $\delta$  the temperature difference of the two transitions, Ising and KT behavior can only be observed if  $t_{\text{ch}}, t_{\text{sp}} \ll \delta$ . In the opposite limit,  $1 \gg t_{\text{ch}}, t_{\text{sp}} \gtrsim \delta$  we expect instead a universal crossover behavior.

The identification of the multicritical point is a problem that is still open and requires further investigation. If the relevant multicritical point is a zero-temperature transition, as the MC data suggest, then the O(4) point discussed in Sec. 7.3 is a possible candidate. Otherwise, one should also consider the finite-temperature multicritical point expected in the phase diagram of the generalized IsXY model [29] with Hamiltonian

$$\mathcal{H}_{\text{IsXY}} = -J \sum_{\langle xy \rangle} [(A + B\sigma_x\sigma_y)\vec{s}_x \cdot \vec{s}_y + C\sigma_x\sigma_y], \quad (54)$$

in frustrated XY models with modulated couplings [16, 22, 103] (they are obtained by generalizing the FFX model (3), setting  $j_{xy} = -\eta$  with  $\eta > 0$  on the antiferromagnetic links), and in  $\phi^4$  theories in which the field-interchange symmetry is broken or in which one of the two O(2) symmetries is broken by adding, for instance, an interaction term of the form  $(\vec{\phi}_{1,x} \cdot \vec{\phi}_{2,x})^2$ .

## Acknowledgments

We thank Pasquale Calabrese for useful discussions, and Alberto Ciampa and Maurizio Davini for their technical assistance to manage the computer clusters where the Monte Carlo simulations have been done. The numerical simulations were performed at the Computational Centers of the Physics Department and of INFN in Pisa.

## Appendix A. Some details on the Monte Carlo algorithms

### Appendix A.1. The FFX model

The algorithm we used for the simulation of the FFX model is based on the results of Ref. [60]. These authors found that the addition of a certain number of overrelaxation (OR) sweeps to a local Metropolis sweep makes the algorithm more efficient. They also suggested an efficient method to generate the proposed new spin in the Metropolis

update. Every sweep over the lattice \* one chooses a single unit vector  $\vec{r} = (\cos \alpha, \sin \alpha)$ , where  $\alpha$  is uniformly distributed in  $[0, 2\pi)$ . Then, for each site  $x$  the proposal is

$$\vec{s}'_x = 2(\vec{r} \cdot \vec{s}_x)\vec{r} - \vec{s}_x. \quad (\text{A.1})$$

This proposal is accepted with the Metropolis probability

$$A = \text{Min} \left[ e^{-(\mathcal{H}' - \mathcal{H})}, 1 \right]. \quad (\text{A.2})$$

The advantage of this proposal compared with more standard ones is that no random numbers are needed and also no expensive trigonometric function is evaluated. Furthermore, the authors of Ref. [60] showed that the autocorrelation times in terms of sweeps of the Metropolis update with this type of proposal (in the following we will refer to it as MR update) are essentially the same as those of a Metropolis update in which the new spin is obtained by a random rotation of the old one. At the chiral transition the acceptance rate of the MR update is approximately 25%, in agreement with Ref. [60].

In most of our simulations we used a demon version [104] of the Metropolis update. We indicate the demon version of any update by a adding a letter D. The demon version of the MR update is therefore denoted by DMR. In this framework, one introduces a demon field  $d_x \in [0, \infty)$  with distribution  $\exp(-\sum_x d_x)$  and replaces the Metropolis accept/reject step in the following way. One defines

$$d'_x = d_x - \mathcal{H}' + \mathcal{H}. \quad (\text{A.3})$$

If  $d'_x \geq 0$ , the proposal is accepted and  $\vec{s}_x, d_x$  are replaced by  $\vec{s}'_x, d'_x$ . Otherwise, the demon and the spin keep their old value. This way the generation of a random number and, more importantly, the evaluation of the exponential is avoided. However, these updates do not change the sum

$$\sum_x d_x + \mathcal{H}. \quad (\text{A.4})$$

Therefore, one must also perform heat-bath updates of all demons, by taking  $d_x = -\ln z_x$ , where  $z_x$  is a random number uniformly distributed in  $(0,1]$ . It is easy to see that by updating  $d_x$  before the update of  $\vec{s}_x$ , one recovers the standard Metropolis algorithm. Also note that the acceptance rate of the demon version of the Metropolis update is exactly the same as that of the standard one, although the autocorrelation times might increase.

The local overrelaxation (OR) update is given by

$$\vec{s}'_x = \frac{2\vec{s}_x \cdot \vec{S}}{S^2} \vec{S} - \vec{s}_x, \quad (\text{A.5})$$

where  $\vec{S} = \sum_{y, nn.x} j_{xy} \vec{s}_y$  is the sum of  $\vec{s}_y$  over the nearest neighbors  $y$  of site  $x$ . One advantage of the OR update is that no random numbers and no evaluations of the exponential function are needed. In the case of the standard XY model one finds that

\* We have generated a new  $\vec{r}$  more frequently, namely for each row of the lattice. We have not tested whether or not this gives an advantage over choosing a new  $\vec{r}$  just once every sweep.

**Table A1.** Integrated autocorrelation times  $\tau_{\text{ch}}$  for the chiral susceptibility of the FFXY model close to the chiral transition.  $\tau_{\text{ch}}$  is reported in number of measurements. # meas. is the total number of measurements and  $N_{\text{local}}$  is the number of update cycles between two measurements.

$L$	$J$	# meas.	$N_{\text{local}}$	$\tau_{\text{ch}}$
256	2.2053	22000	500	1.76(10)
384	2.2062	56600	700	2.67(13)
512	2.2063	39500	1000	3.3(3)
800	2.2066	20500	2000	3.6(3)
1000	2.2063	35700	2000	6.2(5)

for the optimal mixture of Metropolis and OR updates the dynamical critical exponent is reduced to  $z \approx 1.2$  [105]. In contrast, for the FFXY model at the chiral transition the authors of Ref. [60] find only a speed-up by a constant factor.

A complete cycle of the algorithm we used is:

- Heat-bath of the demons;
- $5 \times [(\text{DMR} + \text{OR}) \text{ sweep} + N_{\text{or}} \text{ OR sweeps}]$ .

Here (DMR + OR) means that a single-site DMR update is followed by an elementary OR update at the same site. At the chiral transition we used  $N_{\text{or}} = 3$ , while at the KT transition larger values of  $N_{\text{or}}$  were used.

We have implemented a parallel program using the MPI library. To this end, we have divided the lattice in one direction into sublattices of size  $l \times L$ , where  $l \times n_P = L$  and  $n_P$  is the number of processes that is used. In order to speed up the simulation, we also did some kind of parallelization in the second direction, running the OR sweep in the second direction in the following way:

```
for (x1=0;x1<L/2;x1++) {OR site (x0,x1); OR site (x0,x1+L/2)};
```

where  $(\mathbf{x}_0, \mathbf{x}_1)$  is a lattice point. This small change allows a better use of the floating-point pipelines and gives a speedup of approximately 30%. On a server with 4 1.8GHz Opteron CPUs, one complete update cycle takes 0.26s for  $L = 1000$ . Roughly speaking, one cycle takes 1 s on one Opteron processor with one core.

In table A1 we report the integrated autocorrelation times of the chiral susceptibility for  $L \geq 256$ . The couplings  $J$  are close to the chiral critical value  $J_{\text{ch}} = 2.20632(5)$ . Fitting all data given in table A1 we get  $N_{\text{local}}\tau_{\text{ch}} = 0.022(8) \times L^{1.91(6)}$  with  $\chi^2/\text{d.o.f.} = 0.99$ .

At the KT transition, critical slowing down can be efficiently reduced by using overrelaxation updates. In the case of the standard XY model, at the transition one should increase  $N_{\text{or}}$  as  $N_{\text{or}} \propto L$ . We found that also in the case of the FFXY model at the KT transition this procedure leads to very small autocorrelation times. For  $J = 2.242$  [ $J_{\text{sp}} = 2.2415(5)$ ] and  $L = 1024$ , by using  $N_{\text{or}} = 12$  we find an integrated autocorrelation time  $\tau_{\text{sp}} \approx 5.4(5)$  in units of cycles (heat bath of the demons followed by  $5 \times [(\text{DMR} + \text{OR}) + 12 \text{ OR}]$  sweeps). For  $L \approx 1000$  the autocorrelation time is smaller by a factor of 500 than that at the chiral transition.

**Table A2.** Integrated autocorrelation times  $\tau_{\text{ch}}$  for the chiral susceptibility in the IsXY model at  $C = 0$ , close to the chiral transition.  $\tau_{\text{ch}}$  is reported in units of measurements. # meas. is the total number of measurements,  $N_{\text{local}}$  is the number of local update cycles, and  $N_{\text{single}}$  is the number of single-cluster updates per measurement.

$L$	$J$	# meas.	$N_{\text{local}}$	$N_{\text{single}}$	$\tau_{\text{ch}}$
64	1.4660	100000	500	20	0.92(2)
90	1.4672	100000	700	20	1.22(3)
128	1.4678	100000	1000	40	1.62(5)
180	1.4681	100000	1000	200	3.05(12)
256	1.4681	75000	1000	100	6.2(3)
360	1.4585	50000	2000	80	6.1(4)

### Appendix A.2. The Ising-XY model

For the IsXY model we used three types of updates. We performed single-cluster [83] and overrelaxation updates of the spins  $\vec{s}$  keeping the chiral field  $\sigma$  fixed, and Metropolis updates in which  $\sigma$  and  $\vec{s}$  are both changed. The proposal for the Metropolis update is

$$\sigma'_x = -\sigma_x, \quad \vec{s}'_x = (\cos \alpha, \sin \alpha), \quad (\text{A.6})$$

where  $\alpha$  is a random number uniformly distributed in  $[0, 2\pi)$ . Close to the chiral transition, the acceptance rate of this update is approximately 11% for  $C = 0$  and 3% for  $C = -7$ . We mostly used the demon version of this update (in the following we refer to it as DM update).

Between two measurements we perform  $N_{\text{local}}$  local cycles [a local cycle consists in a heat bath of the demons and in  $5 \times (\text{DM sweep} + \text{OR sweep})$ ] followed by  $N_{\text{single}}$  single-cluster updates. On one 2.2 GHz Opteron CPU, one local cycle takes approximately 0.20s for  $L = 512$ .

In Table A2 we report the integrated autocorrelation times of the chiral susceptibility for lattices with  $64 \leq L \leq 360$ . The couplings  $J$  are close to the chiral critical value  $J_{\text{ch}} = 1.4684(1)$ . The number of single-cluster updates was chosen *ad hoc*, since the cluster update has little influence on the autocorrelation times. Fitting  $N_{\text{local}}\tau_{\text{ch}}$  for  $L \geq 128$  (we are neglecting here the role of the single-cluster updates) we obtain  $N_{\text{local}}\tau_{\text{ch}} = 0.12(4) \times L^{1.95(6)}$  with  $\chi^2/\text{d.o.f.} = 0.53$ . At the chiral transition, the cluster algorithm leaves the dynamic critical exponent substantially unchanged, i.e.  $z \approx 2$ . A similar observation holds for other values of  $C$ , whenever the transition is of second order.

Critical slowing down at the KT transition and in the LT phase is essentially eliminated by the single-cluster updates. For instance, for  $L = 512$  and  $J = 1.492$  we get  $\tau_{\text{sp}} = 0.94(1)$  in units of measurements, where a measurement was performed after 4 single-cluster updates and 20 local cycles.

Appendix A.3. The  $\phi^4$  model

Also here, we used a combination of local Metropolis updates and single-cluster updates. The single-cluster algorithm was used to update the angle of either  $\vec{\phi}_1$  or  $\vec{\phi}_2$ .

We used different versions of the local Metropolis update, depending on the value of  $D$ . For  $D \leq 4$  we used a Metropolis update with the following proposal (update M4):

$$\phi'_{ij,x} = \phi_{ij,x} + s(r_{ij,x} - 0.5) , \quad (\text{A.7})$$

where  $\vec{\phi}_{j,x} \equiv (\phi_{1j,x}, \phi_{2j,x})$  and  $r_{ij,x}$  are random numbers with uniform distribution in  $[0, 1)$ . The step size  $s$  was chosen so that the acceptance rate is roughly 50%.

This update becomes inefficient for large values of  $D$ . Indeed, for  $D$  large,  $|\vec{\phi}_{1,x}| \gg |\vec{\phi}_{2,x}|$  or vice versa, so that the Metropolis proposal (A.7) leads to changes of the fields that are of the typical size of the smaller one. Hence, the algorithm becomes inefficient. To deal with this problem, we constructed proposals that are specifically adapted to this situation:

- (M2) We change only one field at each time. With probability 1/2 we change either  $\phi_1$  or  $\phi_2$  using the proposal

$$\phi'_{11,x} = \phi_{11,x} + s(r_{1,x} - 0.5), \quad \phi'_{12,x} = \phi_{12,x} + s(r_{2,x} - 0.5) \quad (\text{A.8})$$

or the analogous one for  $\phi_{2,x}$ . Here  $r_{1,x}$  and  $r_{2,x}$  are random numbers with uniform distribution in  $[0, 1)$ . The step size  $s$  is chosen so that the acceptance rate is approximately 25%. This way, we achieve an efficient update of the large component of the field.

- (MLE) We exchange the lengths of the two fields. The proposal is given by

$$\vec{\phi}'_{1,x} = \frac{|\vec{\phi}_{2,x}|}{|\vec{\phi}_{1,x}|} \vec{\phi}_{1,x}, \quad \vec{\phi}'_{2,x} = \frac{|\vec{\phi}_{1,x}|}{|\vec{\phi}_{2,x}|} \vec{\phi}_{2,x} . \quad (\text{A.9})$$

This type of update should speed up the chiral degrees of freedom. The acceptance rate is 14% at the chiral transition at  $D = 49$ . One could have also exchanged the components of the two fields, using

$$\vec{\phi}'_{1,x} = \vec{\phi}_{2,x}, \quad \vec{\phi}'_{2,x} = \vec{\phi}_{1,x}. \quad (\text{A.10})$$

However, this proposal has a smaller acceptance rate than (A.9).

Beside these updates we also used local updates that leave invariant part of the Hamiltonian and are close in spirit to overrelaxation updates. A first possibility (OR4) consists in performing a field reflection that keeps the O(4)-invariant part of the Hamiltonian constant:

$$\vec{\phi}'_x = 2 \frac{\vec{\phi}_x \cdot \vec{S}}{\vec{S}^2} \vec{S} - \vec{\phi}_x \quad (\text{A.11})$$

where  $\vec{S}$  is the sum over the fields of the four neighbors of  $x$ . For convenience, we define the four-component vector  $\vec{\phi}_x = (\phi_{11,x}, \phi_{12,x}, \phi_{21,x}, \phi_{22,x})$ . This type of update has no free parameters. The remaining part of the Hamiltonian is taken into account in an

accept/reject step. We expect the acceptance rate to decrease with increasing  $D$ . At the chiral transition we find 87%, 70%, 61%, 43%, 40% for  $D = 1/2, 2, 4, 34, 99$ . Note that it seems to have a finite limit as  $D \rightarrow \infty$ . In the simulations we used a demon version (DOR4) with a single demon (not one for each site).

A second possibility is the overrelaxation of one component of the field (OR1). The Hamiltonian for a single component  $\phi_{ij,x}$  of the field, keeping all other fields fixed, has the form

$$\bar{H}(\phi_{ij,x}) = a\phi_{ij,x} + b\phi_{ij,x}^2 + c\phi_{ij,x}^4. \quad (\text{A.12})$$

The proposal

$$\phi'_{ij,x} = -\phi_{ij,x} - a/b \quad (\text{A.13})$$

keeps the value of  $a\phi_{ij,x} + b\phi_{ij,x}^2$  constant. The quartic part of the Hamiltonian is taken into account in an accept/reject step. The acceptance rate for this type of move is 67% at the chiral transition for  $D = 49$  (56% for  $D = 0.5$ ). Such a step, in a demon version, was performed subsequently for each of the four components of the field at a given site. We used a single demon for the whole lattice, refreshing it before the update of each site (this is equivalent to using a demon for each lattice site and updating it before each sweep).

Because of the different features of the model for large and small values of  $D$  we used different local update cycles in the two regimes. For  $D \leq 4$  we used a local cycle with an M4 sweep followed by  $N_{\text{or}}$  DOR4 sweeps. In most of the cases we used  $N_{\text{or}} = 8$ , but there is no sharp dependence of the efficiency on  $N_{\text{or}}$ . For large values of  $D$  a typical local cycle is instead: (M2+DOR4) sweep, 2 DOR4 sweeps, DOR1 sweep, 2 DOR4 sweeps, (MLE+DOR4) sweep, and finally 2 DOR4 sweeps. Here (M2+OR4) means a local M2 update followed by a local DOR4 update on the same site; (MLE+DOR4) has the same meaning. Beside the local cycle we also performed single-cluster updates: between two measurements we perform  $N_{\text{local}}$  local update cycles followed by  $N_{\text{single}}$  single-cluster updates on each field.

Let us look in more detail at the performance at  $D = 1/2$ . At the chiral transition, by using the local cycle (M4 + 8 DOR4), we obtain the autocorrelation times reported in Table A3. They are consistent with a critical exponent  $z = 2$ .

At the KT transition the cluster algorithm allows us to eliminate the slowing down of the spin degrees of freedom. For  $J = 1.47$  and  $L = 2048$  we find  $\tau_{\text{sp}} = 2.2(3)$  in units of measurements. Between two measurements we performed 10 local cycles and 10 single-cluster updates on each field.

## Appendix B. Some results for the low-temperature phase of 2- $d$ XY models

In the spin-wave limit the partition function of the 2- $d$  XY model is

$$Z = \sum_{n_1, n_2} \int \text{D}[\phi] \exp \left[ -\frac{\beta_{\text{SW}}}{2} \sum_{x, \mu} (\phi_x - \phi_{x+\hat{\mu}} - 2\pi n_\mu \delta_{x, L_\mu})^2 \right]$$

**Table A3.** Integrated autocorrelation times  $\tau_{\text{ch}}$  for the chiral susceptibility in the  $\phi^4$  model at  $D = 1/2$ , close to the chiral transition.  $\tau_{\text{ch}}$  is reported in units of measurements. # meas. is the total number of measurements,  $N_{\text{local}}$  is the number of local update cycles (one cycle corresponds to  $M4 + 8 \text{ DOR4}$ ) and  $N_{\text{single}}$  the number of single-cluster updates for each field per measurement.

$L$	$J$	# meas.	$N_{\text{local}}$	$N_{\text{single}}$	$\tau_{\text{ch}}$
360	1.4663	100000	200	10	11.0(6)
512	1.4665	43000	320	10	14.5(1.1)
600	1.4666	40000	200	10	40(8)
800	1.4665	127000	100	10	95(11)
1200	1.4666	37600	200	10	>100

$$= \sum_{n_1, n_2} W(n_1, n_2) \int D[\phi] \exp \left[ -\frac{\beta_{SW}}{2} \sum_{x, \mu} (\phi_x - \phi_{x+\hat{\mu}})^2 \right], \quad (\text{B.1})$$

where  $n_1$  and  $n_2$  are integer. The shift  $2\pi n_\mu \delta_{x_\mu, L_\mu}$  at the boundary takes into account winding XY configurations on lattices with periodic boundary conditions. The weights are given by

$$W(n_1, n_2) = \exp \left[ -2\pi^2 \beta_{SW} \left( \frac{L_2}{L_1} n_1^2 + \frac{L_1}{L_2} n_2^2 \right) \right]. \quad (\text{B.2})$$

Note that the contributions from  $(n_1, n_2) \neq (0, 0)$  are tiny: for instance, we have  $W(1, 0) = 3.487... \times 10^{-6}$  for  $L_1 = L_2$  at  $\beta_{SW} = 2/\pi$ . The LT phase of the XY model is effectively described by the spin-wave model for  $\beta_{SW} \geq 2/\pi$ . For smaller values of  $\beta_{SW}$ , vortices become relevant and disorder the system. Setting  $s_x = \cos \phi_x$ , the XY correlation functions are given by

$$\langle s_x s_y \rangle = \frac{\sum_{n_1, n_2} W(n_1, n_2) \cos[p_1 n_1 (x_1 - y_1) + p_2 n_2 (x_2 - y_2)] \langle \exp[i2\pi(\phi_x - \phi_y)] \rangle_G}{\sum_{n_1, n_2} W(n_1, n_2)}, \quad (\text{B.3})$$

where  $p_\mu = 2\pi/L_\mu$ .  $\langle \cdot \rangle_G$  denotes the expectation value in a Gaussian system without boundary shift. Using the Wick rule

$$\langle (\phi_x - \phi_y)^{2n} \rangle_G = (2n - 1)!! \langle (\phi_x - \phi_y)^2 \rangle_G^n, \quad (\text{B.4})$$

we can express the exponential in terms of the propagator of the Gaussian field:

$$\langle \exp[i2\pi(\phi_x - \phi_y)] \rangle_G = \exp \left[ -2\pi^2 \langle (\phi_x - \phi_y)^2 \rangle_G \right]. \quad (\text{B.5})$$

The exponent  $\eta$  of the magnetic susceptibility is given by

$$\eta = \frac{1}{2\pi\beta_{SW}}. \quad (\text{B.6})$$

The ratio  $R \equiv \xi/L$  is computed numerically using Eqs. (B.3) and (B.5). One can also derive the helicity modulus. For a lattice with  $L_1 = L_2$  we have [85]

$$\Upsilon = \beta_{SW} - \frac{4\pi^2 \beta_{SW}^2 \sum_{n=-\infty}^{\infty} n^2 \exp(-2\pi^2 \beta_{SW} n^2)}{\sum_{n=-\infty}^{\infty} \exp(-2\pi^2 \beta_{SW} n^2)}. \quad (\text{B.7})$$

One may use Eq. (B.6) to replace  $\beta_{SW}$  with  $\eta$  in Eq. (B.7), and obtain the universal relation between the helicity modulus and critical exponent  $\eta$  in the large- $L$  limit of a square  $L \times L$  lattice. An analogous relation can be obtained for the ratio  $\xi/L$ .

According to the KT theory, the leading corrections to  $\chi$ ,  $\xi/L$  and  $\Upsilon$  in the LT phase are proportional to  $L^{-2x}$  with  $x = \pi\beta - 2$ . Using Eq. (B.6), we have  $2x = 1/\eta - 4$ . In the case of  $\chi$  and  $\xi$  we also have corrections from the analytic background—they are of order  $L^{\eta-2}$ —which dominate for  $2 - \eta < 2x$ .

## References

- [1] Villain J, Spin glass with non-random interactions, 1977 *J. Phys. C: Solid State Phys.* **10** 1717; Two-level systems in a spin-glass model. I. General formalism and two-dimensional model, 1977 *J. Phys. C: Solid State Phys.* **10** 4793
- [2] Ling X S, Lezec H J, Higgins M J, Tsai J S, Fujita J, Numata H, Nakamura Y, Ochiai Y, Tang C, Chaikin P M and Bhattacharya S, Nature of phase transitions of superconducting wire networks in a magnetic field, 1996 *Phys. Rev. Lett.* **76** 2989; erratum 1996 *Phys. Rev. Lett.* **77** 410
- [3] Martinoli P and Leemann Ch, Two dimensional Josephson junction arrays, 2000 *J. Low Temp. Phys.* **118** 699
- [4] Affolter J, Tesei M, Pastoriza H, Leemann Ch and Martinoli P, Observation of Ising-like critical fluctuations in frustrated Josephson junction arrays with modulated coupling energies, 2002 *Physica C* **369** 313 [cond-mat/0111215]
- [5] Yosefin M and Domany E, Phase transitions in fully frustrated spin systems, 1985 *Phys. Rev. B* **32** 1778
- [6] Teitel S and Jayaprakash C, Phase transitions in frustrated two-dimensional XY models, 1983 *Phys. Rev. B* **27** R598
- [7] Shih W Y and Stroud D, Superconducting arrays in a magnetic field: effects of lattice structure and a possible double transition, 1984 *Phys. Rev. B* **30** 6774
- [8] Miyashita S and Shiba H, Nature of the phase transition of the two-dimensional antiferromagnetic plane rotator model on a triangular lattice, 1984 *J. Phys. Soc. Japan* **53** 1145
- [9] Choi M Y and Doniach S, Phase transitions in uniformly frustrated XY models, 1985 *Phys. Rev. B* **31** 4516
- [10] Halsey T C, Topological defects in the fully frustrated XY model and in  $^3\text{He-A}$  films, 1985 *J. Phys. C: Solid State Phys.* **18** 2437
- [11] Choi M Y and Stroud D, Critical behavior of pure and diluted XY models with uniform frustrations, 1985 *Phys. Rev. B* **32** 5773
- [12] Minnhagen P, Empirical evidence of a nonuniversal Kosterlitz-Thouless jump for frustrated two-dimensional XY models, 1985 *Phys. Rev. B* **32** 7548
- [13] Lee D H, Joannopoulos J D, Negele J W and Landau D P, Symmetry analysis and Monte Carlo study of a frustrated antiferromagnetic planar (XY) model in two dimensions, 1986 *Phys. Rev. B* **33** 450; Discrete-symmetry breaking and novel critical phenomena in an antiferromagnetic planar (XY) model in two dimensions, 1984 *Phys. Rev. Lett.* **52** 433
- [14] Korshunov S E and Uimin G V, Phase transitions in 2D uniformly frustrated XY-models. I. Antiferromagnetic model on a triangular lattice, 1986 *J. Stat. Phys.* **43** 1; Korshunov S E, Phase transitions in 2D uniformly frustrated XY-models. II. General scheme, 1986 *J. Stat. Phys.* **43** 17
- [15] Van Himbergen J E, Monte Carlo study of a generalized-planar-model antiferromagnet with frustration, 1986 *Phys. Rev. B* **33** 7857

- [16] Berge B, Diep H T, Ghazali A and Lallemand P, Phase transitions in two-dimensional uniformly frustrated XY spin systems, 1986 *Phys. Rev. B* **34** 3177
- [17] Granato E, Kosterlitz J M and Poulter J, Critical behavior of coupled XY models, 1986 *Phys. Rev. B* **33** 4767; erratum 1988 *Phys. Rev. B* **37** 5886
- [18] Foda O, A supersymmetric phase transition in Josephson-tunnel-junction arrays, 1988 *Nucl. Phys. B* **300** 611
- [19] Thijssen J M and Knops H J F, Monte Carlo study of the Coulomb-gas representation of frustrated XY models, 1988 *Phys. Rev. B* **37** 7738
- [20] Scheinine A L, Fourier-accelerated Langevin simulation of the frustrated XY model, 1989 *Phys. Rev. B* **39** 9368
- [21] Grest G S, Critical behavior of the two-dimensional uniformly frustrated charged Coulomb gas, 1989 *Phys. Rev. B* **39** 9267
- [22] Eikmans H, van Himbergen J E, Knops H J F and Thijssen J M, Critical behavior of an array of Josephson junctions with variable couplings, 1989 *Phys. Rev. B* **39** 11759
- [23] Gabay M, Garel T, Parker G N and Saslow W M, Phase diagram for the generalized Villain model, 1989 *Phys. Rev. B* **40** 264
- [24] Henley C L, Ordering due to disorder in a frustrated vector antiferromagnet, 1989 *Phys. Rev. Lett.* **62** 2056
- [25] Thijssen J M and Knops H J F, Monte Carlo transfer-matrix study of the frustrated XY model, 1990 *Phys. Rev. B* **42** 2438
- [26] Granato E, Kosterlitz J M, Lee J and Nightingale M P, Phase transitions in coupled XY-Ising systems, 1991 *Phys. Rev. Lett.* **66** 1090
- [27] Lee J, Kosterlitz J M and Granato E, Monte Carlo study of frustrated XY models on a triangular and square lattice, 1991 *Phys. Rev. B* **43** 11531
- [28] Nicolaidis D B, Monte Carlo simulation of the fully frustrated XY model, 1991 *J. Phys. A: Math. Gen.* **24** L231
- [29] Lee J, Granato E and Kosterlitz J M, Nonuniversal critical behavior and first-order transitions in a coupled XY-Ising model, 1991 *Phys. Rev. B* **44** 4819
- [30] Fernandez J F F, Puma M and Angulo R F, Critical behavior of a fully frustrated classical XY model in two dimensions, 1991 *Phys. Rev. B* **44** 10057
- [31] den Nijs M, Competition between surface roughening and reconstruction in (110) facets of fcc crystals, 1992 *Phys. Rev. B* **46** 10386
- [32] Lee J-R and Teitel S, Phase transitions in classical two-dimensional Coulomb gases, 1992 *Phys. Rev. B* **46** 3247
- [33] Ramirez-Santiago G and José J V, Correlation functions in the fully frustrated 2D XY model, 1992 *Phys. Rev. Lett.* **68** 1224; Critical exponents of the fully frustrated two-dimensional XY model, 1994 *Phys. Rev. B* **49** 9567
- [34] Saslow W M, Gabay M and Zhang W-M, Spiraling algorithm: collective Monte Carlo trial and self-determined boundary conditions for incommensurate spin systems, 1992 *Phys. Rev. Lett.* **68** 3627
- [35] Granato E, Critical behavior of a one-dimensional frustrated quantum XY model, 1992 *Phys. Rev. B* **45** 2557; Decoupling in the one-dimensional frustrated quantum XY model and Josephson-junction ladders: Ising critical behavior, 1993 *Phys. Rev. B* **48** 7727
- [36] Granato E and Nightingale M P, Chiral exponents of the square-lattice frustrated XY model: a Monte Carlo transfer-matrix calculation, 1993 *Phys. Rev. B* **48** 7438 [cond-mat/9307018]
- [37] Lee J-R, Phase transitions in the two-dimensional classical lattice Coulomb gas of half-integer charges, 1994 *Phys. Rev. B* **49** 3317
- [38] Lee S and Lee K-C, Phase transitions in the fully frustrated XY model studied with use of the microcanonical Monte Carlo technique, 1994 *Phys. Rev. B* **49** 15184
- [39] Knops Y M M, Nienhuis B, Knops H J F and Blöte H W J, 19-vertex version of the fully frustrated XY model, 1994 *Phys. Rev. B* **50** 1061

- [40] Olsson P, Two phase transitions in the fully frustrated XY model, 1995 *Phys. Rev. Lett.* **75** 2758 [cond-mat/9506082]; 1996 *Phys. Rev. Lett.* **77** 4850
- [41] Lee S, Lee J-R and Kim B, Dynamics of spin and chiral ordering in the two-dimensional fully frustrated XY model, 1995 *Phys. Rev. E* **51** R4
- [42] Nightingale N P, Granato E and Kosterlitz J M, Conformal anomaly and critical exponents of the XY Ising model, 1995 *Phys. Rev. B* **52** 7402 [cond-mat/9505048]
- [43] José J V and Ramirez-Santiago G, Comment of “Two phase transitions in the fully frustrated XY model”, 1996 *Phys. Rev. Lett.* **77** 4849
- [44] Xu H-J and Southern B W, Phase transitions in the classical XY antiferromagnet on the triangular lattice, 1996 *J. Phys. A: Math. Gen.* **29** L133
- [45] Granato E, Kosterlitz J M and Nightingale M P, Critical behavior of Josephson-junction arrays at  $f = 1/2$ , 1996 *Physica B* **222** 266 [cond-mat/9512038]
- [46] Cataudella V and Nicodemi M, Efficient cluster dynamics for the fully frustrated XY model, 1996 *Physica A* **233** 293
- [47] Olsson P, Monte Carlo study of the Villain version of the fully frustrated XY model, 1997 *Phys. Rev. B* **55** 3585 [cond-mat/9609181]
- [48] Benakli M, Zheng H and Gabay M, Thermal excitations of frustrated XY spins in two dimensions, 1997 *Phys. Rev. B* **55** 278 [cond-mat/9609269]
- [49] Benakli M and Granato E, Phase transitions in a frustrated XY model with zig-zag couplings, 1997 *Phys. Rev. B* **55** 8361 [cond-mat/9701022]
- [50] Jeon G S, Park S Y and Choi M Y, Double transitions in the fully frustrated XY model, 1997 *Phys. Rev. B* **55** 14088
- [51] Lee S, Lee K-C and Kosterlitz J M, Phase diagram of the restricted solid-on-solid model coupled to the Ising model, 1997 *Phys. Rev. B* **56** 340 [cond-mat/9612242]
- [52] Simon P, The 2D  $J_1$ - $J_2$  XY and XY-Ising models, 1997 *Europhysics. Lett.* **39** 129 [cond-mat/9706078]
- [53] Lee J-R, Lee S J, Kim B and Chang I, Ordering kinetics in the two-dimensional classical Coulomb gas of half-integer charges on a square lattice: temperature dependent growth and roughening transition, 1997 *Phys. Rev. Lett.* **79** 2172
- [54] Honda Y and Horiguchi T, Critical behavior of a 19-vertex model with full frustration, 1998 *Phys. Rev. B* **58** 11501.
- [55] Kawamura H, Universality of phase transitions of frustrated antiferromagnets, 1998 *J. Phys.: Condens. Matter* **10** 4707 [cond-mat/9805134]; Spin and chirality orderings of frustrated magnets: stacked-triangular antiferromagnets and spin glasses, 2001 *Can. J. Phys.* **79** 1447 [cond-mat/0111060]; Classical and quantum chiral order in frustrated XY magnets, 2002 cond-mat/0202109
- [56] Luo H J, Schülke L and Zheng B, Dynamic approach to the fully frustrated XY model, 1998 *Phys. Rev. Lett.* **81** 180 [cond-mat/9801253]; Universal short-time behavior of the dynamic fully frustrated XY model, 1998 *Phys. Rev. E* **57** 1327 [cond-mat/9705222]
- [57] Lee S and Lee K-C, Phase transitions in the fully frustrated triangular XY model, 1998 *Phys. Rev. B* **57** 8472
- [58] Capriotti L, Vaia R, Cuccoli A and Tognetti V, Phase transitions induced by easy-plane anisotropy in the classical Heisenberg antiferromagnet on a triangular lattice: A Monte Carlo simulation, 1998 *Phys. Rev. B* **58** 273 [cond-mat/9711104]
- [59] Boubcheur E H and Diep H T, Critical behavior of the two-dimensional fully frustrated XY model, 1998 *Phys. Rev. B* **58** 5163
- [60] Große Pawig S and Pinn K, Monte Carlo algorithms for the fully frustrated XY model, 1998 *Int. J. Mod. Phys. C* **9** 727 [cond-mat/9807137]
- [61] Loison D and Simon P, Monte Carlo analysis of the phase transition in the two-dimensional  $J_1$ - $J_2$  XY model, 2000 *Phys. Rev. B* **61** 6114 [cond-mat/9912438]
- [62] Franzese G, Cataudella V, Korshunov S E and Fazio R, Fully frustrated XY model with next-

- nearest-neighbor interaction, 2000 *Phys. Rev. B* **62** R9287 [cond-mat/0004495]
- [63] Chen Q-H, Luo M-B and Jiao Z-K, Second-order phase transition in the fully frustrated XY model with next-nearest-neighbor coupling, 2001 *Phys. Rev. B* **64** 212403
- [64] Marconi V I and Dominguez D, Nonequilibrium transitions in fully frustrated Josephson junction arrays, 2001 *Phys. Rev. Lett.* **87** 017004 [cond-mat/0102356]
- [65] Calabrese P and Parruccini P, Critical behavior of two-dimensional frustrated spin models with noncollinear order, 2001 *Phys. Rev. B* **64** 184408 [cond-mat/0105551]
- [66] Nussinov Z, Topological charge-order in a frustrated XY model and related systems, 2001 cond-mat/0107339
- [67] Noh J D, Rieger H, Enderle M and Knorr K, Critical behavior of the frustrated antiferromagnetic six-state clock model on a triangular lattice, 2002 *Phys. Rev. E* **66** 026111 [cond-mat/0204087]
- [68] Korshunov S E, Kink pairs unbinding on domain walls and the sequence of phase transitions in fully frustrated XY models, 2002 *Phys. Rev. Lett.* **88** 167007 [cond-mat/0106151]
- [69] Zheng B, Ren F and Ren H, Corrections to scaling in two-dimensional dynamic XY and fully frustrated XY models, 2003 *Phys. Rev. E* **68** 046120
- [70] Calabrese P, Orlov E V, Parruccini P and Sokolov A I, Chiral critical behavior of frustrated spin systems in two dimensions from five-loop renormalization-group expansions, 2003 *Phys. Rev. B* **67** 024413 [cond-mat/0207187]
- [71] Ozeki Y and Ito N, Nonequilibrium relaxation analysis of fully frustrated XY models in two dimensions, 2003 *Phys. Rev. B* **68** 054414
- [72] Jeon G S, Lee S J and Chang I, Relaxation and coarsening dynamics in superconducting arrays, 2003 *Phys. Rev. B* **67** 014501 [cond-mat/0211599]
- [73] Granato E and Dominguez D, Resistivity scaling and critical dynamics of fully frustrated Josephson-junction arrays with on-site dissipation, 2005 *Phys. Rev. B* **71** 094521 [cond-mat/0502190]
- [74] Olsson P and Teitel S, Kink-antikink unbinding transition in the two-dimensional fully frustrated XY model, 2005 *Phys. Rev. B* **71** 104423 [cond-mat/0304593]
- [75] Polini M, Fazio R, MacDonald A H and Tosi M P, Realization of fully frustrated Josephson-junction arrays with cold atoms, 2005 *Phys. Rev. Lett.* **95** 010401 [cond-mat/0501387].
- [76] Kosterlitz J M and Thouless D J, Ordering, metastability and phase transitions in two-dimensional systems, 1973 *J. Phys. C: Solid State Phys.* **6** 1181; Kosterlitz J M, The critical properties of the two-dimensional XY model, 1974 *J. Phys. C: Solid State Phys.* **7** 1046
- [77] José J V, Kadanoff L P, Kirkpatrick S and Nelson D R, Renormalization, vortices, and symmetry-breaking perturbations in the two-dimensional planar model, 1977 *Phys. Rev. B* **16** 1217
- [78] Hasenbusch M, Pelissetto A and Vicari E, Transitions and crossover phenomena in fully frustrated XY systems, 2005 *Phys. Rev. B* in press [cond-mat/0506345]; Critical behavior of two-dimensional fully frustrated XY systems, 2006 *J. Phys. (Proc. Suppl.)*, in press [cond-mat/0509511].
- [79] Calabrese P, Parruccini P, Pelissetto A and Vicari E, Critical behavior of  $O(2)\otimes O(N)$ -symmetric models, 2004 *Phys. Rev. B* **70** 174439 [cond-mat/0405667]
- [80] Pelissetto A and Vicari E, Critical phenomena and renormalization-group theory, 2002 *Phys. Rept.* **368** 549 [cond-mat/0012164]
- [81] Stella A L and Vanderzande C, Bulk, surface and hull fractal dimension of critical Ising clusters in  $d=2$ , 1989 *Phys. Rev. Lett.* **62** 1067
- [82] Janke W and Schakel M J, Fractal structure of spin clusters and domain walls in the two-dimensional Ising model, 2005 *Phys. Rev. E* **71** 036703 [cond-mat/0410364]
- [83] Wolff U, Collective Monte Carlo updating for spin systems, 1989 *Phys. Rev. Lett.* **62** 361
- [84] Mermin N D and Wagner H, Absence of ferromagnetism or antiferromagnetism in one- or two-dimensional isotropic Heisenberg models, 1966 *Phys. Rev. Lett.* **17** 1133
- [85] Hasenbusch M, The two dimensional XY model at the transition temperature: a high precision Monte Carlo study, 2005 *J. Phys. A: Math. Gen.* **38** 5869 [cond-mat/0502556]

- [86] Hasenbusch M, A Monte Carlo study of leading order scaling corrections of  $\phi^4$  theory on a three-dimensional lattice, 1999 *J. Phys. A: Math. Gen.* **32** 4851 [hep-lat/9902026]
- [87] Campostrini M, Hasenbusch M, Pelissetto A, Rossi P and Vicari E, Critical behavior of the XY universality class, 2001 *Phys. Rev. B* **63** 214503 [cond-mat/0010360]; Critical exponents and equation of state of the three-dimensional Heisenberg universality class, 2002 *Phys. Rev. B* **65** 144520 [cond-mat/0110336]
- [88] Salas J and Sokal A D, Universal amplitude ratios in the critical two-dimensional Ising model on a torus, 2000 *J. Stat. Phys.* **98** 551 [cond-mat/9904038]
- [89] Calabrese P, Caselle M, Celi A, Pelissetto A and Vicari E, Nonanalyticity of the Callan-Symanzik  $\beta$ -function of two-dimensional  $O(N)$  models, 2000 *J. Phys. A: Math. Gen.* **33** 8155 [hep-th/0005254]
- [90] Caselle M, Hasenbusch M, Pelissetto A and Vicari E, Irrelevant operators in the two-dimensional Ising model, 2002 *J. Phys. A: Math. Gen.* **35** 4861 [cond-mat/0106372]
- [91] Vollmayr K, Reger J D, Schencher M and Binder K, Finite size effects at thermally-driven first order transitions: a phenomenological theory of the order parameter distribution, 1993 *Z. Phys. B* **91** 113
- [92] Wilding N B and Nielaba P, Liquid-vapor asymmetry in pure fluids: A Monte Carlo simulation study, 1995 *J. Chem. Phys.* **102** 2562; Liquid-vapor phase behavior of a symmetrical binary fluid mixture, 1996 *Phys. Rev. E* **53** 926
- [93] Caracciolo S, Montanari A and Pelissetto A, Asymptotically free models and discrete non-Abelian groups, 2001 *Phys. Lett. B* **513** 223 [hep-lat/0103017]; Caracciolo S, Montanari A and Pelissetto A, Discrete non-Abelian groups and asymptotically free models, 2001 *Proc. Int. Europhysics Conf. on High-Energy Physics, HEP01, Budapest, PrHEP-hep2001/230* [hep-lat/0110221].
- [94] Caracciolo S and Pelissetto A, Lattice perturbation theory for  $O(N)$ -symmetric  $\sigma$ -models with general nearest-neighbour action. I. Conventional perturbation theory, 1994 *Nucl. Phys. B* **420** 141 [hep-lat/9401015].
- [95] Lawrie D and Sarbach S, 1984 Theory of tricritical points, *Phase Transitions and Critical Phenomena*, edited by C. Domb and J. L. Lebowitz (London: Academic Press), Vol. 9.
- [96] Nelson D R, Kosterlitz J M and Fisher M E, Renormalization-group analysis of bicritical and tetracritical points, 1974 *Phys. Rev. Lett.* **33** 813; Kosterlitz J M, Nelson D R and Fisher M E, Bicritical and tetracritical points in anisotropic antiferromagnetic systems, 1976 *Phys. Rev. B* **13** 412
- [97] Sheng Q and Henley C L, Ordering due to disorder in a triangular Heisenberg antiferromagnets with exchange anisotropy, 1992 *J. Phys.: Condens. Matter* **4** 2937
- [98] Wintel M, Everts H U and Apel W, Monte Carlo simulation of Heisenberg antiferromagnets on a triangular lattice: topological excitations, 1995 *Phys. Rev. B* **52** 13480 [cond-mat/9508128]
- [99] Caffarel M, Azaria P, Delamotte B and Mouhanna D, Spin stiffness and topological defects in two-dimensional frustrated spin systems, 2001 *Phys. Rev. B* **64** 014412 [cond-mat/0012397]
- [100] Azaria P, Delamotte B and Mouhanna D, Low-temperature properties of two-dimensional frustrated quantum antiferromagnets, 1992 *Phys. Rev. Lett.* **68** 1762
- [101] Hasenbusch M and Pinn K, Computing the roughening transition of Ising and solid-on-solid models by BCSOS model matching, 1997 *J. Phys. A: Math. Gen.* **30** 63 [cond-mat/9605019]
- [102] Calabrese P, Pelissetto A and Vicari E, Multicritical behavior of  $O(n_1) \oplus O(n_2)$ -symmetric systems, 2003 *Phys. Rev. B* **67** 054505 [cond-mat/0209580]
- [103] Granato E, Kosterlitz J M and Simkin M V, Edge effects in a frustrated Josephson-junction array with modulated couplings, 1998 *Phys. Rev. B* **57** 3602 [cond-mat/9710242]
- [104] Creutz M, Microcanonical Monte Carlo Simulation, 1983 *Phys. Rev. Lett.* **50** 1411
- [105] Gupta R, DeLapp J, Batrouni G G, Fox G C, Baillie C F and Apostolakis J, The phase transition in the 2-D XY model, 1988 *Phys. Rev. Lett.* **61** 1996